ABSTRACT

Title of Dissertation: COIL-TO-HELIX TRANSITION OF POLY(ETHYLENE OXIDE) IN SOLUTION

Michael L. Alessi, Doctor of Philosophy 2004

Dissertation Directed By: Professor Sandra C. Greer, Department of Chemical Engineering and Department of Chemistry and Biochemistry

Poly(ethylene oxide) (PEO) is a simple polymer with repeating units [- C - C - O -] soluble in organic and aqueous solvents. The carbon atoms are hydrophobic; the oxygen atoms are hydrophilic and participate in hydrogen bonding. In all solvents in which PEO has previously been studied, PEO forms a coil in solution. Neutron scattering studies of PEO in isobutyric acid show that PEO undergoes a coil-to-rod transition in a solution of isobutyric acid (IBA). The stiffening is seen to progress smoothly with the addition of IBA, from a coil in D_2O to a rod in pure deuterated-IBA. In addition to a solvent driven transition, a reversible rod-to-coil transition was seen to occur as a function of temperature, between 55 and 60 ^{o}C. Polarimetry experiments show that the rod formed by the PEO in solution is actually a helix, the conformation that PEO has in the solid state. It is also shown that, through the use of chiral impurities and temperature, the direction of the helix can be affected, allowing polymer folding to be influenced on a molecular level.

COIL-TO-HELIX TRANSITION OF POLY(ETHYLENE OXIDE) IN SOLUTION

By

Michael L. Alessi

Dissertation submitted to the Faculty of the Graduate School of the
University of Maryland, College Park, in partial fulfillment
of the requirements for the degree of
Doctor of Philosophy
2004

Advisory Committee:
Professor Sandra C. Greer, Chair
Professor Robert M. Briber
Professor Panagiotis Dimitrakopoulos
Professor Srinivasa R. Raghavan
Professor Robert A. Walker

Dedication

For Clyde, a very good dog.

Acknowledgements

I would like to first thank Dr. Derek Ho of the NIST Center for Neutron Scattering. Dr. Ho never hesitated to help me understand a theoretical aspect of neutron scattering and provided hours of assistance during the experimental phase of the neutron scattering. I will always be grateful for his help in this endeavor.

This work would not have been possible without the help and guidance of Dr. Sandra C. Greer. She has set a standard for ethics and professionalism that I will always strive to attain. Thank you Dr. Greer.

Table of Contents

List of Tables

List of Figures

Chapter 1: Introduction

Poly(oxyethylene) is a polymer consisting of ethylene glycol monomers. This polymer is generally referred to as poly(ethylene glycol) (PEG) when the molecular weight is less than 20,000 and poly(ethylene oxide) (PEO) when the molecular weight is greater than 20,000. For simplicity, this work will refer to poly(oxyethylene) as PEO, regardless of molecular weight. PEO can be synthesized through the ionic ring opening polymerization of an oxirane monomer, shown below is an example of anionic ring opening polymerization.

Initiation

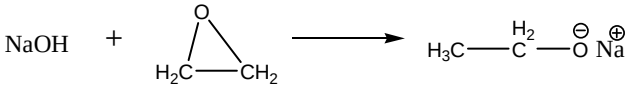

Propagation

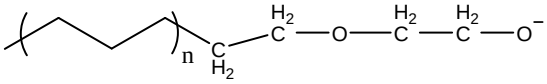

Figure 1. Anionic ring opening polymerization mechanism

Because synthetic polymerization reactions are statistical in nature, polymers are formed with a range of molecular weights instead of a single molecular weight. The breadth of the molecular weight distribution or polydispersity index (PI) is of great interest to both theorists and industry since the behavior of a polymeric system is strongly dependent upon its molecular weight. The PI is measured in terms of a ratio of the second and first moments of the molecular weight. These moments are also known as the weight average (M_w) and number average (M_n) molecular weights, respectively. The lowest possible PI would be 1.0, which represents a monodisperse polymer system, only seen in proteins. Broader distributions (PI>>1.0) can complicate the theoretical treatment of the system, since then it cannot be treated as a simple system and must be treated as a multi-component system with a nearly infinite number of components. This can make for an intractable calculation. Industrial applications are also interested in the breadth of the molecular weight distribution, since polymer properties depend upon its PI.

PEO is an interesting system because it is soluble in both water and several organic solvents, due to the presence of both hydrophobic and hydrophilic segments. Since this polymer is soluble in many different solvents, it is widely used in both industrial and biological applications. Industrial applications of PEO include use as a support for organic synthesis reactions, use as a conductive polymer matrix when mixed with salt, and use as a membrane material for the separation of acid gases.[1] In biology, PEO is used to crystallize proteins and is considered biologically inert by the FDA, allowing it to be used in medical applications. PEO is also used as a drug delivery matrix and as a coating to avoid immune responses to implants. PEO has

also been a fertile area for scientific interest. A literature search for poly(ethylene oxide) or poly(ethylene glycol) will result in over 89,000 articles. The system is of such interest because of the hydrophobic and hydrophilic segments that allow it to dissolve in polar and nonpolar solvents. The combination of these segments in one macromolecule allows the polymer to be treated as a cheap and stable model protein that is "shelf stable" and easily modified for molecular weight or hydrophobicity.

As mentioned earlier, the breadth of the molecular weight distribution is of vital importance. A common technique used to narrow the molecular weight distribution of a polymer is fractionation. The molecular weight and polydispersity of the polymer are often controlled by using fractionation between coexisting liquid phases. Flory's theory of polymer solutions[2] treats the phase separation of polymers as a competition between the enthalpic gain due to phase separation versus the entropic cost of phase separation. When phase separation occurs, the larger molecules are expected to move into the polymer rich phase, while the shorter chains will be in the solvent rich phase. Extracting the lower phase and carrying out repeated fractionations allows a narrow molecular weight distribution polymer sample to be isolated.

Recent work by Shresth *et al.*studied the fractionation of PEO in two binary solutions.[3] The authors took critical solutions of water/isobutyric acid (IBA) and water/lutidine and dissolved PEO with a broad molecular weight distribution in both systems. These solutions were chosen because they exhibit an upper critical solution temperature, (UCST) (see Figure 2[4,5]) and a lower critical solution temperature (LCST), respectively. The temperature was adjusted to bring both systems into their

two-phase regions. A sampling manifold was then used to simultaneously extract samples from the coexisting phases. The polymer samples were analyzed using gel permeation chromatography (GPC). The water/lutidine system did not show a particularly strong fractionation and almost no decrease in the polydispersity. In the water/isobutyric acid system, however, the authors observed a strong fractionation in which most of the PEO goes into the isobutyric acid-rich phase and larger PEO molecules go to the water-rich phase, with a dramatic decrease in the polydispersity of the PEO in the aqueous phase that is independent of temperature. The results are summarized in Table 1.

Table 1. Molecular weights and polydispersities from Shresth *et al.*[3]

	M_n	PI
Parent Phase	18,900	1.36
IBA Phase	13,100	1.37
Water Phase	34,200	1.07

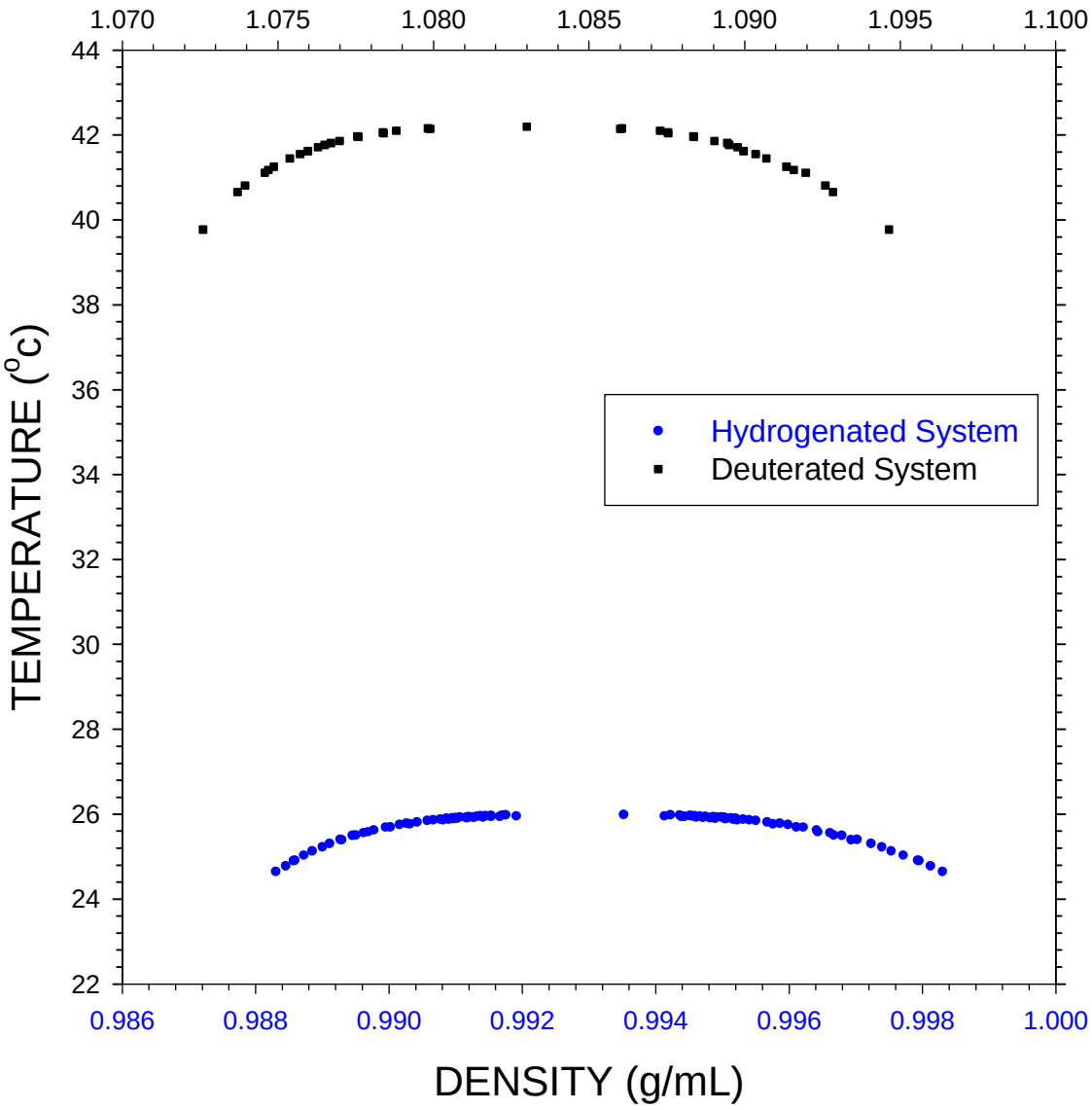

Figure 2. Phase diagram of isobutyric acid and water for both the hydrogenated and deuterated systems using density as the order parameter.[4,5]

This dramatic fractionation was the motivation for the experiments presented here, since a molecular explanation of this fractionation was not previously attempted. In the present work, neutron scattering was used to observe the behavior of PEO molecules in this system. Neutron scattering represents a powerful nondestructive technique in polymer analysis. Unlike the interaction of x-rays, which follows the periodic table, neutrons interact with atoms in an almost random way. Neutrons not only interact with lighter elements such as H, they also can interact differently with different isotopes of the same element. An example of this is the difference in neutron scattering length between hydrogen (-3.74 fm) and deuterium (6.67 fm).[6]

Another powerful aspect of neutron scattering is the ability to observe a number of length scales in the same experiment by choosing a wide enough q range. These different q ranges are shown in the curve show in Figure 3. When $q^{-1}<R_g$, the individual molecules appear as points and only aggregations and thermodynamic properties are seen. In the Guinier regime, $q^{-1}\sim R_g$, the entire molecule is observed, but only the dimension of the molecule can be measured and not details about the shape of the molecule. The fractal regime is an area where the chains are now seen and the shape of these molecules can be deciphered. The highest q regime, the Porod regime, gives a measure of the contrast between the scatterer and the solvent.

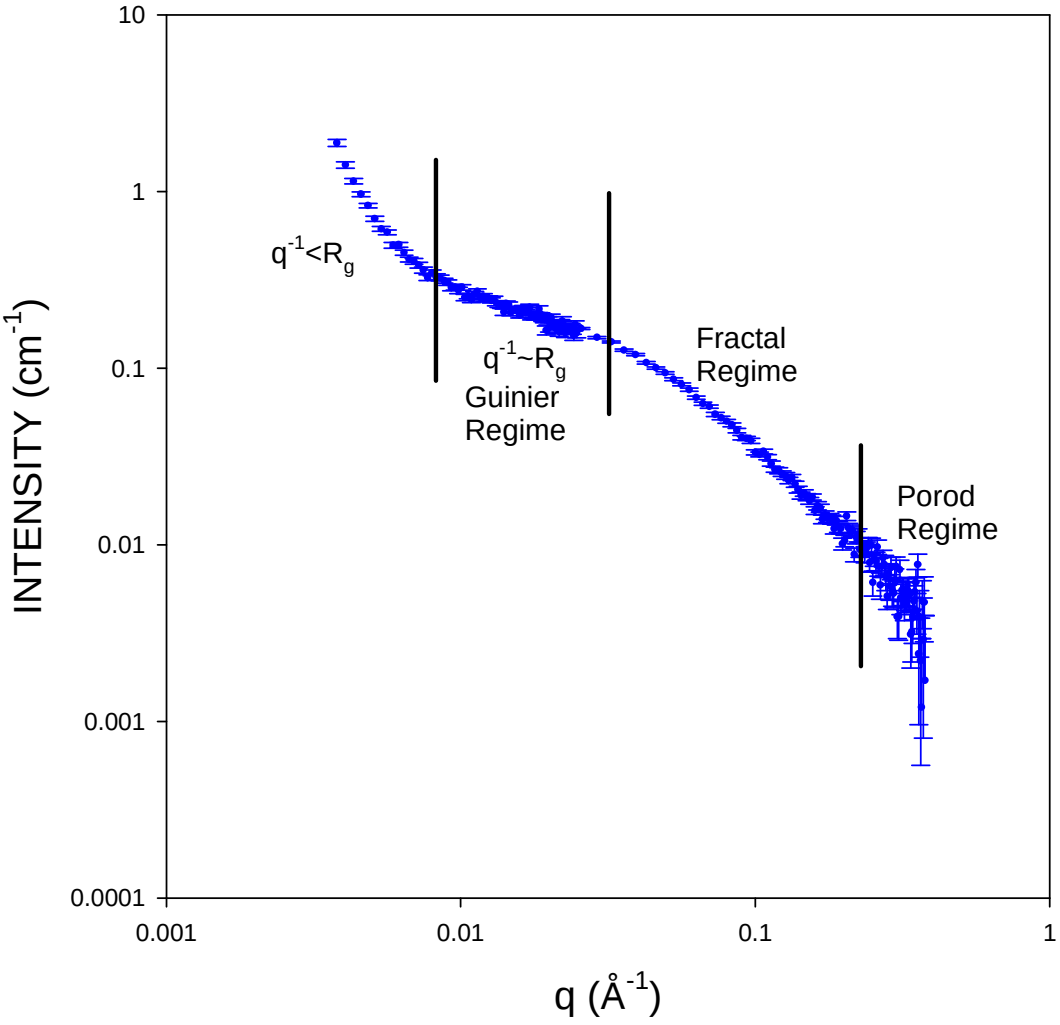

Figure 3. Representative scattering curve showing different q regimes.

The neutron scattering studies carried out in this work have indicated that PEO forms a stiff rod in IBA solutions. As will be discussed later, it has been theorized that PEO forms a helix in water,[7] although this global helix has never been observed, only a local helical structure on the order of a few monomers. The stiff rods, observed here for the first time in IBA, are also believed to be helical. Polarimetry measurements on PEO in hydrogenated isobutyric acid solutions showed

an optical rotation, which was not seen with PEO in water. It is felt that this provides strong evidence that the rigid rods seen in the deuterated system are not only present in the hydrogenated system, but also helical. This result is significant since it legitimizes our use of isotopic substitution, the most commonly used scattering technique in which either the solvent or the polymer is deuterated by replacing protons with deuterium, creating a good contrast for analysis. One assumption of this technique, however, is that the substitution will not have a dramatic effect on the behavior of the system.[6] The minimal disruption due to the deuteration contrasting technique has not been found to hold for PEO in D_2O.[8-10] The global conformation of the polymer was not changed, but the authors found that the local conformation of the chain was less ordered in D_2O than in water. It appears that this effect is not significant in isobutyric acid solutions.

Chapter 2: Prior Work

Aqueous Solutions of Poly(ethylene oxide)

Theory

The fact that PEO is so ubiquitous has resulted in a large amount of research on its behavior in aqueous solutions. Sadly, the large amount of work on this system has not led to a fundamental understanding of this fascinating system. Why PEO is soluble in water is still poorly understood on a molecular level. While PEO is soluble in water, poly(oxymethylene), poly(oxypropylene), and poly(oxybutylene) are all insoluble in water, even though they are simply homologues of PEO.[11] Several attempts have been made to explain PEO's closed-loop phase behavior in aqueous solutions, ranging from conformational hydrophobicity to changes in water structuring.[12,13] Experimental work on this system has been no simpler. The aggregation of PEO polymers in solution has been seen by some authors[14,15] and not seen by others.[16,17]

An early attempt to explain the solubility of PEO in water was undertaken by Kjellander and Florin.[7] The authors used a structural model for PEO in water in which the system was visualized as a solute surrounded by a water cage. The hexagonal structure of water accommodates PEO molecules, since the distance between the alternate oxygen atoms is 4.7 Å, which is the same as the distance between oxygen atoms in hexagonally structured water.[18] If the PEO molecule takes a helical formation, the oxygen-oxygen distance in the polymer is 2.88 Å,[7] which

compares well with the oxygen-oxygen distance in tetrahedrally associated water which is 2.85 Å.[18]

When PEO is put into water at moderate temperatures, the entropy of mixing and dilution are negative, as is the enthalpy of mixing. Since the polymer is hydrated by two water molecules per monomer,[7,19] the conformational freedom of the molecule is reduced, accounting for the negative mixing energies. Contact between two polymer molecules results in the overlap of hydration shells, resulting in an increase in energy. Decreasing the temperature of the system increases the structure of the water and increases the entropic cost. This cost is offset by the improved enthalpic interaction due to PEO fitting into the water structure, which results in the LCST. As the temperature is increased, the structure of the surrounding water is weakened, but the entropic term, $T\Delta S$, still dominates and phase separation occurs. At very high temperatures, the water structure breaks down and combinatorial entropy dominates, resulting in an UCST.

A later work by Karlström, which was based upon a theory by Hirschfelder *et al.*, (HSE) considered a conformational hydrophobicity.[20,21] HSE theory explains the formation of a solubility gap for two molecules by describing their intermolecular potential as having small attractive regions and large repulsive regions.[20] At low temperatures, the molecules are in the attractive regime, and at high temperatures, ordinary mixing entropy will dominate, resulting in one phase for both of these situations. The miscibility gap occurs when the temperature is high enough to be in the repulsive domain, but low enough to not be dominated by mixing entropy.

Karlström adapted this to explain the miscibility gap in aqueous PEO solutions by looking at the conformation of the C-O and C-C bonds of the polymer. The author used a Flory-Huggins type treatment to describe the system, but incorporated an interaction parameter that changed with the conformation of the polymer. When the oxygen atom of the monomer has a gauche orientation around the C-C bond and trans around the C-O bond, the segment has a large dipole moment which interacts favorably with the surrounding water molecules. Other conformations are nonpolar or have small dipole moments and will not interact favorably with water. The author considered these two states as low and high temperature states, respectively. Using these two states, Karlström derived the internal energy and entropy of the system using the Flory-Huggins expression. The Helmholtz energy of the system can then be minimized with respect to pressure to calculate the free energy at a specific composition and can be used to calculate the phase diagram of the system. The theory was compared to Saeki *et al.*'s [22] experimental data. Karlström's theory was in qualitative agreement with Saeki's data and showed a closed loop phase diagram, but was not in good quantitative agreement, the critical composition was shifted to higher mass fractions and the LCST was shifted downward. In addition to the poor agreement with experimental data, this theory requires five interaction parameters.

Attempts were also made to develop a general equation of state for hydrogen bonded systems which can then be applied to aqueous PEO solutions.[23-28] A major step forward for this approach was put forth by Veytsman.[25] The author developed a combinatorial expression for the distribution of hydrogen bonds in a system.

Veytsman split the free energy of the system into a standard free energy of the system without hydrogen bonds and a contribution to the free energy from hydrogen bonds. This approach used statistics to avoid the condition that hydrogen-bonded molecules must be in adjacent lattice sites. This approach was later used by Panayiotou *et al.*[23,24] and Veytsman[25,26] to develop a more rigorous theory of hydrogen bonded fluids.

Matsuyama and Tanka developed a simple lattice model to explain LCST behavior in polymer solutions that undergo hydrogen bonding.[27] This theory takes account of hydrogen bonding between the polymer and solvent, but ignores polymer-polymer and solvent-solvent hydrogen bonding. The authors treat the hydrogen bonded species as clusters and deal with the free energy of the cluster formation. The free energy of the system is again treated as additive, with the free energy of the cluster formation contributing to the free energy of the reference system. The free energy of the reference system is calculated using a normal Flory-Huggins lattice treatment, and the contribution from the clusters is incorporated by using the following multiple chemical equilibria conditions:

$$\mu_{m+1} = \mu_1 + m\mu_0 (m = 0,1,2,..., f) \tag{1}$$

The subscripts in equation 1 are references to the clusters of associated molecules, with 0 being free solvent and 1 unassociated polymer. The volume fraction of each size cluster can then be expressed as

$$\phi_{m+1} = K_m \phi_1 \phi_0^m . \tag{2}$$

The term K_m in equation 2 is an association constant taken in terms of the free energy difference due to bond formation which is split into enthalpic and entropic terms,

$$K_m = \exp\left(m - \beta\left[\Delta H - T\Delta S\right]\right). \quad (3)$$

The theory predicts a decrease in the average number of associated molecules as the temperature is increased, which points to hydrogen bond breakage at higher temperatures as explaining the LCST behavior seen in hydrogen bonded systems. The authors compared their data to experimental results for PEO in both t-butyl acetate and water and had very good agreement with the experimental results. This theory is diminished, however, by the large number of parameters required by the theory. Five different parameters are required: the functionality of the polymer, degree of polymerization of the polymer, entropy change per hydrogen bond, dimensionless bond energy, and the polymer-solvent interaction parameter. These parameters are generally found by fitting the equations to experimental data and the parameter values are often unrealistic.[19]

Panayiotou and Sanchez developed an equation of state approach for hydrogen bonded systems similar to the Matsuyama's treatment.[23,24] The original treatment consisted of developing a formal equation of state for hydrogen bonded fluids. In order to simplify the analysis, the physical portion of the partition function is treated as a normal lattice fluid partition function. The chemical portion of the partition function is developed by extending Veytsman's earlier work and is found by relating the energy of the system to the number of hydrogen bonds in the system. A normal counting scheme for hydrogen bonds would overestimate the number of ways to form hydrogen bonds, since it would not account for the proximity requirement that the molecules be adjacent to each other nor would it ensure that the molecules are in the proper orientation. The overestimation is addressed by multiplying by the

probability that the molecules are both adjacent and in the proper orientation to undergo hydrogen bonding. The probability is a function of the system volume, ρ/rN, and the entropy loss due to the formation of a hydrogen bond, S_{ij},

$$P_{ij} = e^{\frac{S_{ij}}{R}} \frac{\rho}{rN}. \tag{4}$$

The chemical portion of the partition function is found by summing over all of the possible number hydrogen bonds for the system. The total Gibbs partition function is then written as a combination of the chemical, Q_H, and physical, Q_P, partition functions as

$$\Psi = Q_P Q_H e^{\frac{-PV}{RT}}. \tag{5}$$

Panayiotou and Sanchez further developed their theory for hydrogen bonded fluids to include associated polymers.[23] This work only considered solvent-solvent and solvent-polymer interactions and ignored polymer-polymer interactions. The polymer-solvent interactions are considered to form association complexes with the solvent molecules which also associate with each other. These complexes only interact with each other through physical interactions and not hydrogen bonding. The formation of the complexes is treated as three distinct steps: the associations are formed in their reference state in perfect orientation with perfectly oriented monomers, these complexes are disoriented, and finally the disoriented complexes are mixed on the lattice with free solvent and empty sites. The system can then be treated by standard lattice fluid theory to find the normal energy of the system and the contribution of the hydrogen bonding to the energy of the system is accounted for by considering the formation of the association complexes.

The associations are of two kinds, self-association of the solvent molecules A and chains of A associated with a polymer molecule B. These associations are treated using two simple equilibrium constants, K_A and K_B.

$$A_i + A_j \xrightarrow{K_A} A_{i+j} \tag{6}$$

$$B + A_i \xrightarrow{K_{AB}} BA_i \tag{7}$$

The equilibrium constants are related to the free energy change due to hydrogen bond formation by:

$$\begin{aligned} K_A &= e^{\frac{-\Delta F_A}{RT}} \\ K_{AB} &= e^{\frac{-\Delta F_{AB}}{RT}}. \end{aligned} \tag{8}$$

The number of complexes formed can then be related to these equilibrium constants and allow the calculation of the volume fraction of the different species. These volume fractions are then used in the standard lattice fluid equation of state. This theory was compared to experimental data for chloroform and PEO and showed good agreement. This theory, however, requires three fitting parameters: hydrogen bonding energy change, entropy change due to hydrogen bonding, and volume change of hydrogen bonding. These are not measurable *a priori* and so must be found by fitting the equations to experimental data. This limits the application of the theory to systems with similar hydrogen bonding data or systems with a known set of experimental data.

In 1998, Veytsman expanded up on his earlier note to develop a mean-field equation of state for hydrogen bonded systems.[26] In a manner similar to Panyiotou *et al.*,[24] Veytsman treated the partition function of the system as a product of two partition functions, one for the reference system without hydrogen bonds and another

representing the contribution from the hydrogen bonds. An individual partition function, Ξ_i, for a specified number of hydrogen bonds, M_{ij}, which allows the Helmholtz free energy for the specified number of hydrogen bonds to be calculated as

$$A_i = -kT \ln \Xi_i. \tag{9}$$

The equilibrium value of the free energy of the system is found by minimizing the free energy with respect to M_{ij}. The pressure of the system is then calculated by taking the derivative of the free energy with respect to the volume of the system at constant temperature and association number. The free energy has both an implicit and explicit volume dependence, which complicates this derivative. This can be simplified by using the relation

$$\frac{\partial A}{\partial V} = \left(\frac{\partial A_i}{\partial V}\right) + \sum \left(\frac{\partial A_i}{\partial M_{ij}}\right)\left(\frac{\partial M_{ij}}{\partial V}\right). \tag{10}$$

The first part of the second term in equation 10, $\left(\frac{\partial A_i}{\partial M_{ij}}\right)$, is equal to zero from the equilibrium condition used to calculate the free energy with respect to M_{ij}, and simplifies the relationship between pressure and free energy to only account for the explicit volume dependence as

$$P = -\left(\frac{\partial A_i}{\partial V}\right). \tag{11}$$

Recognizing that the free energy of the system is a linear combination of the energy of a reference system and the free energy resulting from hydrogen bonding, the pressure of the system can be written

$$P\left(T, V, N_i\right) = P_{ref}\left(T, V - \sum_{ij} M_{ij} V_{ij}^{H}, N_i\right) - kT \sum_{ij} \frac{M_{ij}}{V}. \tag{12}$$

In equation 12, P_{ref} is the pressure of a reference system which can be calculated using any standard equation of state, and V^H is the volume change produced by one hydrogen bond. Equation 12 allows the calculation of the equation of state of a hydrogen bonded system by calculating the number of hydrogen bonds, M_{ij}, which minimizes the free energy and then using this term to correct a standard equation of state which can be used to calculate P_{ref}. Similar treatments can be carried out to calculate other thermodynamic properties using other derivatives. The primary limitation of this theory, however, is the fact that it is mean-field and cannot be used near the critical point of a system.

The most recent theory was put forward for PEO in aqueous systems by Dormindontova.[19] Dormidontova used a mean-field approach similar to that of Matsuyama[27] except the competition for hydrogen bonding between PEO molecules and water was considered as well. The author viewed the free energy of the system as a linear combination of terms representing the reference energy of the system without hydrogen bonds, F_{ref}, excluded volume interactions of monomers, F_{int}, and a term representing the contribution from hydrogen bonding, F_{assoc}. The free energy due to hydrogen bonding is dependent upon the partition coefficient of the system. The partition function of the system is written as

$$\Xi_{assoc} = P_{comb} W_p \exp\left(\frac{\Delta E_p}{kT} n_p\right) W_w \exp\left(\frac{\Delta E_w}{kT} n_w\right), \tag{13}$$

where P_{comb} is a combinatorial method to form n_p hydrogen bonds between PEO and water molecules and n_w hydrogen bonds between water molecules. W_p and W_w are the probabilities that a proton donor and acceptor are near enough and in the proper orientation for a hydrogen bond to occur between a polymer molecule and a water

molecule and between water molecules respectively, and ΔE is the energy change upon hydrogen bond formation. The author then minimizes the free energy of the system with respect to the fraction of PEO-water hydrogen bonds, x, and water-water hydrogen bonds, p.

A ratio of these two fractions gives a relationship between the energy of the respective bond formation and the fraction of each type of bond. This ratio is written as

$$\frac{x}{p} = \exp\left[\frac{\Delta F_p - \Delta F_w}{kT}\right]\frac{(1-x)}{(1-p)}. \qquad (14)$$

This relationship shows that there is a competition between PEO and water molecules for protons to form hydrogen bonds, and that water-water hydrogen bonding cannot be ignored unless the energy difference between the two types of hydrogen bonds is negligible. Equation 14 was then analyzed for several different volume fractions of polymer. At low concentrations of polymer, (Φ=0.05), the average fraction of PEO-water and water-water hydrogen bonds are larger than for higher polymer concentrations since there are more proton donors (water molecules) available to form hydrogen bonds. When the polymer concentration is intermediate, (Φ=0.5), the average fraction of hydrogen bonds is smaller than that for Φ=0.05, (0.75 versus 0.95), and the difference between the fraction of PEO-water and water-water hydrogen bonds is larger at low temperatures than that of the dilute polymer system. When the concentration of the polymer is high, Φ=0.9, the average fraction of hydrogen bonded species at low temperature is much lower than the other two cases, only around 0.25. Unlike the prior two cases, the fraction of water-water hydrogen bonds shows an increase with temperature to a maximum around 40 ^{o}C. The

difference between the fraction of PEO-water and water-water hydrogen bonds was also larger than either of the two cases. The maximum in the fraction of water-water hydrogen bonds can be explained energetically. At low temperatures the formation of PEO-water hydrogen bonds is favorable because of enthalpic contributions, but at higher temperatures the entropic cost of the hydrogen bond becomes too great and the bonds are disrupted. At low enough temperatures, the freed water molecules can produce an energetic gain by forming hydrogen bonds with other water molecules. Above a certain temperature, in this case 40 ^{o}C, the entropic penalty for the associated water becomes large enough to begin disrupting water-water hydrogen bonds, leading to a decrease in the fraction of associated water molecules. This indicates a preference for water-water hydrogen bonds versus PEO-water hydrogen bonds.

The author compared the theory to experimental phase diagrams for thirteen different PEO samples of different molecular weights from three different research groups.[22,29,30] The theoretical predictions gave excellent agreement with the experimental data. This was an impressive accomplishment, since the theory was able to use the same parameters for systems ranging over almost three orders of magnitude.

Experiment and Simulation

The solution behavior of PEO in aqueous systems has been extensively studied.[11,13-17,22,29,31-37] A graph of LCST temperatures for PEO in water is shown in Figure 4.[22,29,33,38]

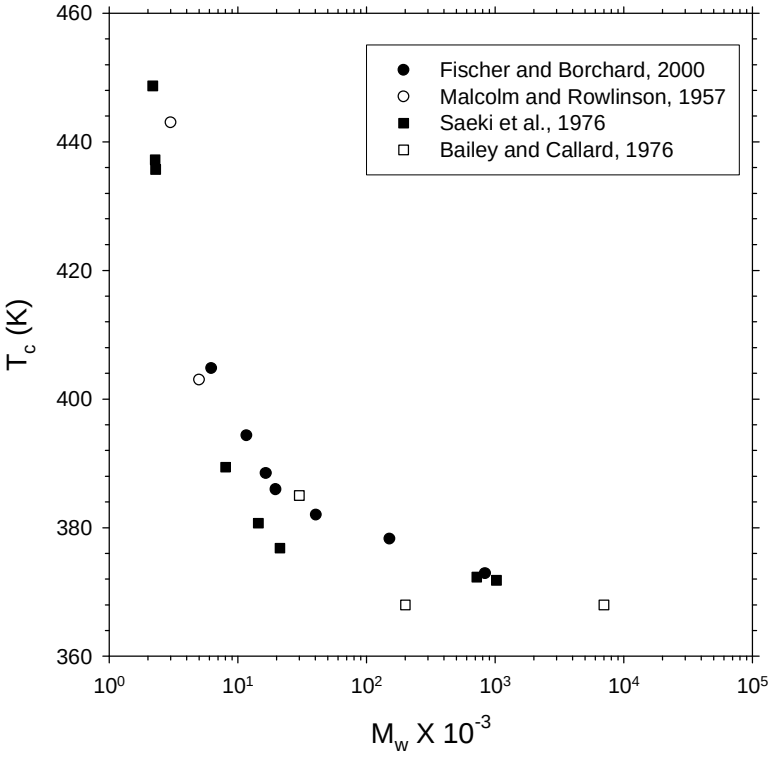

Figure 4. LCST of PEO in H_2O

A recent study by Smith *et al.* used molecular dynamics simulations of PEO dimers in water.[39] The authors calculated the excess thermodynamic properties of mixing. The excess enthalpy of mixing is favorable at room temperature, while the excess entropy of mixing is unfavorable. This entropic term explains the presence of an LCST and agrees with Kjellander's model of the polymer fitting into a water matrix.[7]

Polymers in a Binary Solvent

Theory

The behavior of a polymer in a critical binary solvent is still poorly understood because of the complexity of numerous interactions. The interaction of the polymer with each solvent as well as the solvent interactions must be accounted for. As the critical point is approached, the interactions of the system are affected by the chain length of the polymer and the diverging correlation lengths of the solvent. Theoretical treatments of this problem have been in development since 1949, with varying degrees of success.

The first attempt at developing a method to describe the system was undertaken by Scott in 1949.[40] Scott developed a mean-field theory using a "single liquid approximation" (SLA) in which the binary solvent was treated as a single liquid with an effective interaction parameter, χ_{eff}. This allows the chemical potential to be written as:

$$\frac{\Delta\mu_3}{RT} = \ln\varphi_3 - (m-1)(1-\varphi_3) + m\chi_{eff}(1-\varphi_3)^2 \qquad (15)$$

$$\chi_{eff} = \chi_{13}\varphi_1 + \chi_{23}\varphi_2 - \chi_{12}\varphi_1\varphi_2 \qquad (16)$$

In the previous equations, the subscripts 1 and 2 indicate solvent and 3 the polymer. Equation 16 indicates that two poor solvents for a polymer can combine to improve the quality of the effective solvent. This occurs when the third term of the equation is large enough to decrease the effective interaction parameter. When this occurs there is an energetic drive to minimize solvent-solvent interactions. This can be

accomplished by swelling the polymer and increasing the number of solvent-polymer interactions at the expense of solvent-solvent interactions. The converse can also be true, in which two good solvents can combine to form a poor solvent. This theory, however, does not take into account preferential adsorption of one solvent by the polymer molecule.

A more rigorous treatment incorporating an unequal affinity for the polymer and solvent was developed by Shultz and Flory (SF).[41] This theory assumes the solvent composition inside the polymer coil is different than in the bulk solvent. SF treats the three component system as two homogeneous phases, one inside the polymer coil and the other outside of the coil. The free energy of the polymer phase is the standard free energy of mixing of the three components plus an elastic contribution from the deformation of the chain. The SF effective interaction parameter can be written as:[42]

$$\chi_{SF} = \frac{1}{2} - \frac{1 - 2\varphi_1\chi_{13} - 2\varphi_2\chi_{23} + D\varphi_1\varphi_2}{2\varphi_1 + 2\varphi_2 - 4\varphi_1\varphi_2\chi_{12}} \tag{17}$$

$$D = 2\chi_{12}\chi_{13} + 2\chi_{12}\chi_{23} + 2\chi_{13}\chi_{23} - \chi_{12}^2 - \chi_{13}^2 - \chi_{23}^2 \tag{18}$$

Equation 17 can be rearranged for an equimolar solvent in terms of the effective interaction parameter from the single liquid approximation.[42]

$$\chi_{SF} = \chi_{SLA} + \frac{\gamma^2\chi_{13}^2}{4(2 - \chi_{12})} \tag{19}$$

In equation 19, γ is the preferential adsorption parameter indicating the energetic preference of the polymer for one of the solvents. Since this term is positive, it

decreases the quality of the solvent. As the interaction parameter for the solvents approaches 2, which is the expected critical value for a mean-field theory, the interaction parameter will tend to infinity,[2] which predicts a polymer collapse as the critical point of the system is approached.

In 1980, Brochard and de Gennes developed a theory for a polymer in a mixture of two solvents near their critical point.[43] This theory also accounts for the case of preferential solvent adsorption and its effect on the chain dimensions. Like SF theory, Brochard and de Gennes (BG) theory predicts a chain collapse as the critical point is approached. This effect is thought to be due to monomer attraction. One monomer in the chain is surrounded by the preferentially adsorbed solvent. Nearby monomers are then attracted to cloud of solvent, creating a net chain collapse. The range of this attraction is dependent on the correlation length of the solvent, which diverges as the critical point is approached. When the molecule size is larger than the correlation length, the interaction can be treated as point-like and written:[43]

$$W_{TOT}(r_{ij}) = kT\tilde{v}\delta(r_{ij}) \tag{20}$$

The term, $\tilde{\upsilon}$, is the effective excluded volume, which is the classic excluded volume minus the solvent interactions:

$$\tilde{v} = v - 4\pi e^2 \xi^2 \tag{21}$$

In Equation 21, *e* is a coupling parameter for the monomer concentration inside the coil and the deviation of solvent concentration inside the coil from critical. As the correlation length, ξ, increases in size, the excluded volume becomes negative and the chain collapses. The correlation length limit for coil collapse ($\tilde{\upsilon}$=0) is then calculated to be:

$$\xi = \left(\frac{vkT}{4\pi e^2} \right)^{\frac{1}{2}} \tag{22}$$

Brochard and de Gennes also investigated the effect of the chain collapse on the internal concentration, the shift of the critical point, and the rigorousness of the collapse condition, $\tilde{\upsilon}=0$.

Brochard and de Gennes treated the internal concentration of the coil as follows. The free energy of just the binary solvent system with no polymer is written in terms of its susceptibility. Adding a polymer coil modifies the free energy through monomer interactions and shifts the critical point of the system by dilution effects. The authors also investigated whether the condition $\tilde{\upsilon}=0$ for collapse is too restrictive. This condition holds when the terms comprising the effective excluded volume are small. When the solvents are very good, the first term, *v*, in Equation 21 is large. The attractive interaction though, is still small and is only relevant because of its very long range. This situation can be considered by again looking at the entire polymer coil. Consider a sphere of size ξ containing g monomers. Inside of the sphere, the excluded volume effects are strong and the chain inside the subunit is swollen. The interactions between the different subunits can then be treated as attractive hard spheres. They exhibit an attraction due to the monomers inside the sphere, but when they overlap the excluded volume effects dominate and repel each other. The effective excluded volume between the subunits can be calculated to scale as:

$$V \approx \xi^3 - \xi^3 e^{\frac{g^2 e^2}{kT\xi}} \tag{23}$$

Carrying out an analysis for the correlation length at collapse in the case of a mixture of good solvents similar to Equation 22 yields:

$$\xi \approx \left(\frac{kTa}{4\pi e^2} \right)^{\frac{3}{7}} \tag{24}$$

As can be seen from Equation 24, the onset of collapse in good solvents is proportional to $e^{-6/7}$ versus e^{-1} for the more general case. This difference is small and difficult to observe experimentally.

A later treatment of this problem using renormalization group (RG) theory was carried out by Stapper and Vilgis.[44] Due to the complexity of the problem, the authors studied the case of a polymer without preferential adsorption. The authors solved the RG equation for a bicritical field to calculate the end to end distance of the polymer. This distance was found to depend upon a new critical exponent, υ_B, which is smaller than the classical self-avoiding walk exponent, υ.[44]

$$\left\langle R^2 \right\rangle = D(u) b^2 N^{2\upsilon_B} \tag{25}$$

In Equation 25, D(u) is a system dependent constant, b is the Kuhn length (a stiffness of the polymer chain), and N is the degree of polymerization. The smaller value of υ_B indicates that the polymer will have a smaller end-to-end distance in the mixture of solvents than in either of the solvents alone. This work provided one of the first attempts at using RG theory to consider the behavior of a polymer in a binary solvent, but neglected to incorporate preferential adsorption in the theory due to the complexity, and did not carry the analysis further in order to calculate the temperature dependence of the chain size.

Experiment and Simulation

Simulational verification of the theories for a polymer in a binary solvent has been sparse.[45-47] One of the first attempts was a Monte Carlo simulation by Magda *et al.*[42] The authors use a cubic lattice with the solvents modeled as an Ising fluid and with the polymer modeled as a relatively simple self-avoiding walk. The volume of the solvent molecules and monomers are considered equal, and each lattice site interacts only with its six nearest neighbors. This model does, however, take into account preferential adsorption. The simulation consisted of either polymer moves or solvent moves and to minimize computational cost, the move selection was biased to achieve a ratio of polymer moves to solvent moves equal to 0.3. An advantage of computer simulations is the ability to control the interactions of the system; the authors studied three systems: unfavorable solvent-solvent interactions with no preferential affinity, zero solvent-solvent interactions with preferential affinity, and unfavorable solvent-solvent interactions with preferential affinity.

Case I: Unfavorable solvent-solvent interactions with no preferential affinity.

The simulation for this case was carried out at N=40 and a ratio of solvent-solvent interaction parameter to solvent-polymer interaction parameter equal to 3. Qualitatively, SLA theory gave the best agreement with the simulation, but consistently overestimated R_g while SF theory underestimated R_g for high and low values of Φ_A, at Φ_A equal to 0.5, however, the theories converge and predict the same value for R_g.

Case II: Zero solvent-solvent interactions with preferential affinity.

The authors considered equimolar systems of two good solvents and a combination of good and poor solvents. Since all of these systems had zero solvent-solvent interactions, the system did not have a consolute point. In order to quantify the effect of preferential adsorption, and effective interaction parameter, χ^{EFF} was defined as the interaction parameter for a pure solvent that would result in the same value for R_g. In this case SF theory gave qualitative agreement with the simulation results; however, SF predicts a χ^{EFF} value of 2.9, while the simulation gave a value of 0.43 for N=40. Increasing the degree of polymerization to 100 increased χ^{EFF} to 0.53, this may indicate an agreement with SF theory as $N\rightarrow\infty$. Due to computational limitations, this was not explored further by the authors.

In a mixture of two good solvents, the behavior of two solvents was contrasted. Solvent 1 did not exhibit preferential affinity and solvent 2 exhibited preferential affinity. In solvent 1, R_g was seen to monotonically increase as the polymer-solvent interaction parameter (χ_{AP}) becomes more negative. In contrast, solvent 2 shows a maximum and then decreasing R_g as χ_{AP} becomes more negative. SF theory predicts a maximum value of R_g for $\chi_{AP} \sim 6$, while the simulation finds a maximum for $\chi_{AP} = 4$. The authors found that R_g is smaller than in either of the pure solvents at the same temperature when $\chi_{AP} \leq -12$.

Case III: Preferential affinity with unfavorable solvent-solvent interactions.

A system consisting of a polymer chain exhibiting preferential affinity in a mixture of two unfavorably interacting solvents was studied along with a polymer not exhibiting preferential affinity. The polymer that did not have a preferential affinity for a solvent was found to have a relatively constant R_g as the critical point was

approached, showing only a modest decrease. The polymer with preferential affinity, however, showed a dramatic decrease in R_g as the critical point was approached and then an expansion as the system comes closer. R_g exhibited a minimum when the reduced temperature ($\varepsilon = T/T_c-1$) is 0.1. When ε becomes smaller than 0.1, R_g begins to expand, this behavior is in qualitative agreement with the BG theory. Because the simulation was carried out with relatively small polymer chains, ($40 \leq N \leq 100$) the quantitative value of the simulation is limited since Case II showed finite chain effects.

Several authors have used light scattering experiments to observe the behavior of a polymer in a binary critical solution near its consolute point.[45,47] To and Choi used dynamic light scattering to measure the hydrodynamic radius of the polymer as T_c was approached. Morita *et al.* used fluorescently labeled poly(N-isopropylacrylamide) to obtain R_g as the critical point was approached. To *et al*. saw a decrease in R_h from 106 nm at $T_c-T=9.45$ to 5 nm when $T_c-T<0.3$. The quantitative values of R_h measured using light scattering for $\Delta T<0.3$ are complicated since the scattering in this regime is dominated by critical fluctuations in the solvent. The authors used supplementary viscosity measurements to observe a decrease in viscosity as T_c is approached, demonstrating that R_g is indeed shrinking, but the expected re-expansion was not seen. Morita related the fluorescent emission of the labeled polymer, Q_{intr}, to the radius of gyration as $R_g \sim Q_{intr}^{1/3}$. When $\varepsilon<0.03$, R_g was seen to decrease by 55%. Both of these experiments showed excellent agreement with BG theory.

An example of the complexity of ternary systems of polymers in binary solvents is exemplified by the work of To *et al.*[46] A light scattering study of the behavior of high molecular weight PEO in a critical binary solvent consisting of nitroethane (NE) and 3-methyl-pentane (MP) was carried out by To *et al.* in 1998. The authors found a sharp increase in scattering intensity as the critical composition of the solvent was approached, even though the system was far away from the critical temperature (15 K). Samples of varying solvent concentration with a PEO (M_w = $9*10^5$) concentration of 0.075 mg/cc were studied at constant temperature. The scattering of the system with PEO was found to be the same within the experimental uncertainty as the system without PEO when the volume fraction of MP was less than 0.58. Increasing the volume fraction of MP above 0.58, however, resulted in a two orders of magnitude increase in the scattering intensity. The system was then observed for three days to ensure that precipitation was not occurring. When the volume fraction of MP was increased to above 0.7, the system precipitated and the scattering intensity began decreasing sharply within a day. To check whether this behavior was an artifact of phase separation, the authors conducted the same experiment with different PEO concentrations (0.01 and 0.1 mg/cc) and other molecular weights of PEO (M_w=$4*10^6$ and $5*10^6$) and found the same behavior over the same concentration ranges, indicating that this is not an effect related to phase separation. Moving away from the polymer molecule, the solvent composition will smoothly shift to the bulk concentration. When the bulk solvent composition is greater than φ_c, the solvent composition will always have a composition equal to φ_c at some radial distance. This layer of critical composition solvent could be the cause of

the scattering, since R_g and R_h of the scatterers were larger than that measured for the PEO in water at the same temperature. This explanation seems lacking due to the fact that the solvents were chosen because their refractive indices where 1.38 and 1.39. This should minimize the dn/dc effect of a wetting layer around the polymer molecule. The effect is also observed below φ_c which makes it impossible for a wetting layer of critical composition to be formed around the polymer molecule.

The authors proposed a more reasonable explanation that this behavior may be a wetting layer inversion, which occurs at φ=0.58. Below this concentration the polymer is surrounded by the good solvent (NE), but above 0.58 the polymer is preferentially adsorbed by the poor solvent (MP). This inversion will change the refractive index around the polymer and cause the polymer molecules to aggregate in order to minimize solvent contact. This would account for the large scatterers observed in the system. This is also borne out by the fact that above φ = 0.7 the PEO becomes insoluble and precipitates out.

Chapter 3: Experimental Methods

Materials

Eight molecular weights of poly(ethylene oxide) were studied, in order to cover several orders of magnitude of molecular weight.

Polymer 2kH

The lowest molecular weight studied was Sample # PEG2OH-2K, purchased from Polymer Source Incorporated, Dorval, Canada, with M_n = 2000 and M_w = 2200 to give a PI of 1.10.The sample was characterized by Polymer Source using a Varian liquid chromatograph with UV and RI detectors and Supelco columns. This polymer was terminated, like Polymer 20k, by hydroxy groups.

Polymer 4k

Sample # PEG20CH3-2K, was purchased from Polymer Source Incorporated, Dorval, Canada, and had a listed molecular weight of M_n = 2000 with a polydispersity (PI) of 1.10. Analysis of the polymer by SEC was carried out by Niamke[48] on a Waters GPC system with four columns, Ultrastyragel 500 Å, HR3, HR4, and Shodex K-806M using tetrahydrofuran (THF) at 40^o C as the eluent at 1 mL/min. Niamke found a M_n of 4080 and M_w of 4530 giving a PI=1.11. This polymer was terminated with two methoxy groups as shown below.

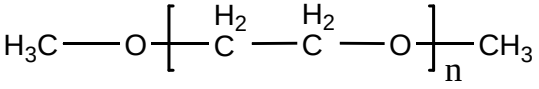

Polymer 10kH

Polymer 10kH was purchased from Polymer Source Incorporated, Dorval, Canada, Sample # PEG2OH-10k. Polymer Source characterized the polymer using the instrument described above for Polymer 2kH. The polymer had a reported M_n = 10500 and M_w = 11300, giving a PI of 1.08, and was hydroxyl terminated.

Polymer 10kM

Polymer 10kM was also purchased from Polymer Source Incorporated, Sample # P2963-2OCH3. The analysis from Polymer Source, using the same conditions as for Polymer 2kH and Polymer 10kH, listed M_n = 12000 and M_w = 13000, giving a PI of 1.08. This polymer was methoxy terminated.

Polymer 20k

The next polymer studied was purchased from Fluka Chemicals, Lot # 425182/1, and had a listed nominal molecular weight of 20,000. The PEO was analyzed by Shresth[49] using a Waters 2000 Chromatograph system with Waters Styragel HR1, HR2, HR3, and HR4 columns with a THF eluent at 1 mL/min. The SEC analysis gave an M_n of 18,900 and M_w of 25,700 for a PI=1.4. Unlike Polymer 2k, this polymer was hydroxyl terminated.

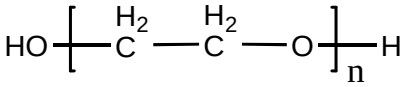

Polymer 200k

Polymer 200k was purchased from Sigma-Aldrich, Product # 181994, Batch # 06725JO. This polymer, like Polymer 20k, was hydroxy terminated and the manufacturer reported a viscosity average molecular weight (M_v) of 200,000. The polymer was analyzed using a Waters GPC with two Polymer Lab Mixed Bed columns with THF at 1 mL/min and showed a broad, single polydisperse species with M_n = 107,000 and M_w = 267,000 to give a PI of 2.5

Unlike the other samples, this polymer was packaged with 200-500 ppm of butylated hydroxytoluene (BHT), shown below, as an inhibitor.

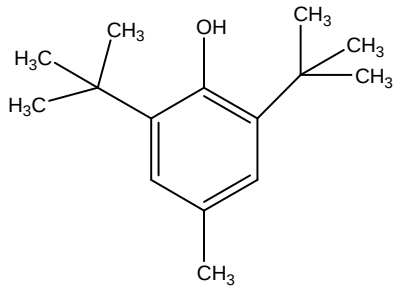

When this polymer was dissolved in the IBA a fine white material was dispersed throughout the solution, which was believed to be BHT. The BHT was removed from the polymer sample by using a binary solvent extraction with acetone and methanol. This worked to dramatically decrease the visible BHT, but it was still present to some extent. This combined with the large PI led us to judge this polymer unsuitable for quantitative measurements.

Polymer 252k

The second highest molecular weight polymer studied was purchased from Polymer Source Incorporated, Product # P3624-EOOCH$_3$. The company reported the M_n as 252,000 and a PI of 1.10. Analysis of the polymer using the same GPC used to analyze Polymer 200k gave M_n=232,000 and M_w=292,000 for a PI = 1.26. Since the results are similar to the manufacturer's values, the Polymer Source values will be used for data analysis, due to the sensitivity of the instrument to the user-provided polymer concentration. The termination of this polymer is shown below.

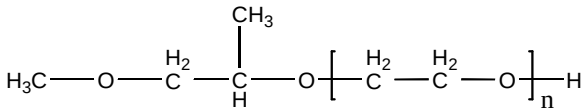

Polymer 337k

The highest molecular weight polymer studied was also purchased from Polymer Source Incorporated, Product # P1590-EO. The manufacturer's reported molecular weight of this polymer was M_n=337,000 and M_w=404,000 with a PI of 1.2. Like Polymer 4k, this polymer was methoxy terminated. This polymer was analyzed using the same equipment used to analyze Polymer 200k, and the analysis gave M_n=348,000 and M_w= 452,000 for a PI of 1.3. The fact that the values listed are again close to those given by the manufacturer, the numbers reported by the manufacturer will be used as the molecular weight during data analysis.

Solvents

Two types of solvents were used in this study, hydrogenated and deuterated. Since a number of solvent manufacturers were used, the specific solvents used for each study will be discussed with each specific experiment. The deuterated solvents showed a good contrast with the hydrogenated polymer as can be seen from the scattering length densities shown below:

Table 2. Scattering length densities of the deuterated solvents and hydrogenated polymer.

Compound	**Scattering Length Density ($Å^{-2}$)**
d-Isobutyric Acid	$5.5 * 10^{-6}$
Deuterium Oxide	$6.33 * 10^{-6}$
h-PEO	$6.4 * 10^{-7}$

Neutron Scattering

The scattering was carried out on the 30 meter instruments at the National Institute for Standards Center for Neutron Research (NCNR). The scattering was carried out with hydrogenated polymers and fully deuterated solvents in four separate runs.

Run 1

This run was carried out in January of 2003 on the NG-7 instrument and studied two molecular weight polymers in critical and off-critical solvent compositions. The off-critical compositions were chosen in an effort to maximize the scattering in the lower and upper phases respectively. The detector was set to a distance of 3 and 15 meters with a neutron wavelength of 8 Å, to cover a q range of 0.00354 to 0.3519 $Å^{-1}$. The solvent mixtures were made of D_2O Ultra-D with

99.999% deuterium enrichment, Lot # IG0056-2, purchased from Isotec, and deuterated isobutyric acid, Lot # A-1450, purchased from MSD Isotopes in 1978. Two polymers were studied in Run 1, Polymer 20k and Polymer 337k. The sample scattering was measured at three set-point temperatures, 43, 45, and 49 ^{o}C; the actual temperatures were 41, 43, and 47 ^{o}C because the actual sample block temperature, as measured by a thermocouple in the sample block, is 2^{o} lower than the set point of the water bath. The sample compositions are listed in the table below:

Table 3. Sample compositions for SANS Run 1.

Sample Name	Polymer	Polymer Mass (g)	Polymer Concentration (mg/mL)	Mass Fraction IBA
C1	20k	0.0031	11	0.39
C2	337k	0.0031	11	0.39
<C1	20k	0.0037	13	0.30
<C2	337k	0.0029	10	0.30
>C1	20k	0.0038	13	0.46
>C2	337k	0.0030	10	0.46

The samples were made in quartz banjo cells from Hellma Worldwide, with a pathlength of 1 mm and a volume of 0.28 mL to give an approximate polymer concentration of 10 mg/mL. The mixed solvents used for this set of experiments were mixed on the bench top. The solutions were then heated to one phase and transferred to the cells, which contained the pre-measured polymer. The cells were then warmed using an IR lamp and shaken to dissolve the polymer. The scattering data are shown in Figures 5-10, grouped by solvent composition and polymer sample and shown at three temperatures.

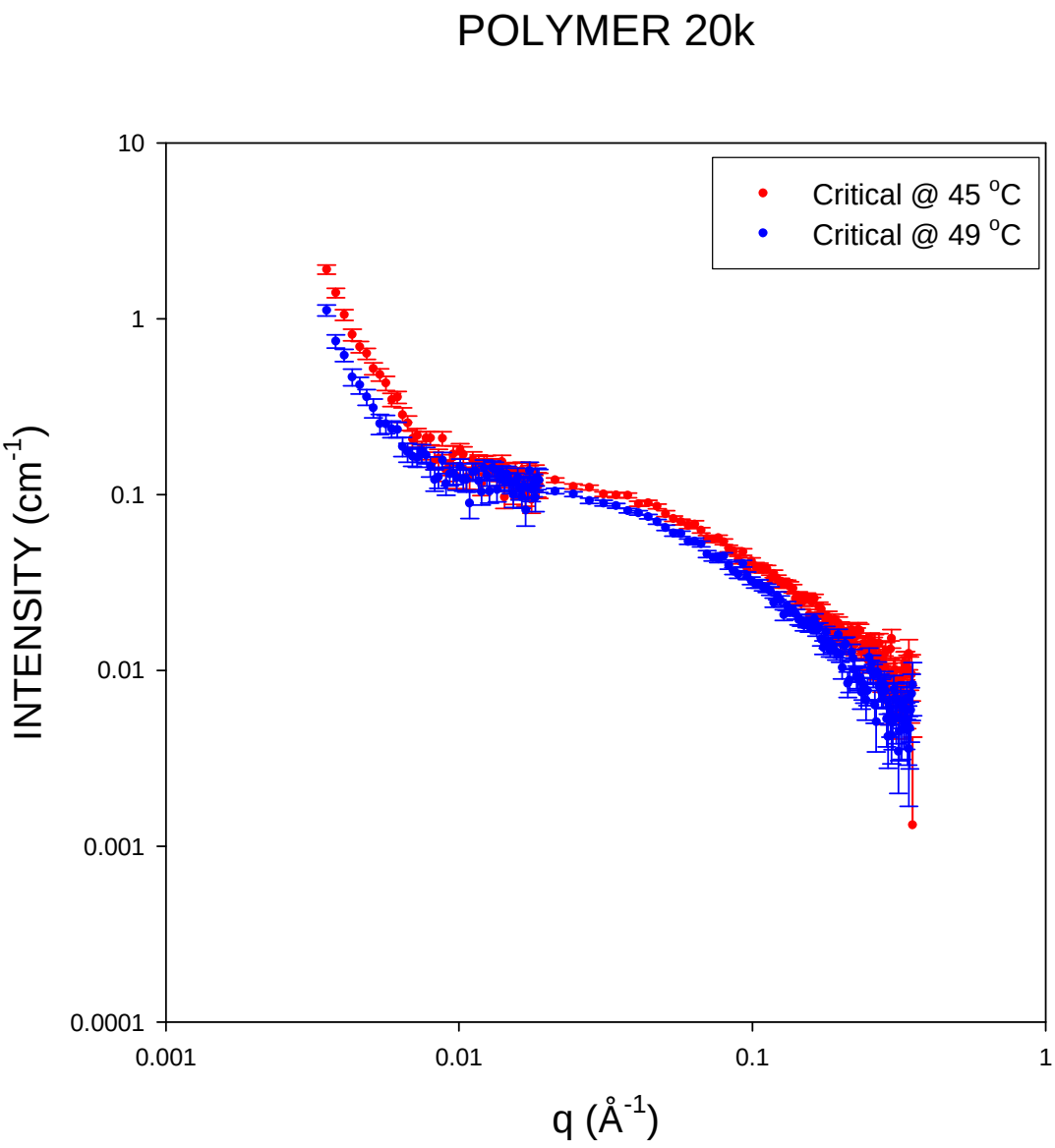

Figure 5. Polymer 20k in a critical solution with x_m = 0.39 isobutyric acid at two temperatures.

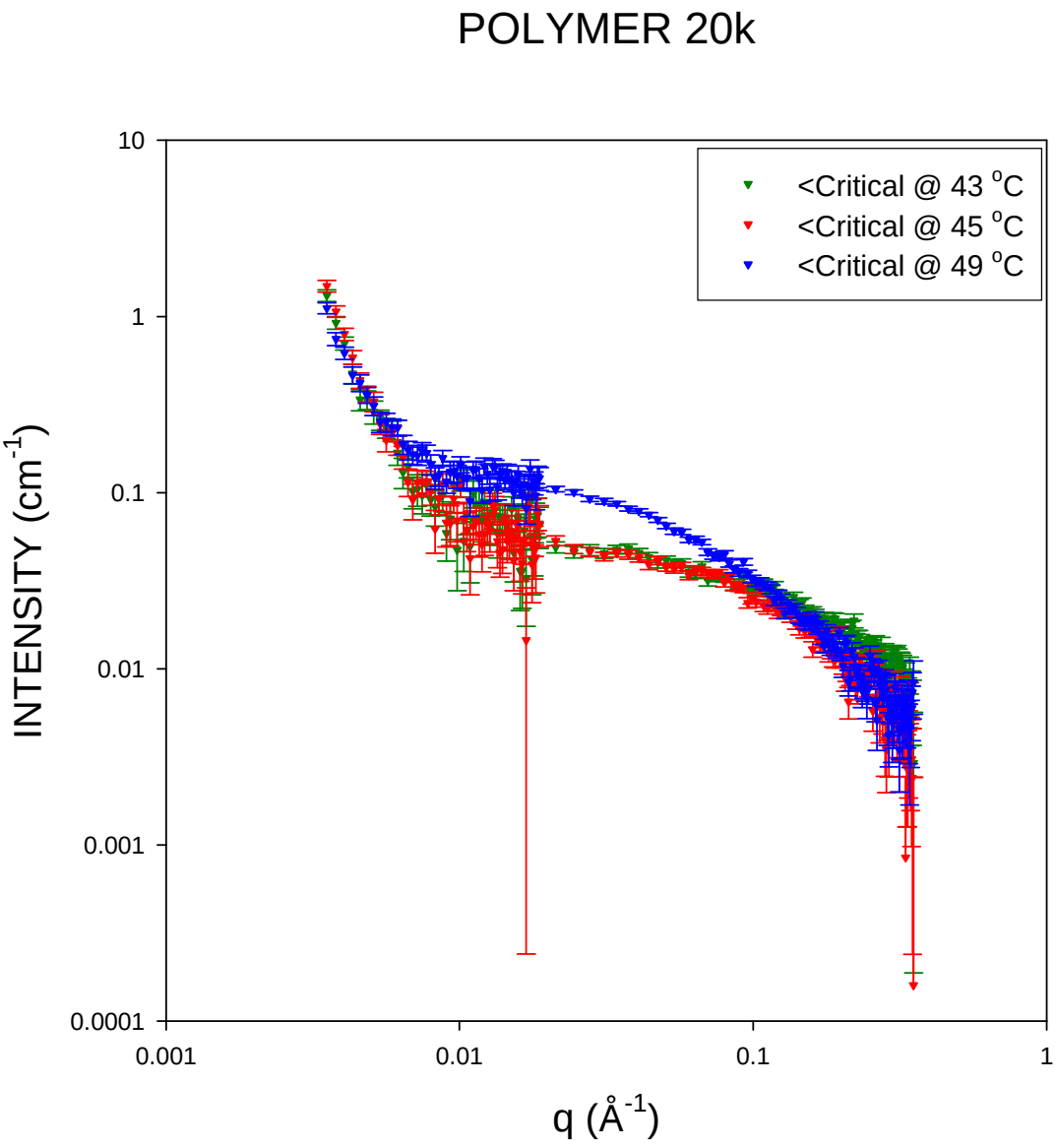

Figure 6. Polymer 20k in a solution with x_m = 0.30 at three temperatures.

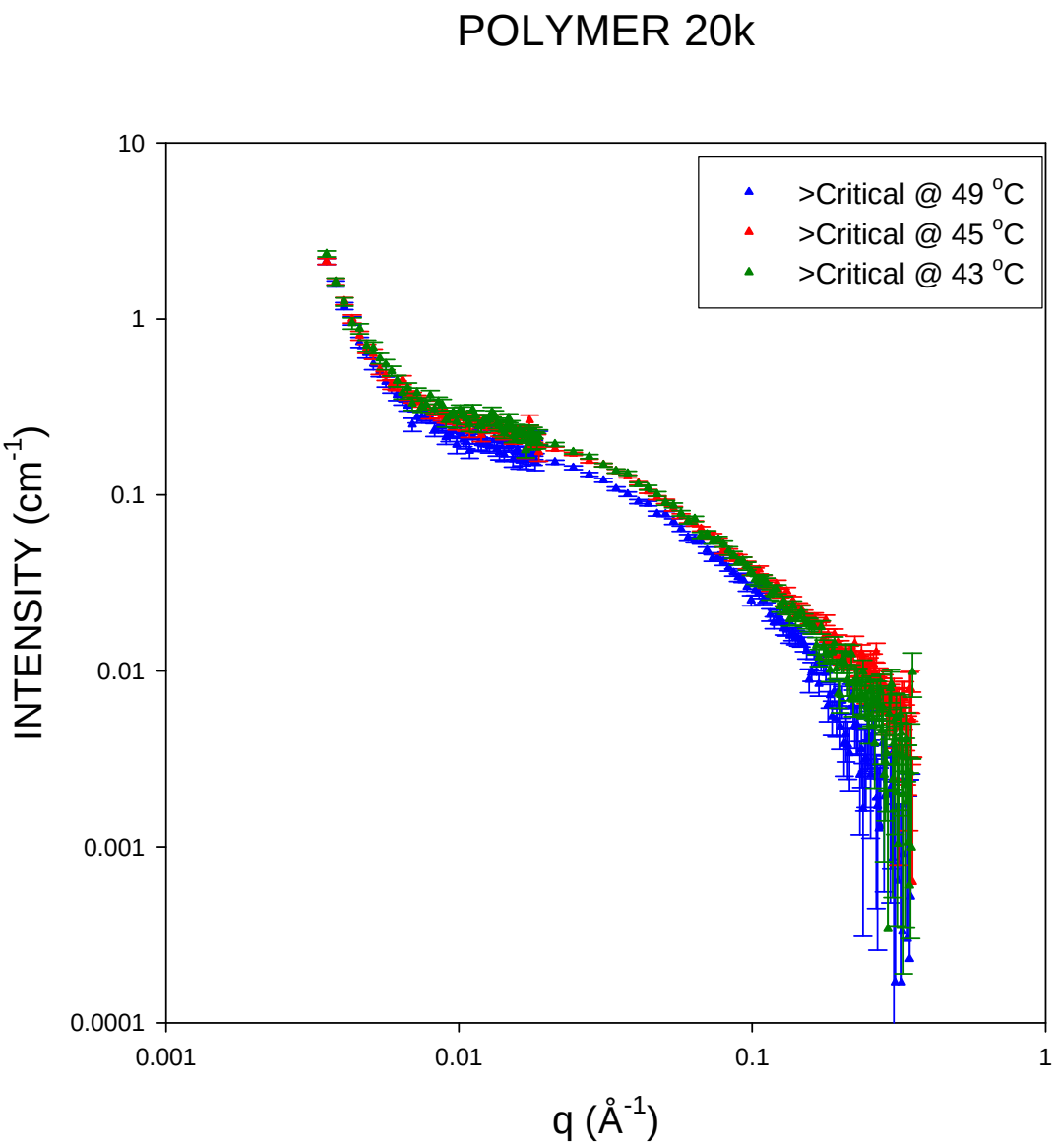

Figure 7. Polymer 20k in a solution with an isobutyric acid mass fraction of 0.46 at three temperatures.

Figure 5 shows Polymer 20k in a critical solution. There is no dramatic change between the run at 45 ^{o}C and 49 ^{o}C. Both curves also show an upturn in the low-q regime, which is indicative of large aggregations.[15,32] The slope of both curves in the intermediate q range was 1.0 for both samples for the q range of 0.0376-0.1781 Å^{-1}. In Figure 6, Polymer 20k in solution of less than critical composition of isobutyric acid, the aggregation upturn seen in Figure 5 is still present. At first glance there appears to be a dramatic effect of temperature between 49 ^{o}C and the two lower temperatures. However, the two lower temperatures show a relatively flat intermediate q regime, indicating a lack of free polymer chains. That is, most of the polymer exists in the large aggregates. In the sample of greater than critical composition (Figure 7), the aggregation features are seen and the slopes of the curves in the mid-q range are roughly equal, indicating little temperature effect.

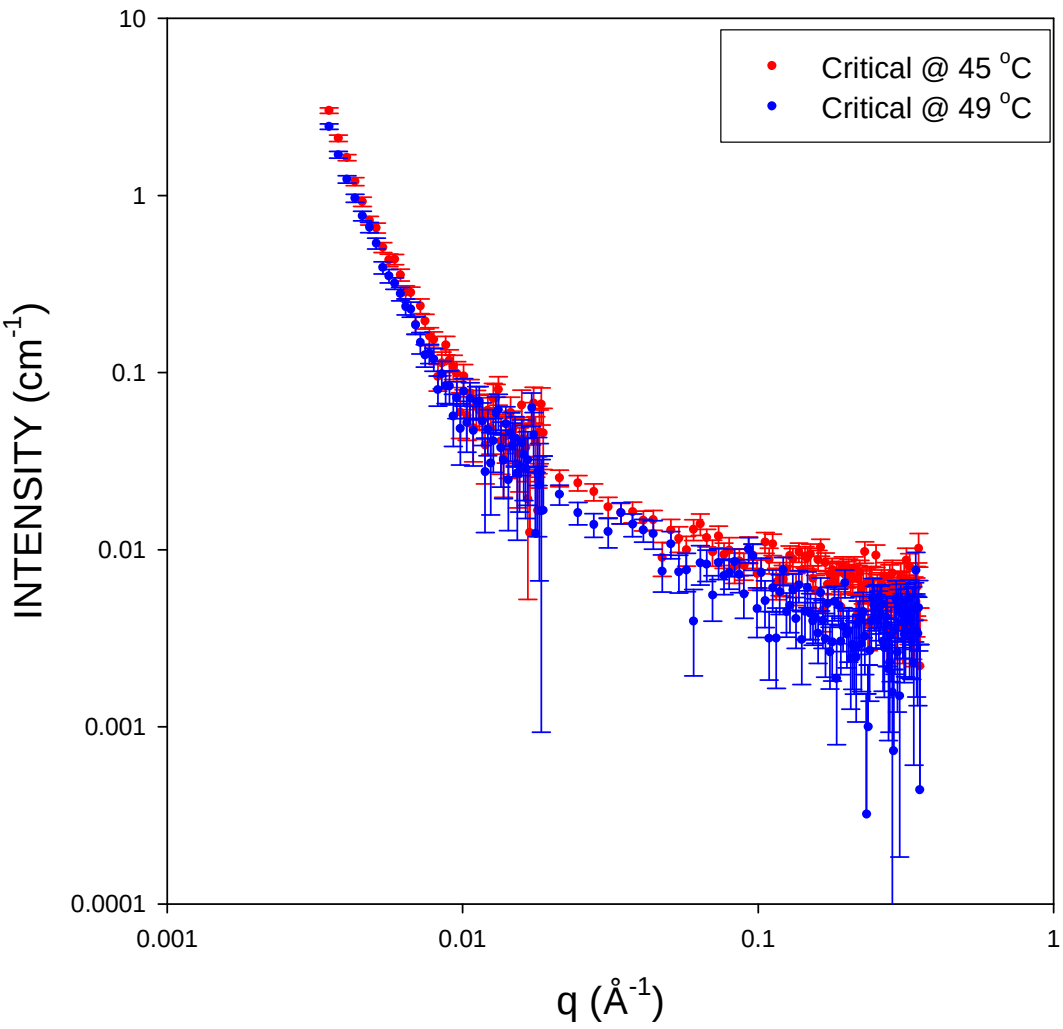

Figure 8. Polymer 337k in a solution with an isobutyric acid mass fraction = 0.39 at three temperatures

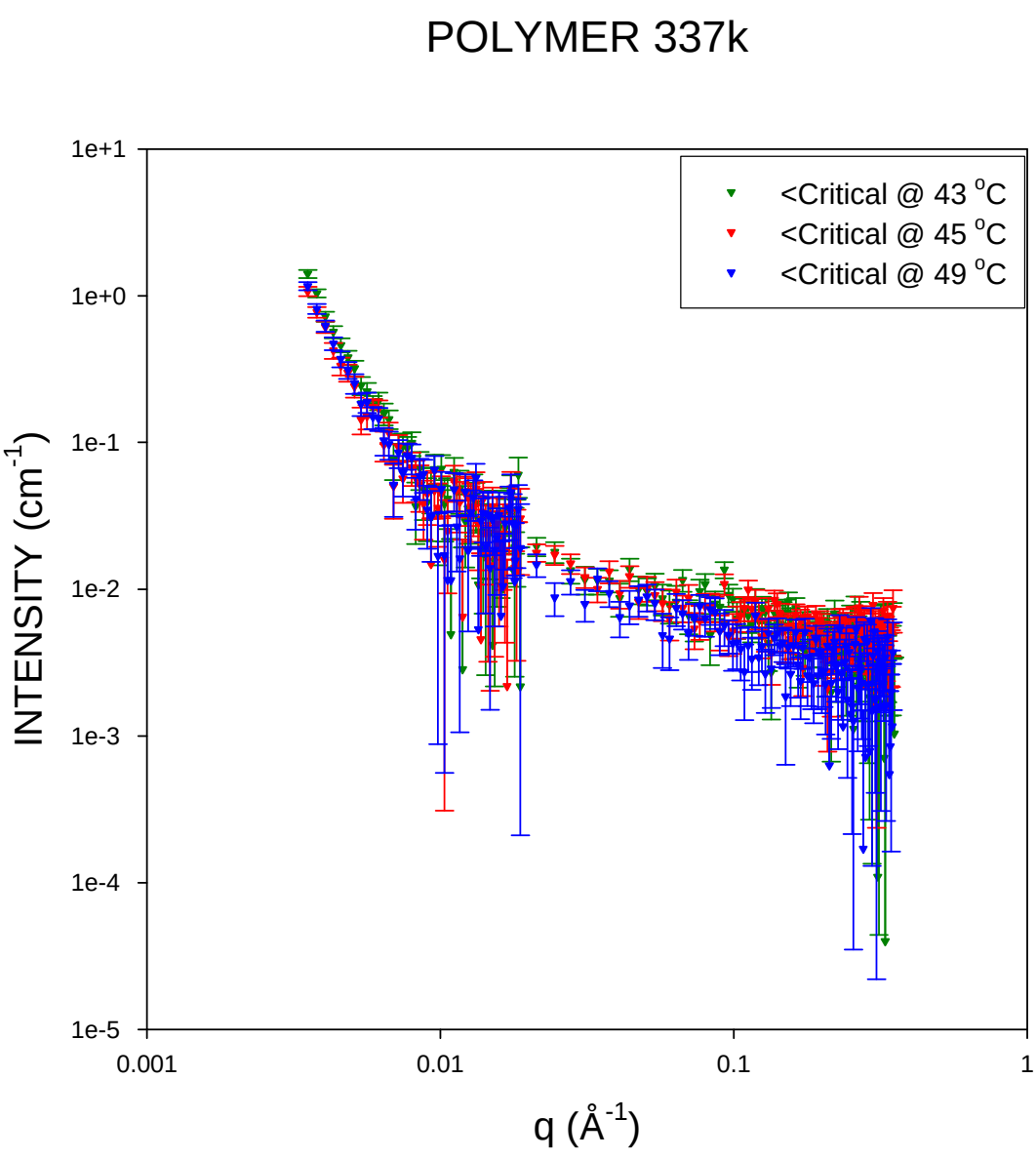

Figure 9. Polymer 337k in a solution with an isobutyric acid x_m = 0.30 at three temperatures.

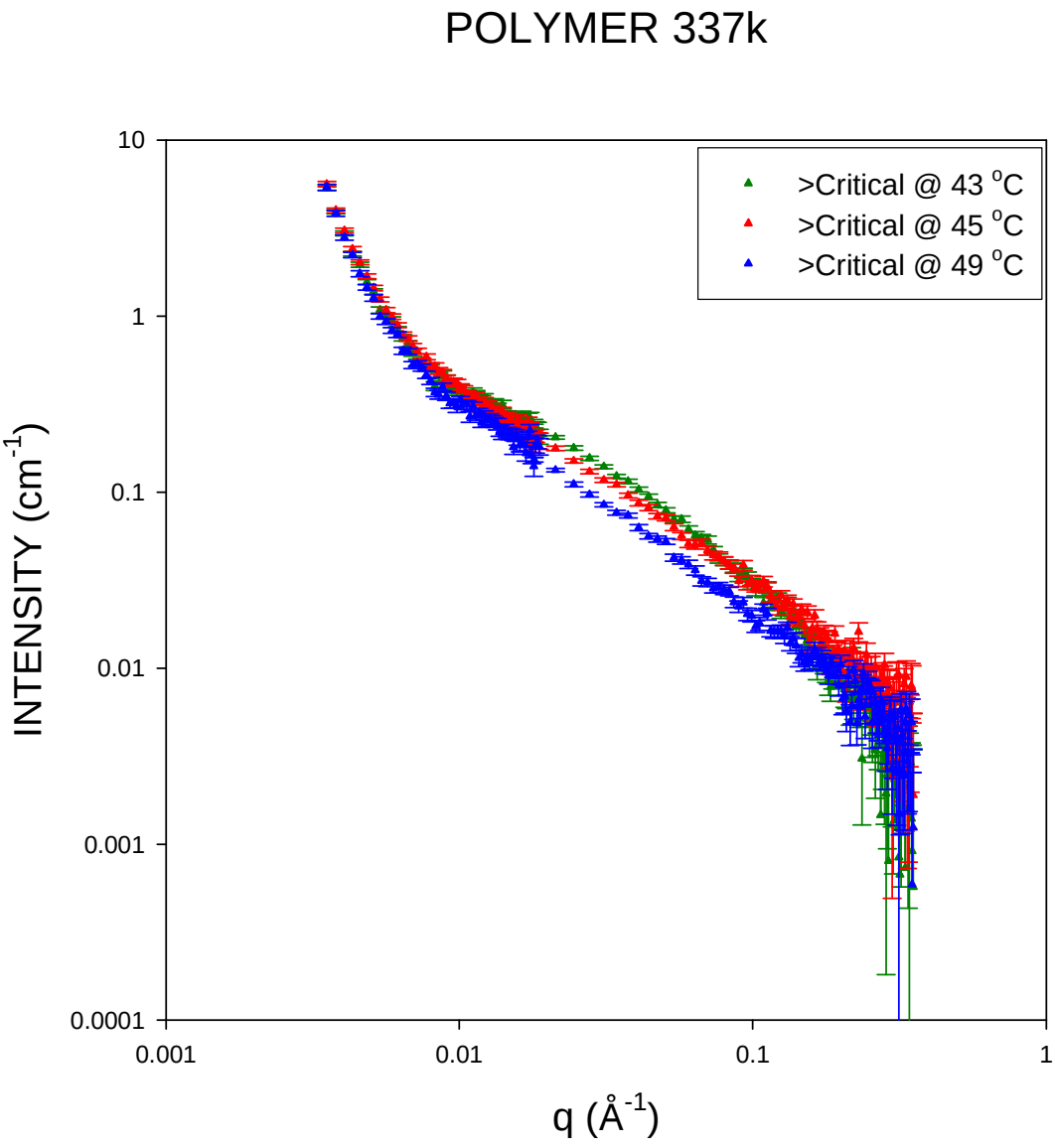

Figure 10. Polymer 337k in a solution at greater than critical composition of isobutyric acid (x_m=0.46) at three temperatures.

Figure 8 shows Polymer 337k in a critical solution. The curves show very strong aggregation and a relatively flat (slope <1.0) mid-q range, indicating most of the chains exist as aggregates. The Guinier regime is difficult to decipher in this run. Figure 9 has similar features to Figure 8 in that there are few free chains and strong aggregation peaks. Figure 10, like Figures 8 and 9, shows aggregation but has free chains for analysis. There does not appear to be a strong temperature dependence for this set of samples either.

Run 1 had numerous problems. Several of the samples were found to have leaked and the isotopic enrichment of the isobutyric acid was suspect due to the age of the solvent (~25 years). In addition, the concentration of Polymer 337k was above the calculated overlap concentration, c^*, when a different relation for the R_g of PEO in water[17] was discovered after Runs 1-3 and compared to the first relation used.[14] Both relations and the effect of polymer shape upon c^* will be discussed in the Analysis section. All of the samples were analyzed for R_g values using Guinier fits, which are discussed in the Results section.

Run 2 and 2a

The second round of neutron scattering was carried out in June 2003 on the NG-3 instrument. This experiment had several improvements over Run 1. Since in Run 1 there seemed to be more of a solvent effect than a temperature effect, the samples in Run 2 were chosen so as to cover a wider range of solvent compositions and temperatures with the same two polymers. Two samples were also made using deuterated acetic acid to investigate a possible pH effect, and were run two weeks after the IBA samples when some beam time became free.

The cells in Run 2 were closed using Teflon plugs with an extra layer of Teflon tape, instead of the rubber sleeves used to seal the cells in Run 1 in order to prevent solvent leakage. The counting statistics for this run were improved by using 2 mm pathlength cells for the mixed solvent runs and by using NG-3, which has a slightly better flux than NG-7. In order to minimize solvent cost, 1 mm cells were used for the pure d-IBA. The solvents used in this run are listed in the following table.

Table 4. Solvents used in SANS Run 2.

Solvent	Manufacturer	Lot #	Deuterium Enrichment
Deuterated Isobutyric Acid	Isotec Custom Synthesis, 2003	CR0519	98%
Deuterium Oxide	Isotec	IG0056-2	99.999%
Deuterated Acetic Acid	Aldrich	1186-52	99.9%

The samples were mixed on the bench top in the same manner as that used to make the samples for Run 1. The samples were then stored in an oven set to 60^{o} for 6

hours while the instrument was set up. In this run, the mixed solvent and pure d-IBA samples were run at five set temperatures: 30, 40, 43, 45, and 55 ^{o}C. The acetic acid and D_2O runs were only carried out at three temperatures: 25, 43, 55,^{o}C and 30, 43, 55 ^{o}C respectively. The detector was set to 13 meters and 1.35 meters with 8 Å neutrons to cover a q range of 0.002568-0.32250 Å^{-1}. The sample compositions are listed below.

Table 5. Sample compositions for SANS Run 2.

Sample	Polymer	Polymer Mass (mg)	Polymer Concentration (mg/mL)	Mass Fraction d-IBA
A	20k	6.4	12	0.30
B	20k	6.1	11	0.39
C	20k	6.3	12	0.46
D	337k	6.3	12	0.30
E	337k	5.8	11	0.39
F	337k	6.4	12	0.46
G	20k	6.2	11	0.0 (Pure D_2O)
H	20k	3.6	12	1.0
I	337k	6.8	12	0.0 (Pure D_2O)
J	337k	3.1	11	1.0
1	20k	6.8	12	Pure d-Acetic Acid
2	20k	6.4	12	0.39 d-Acetic Acid

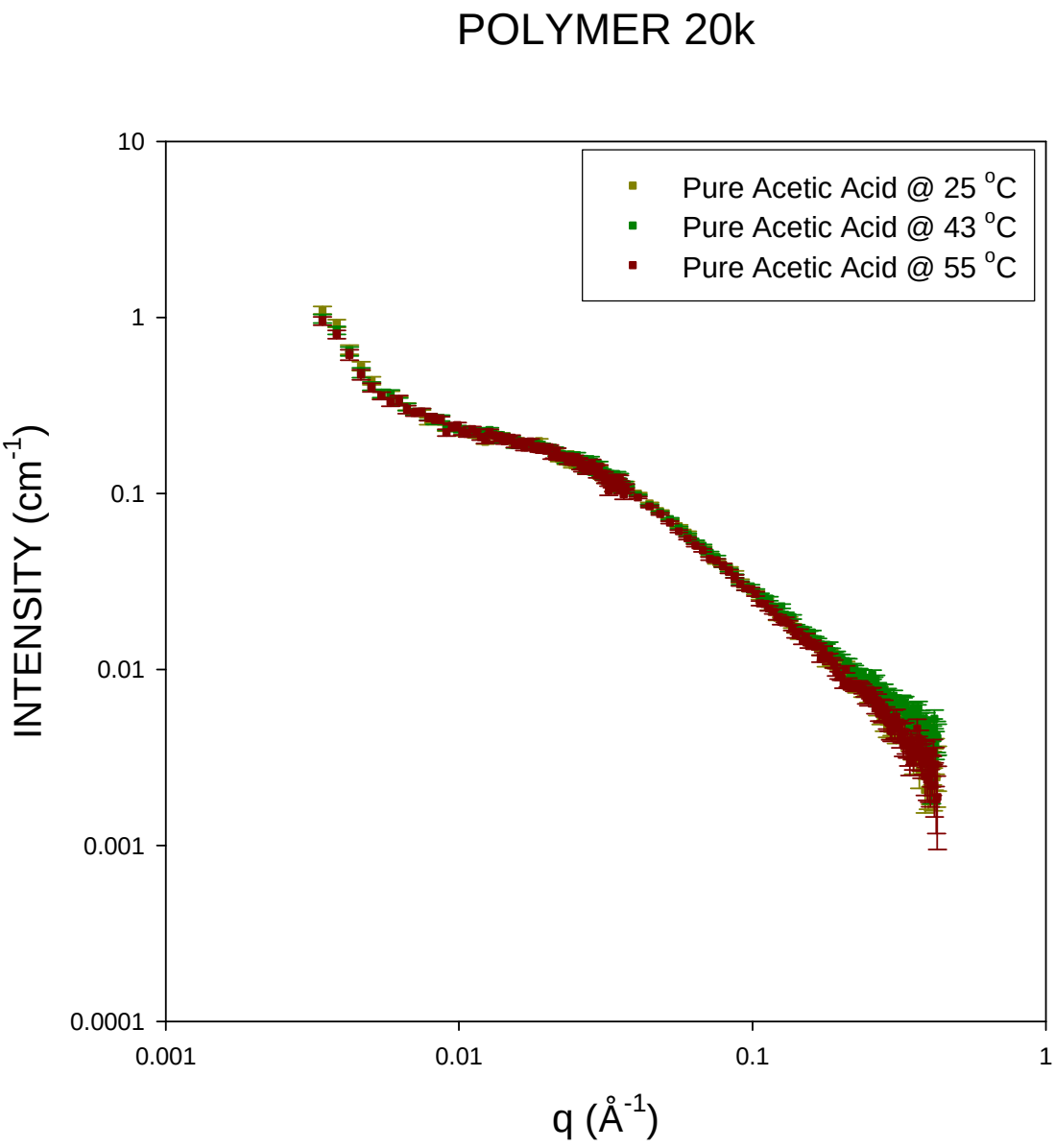

Figure 11. Neutron scattering data for Polymer 20k in pure deuterated acetic acid at three temperatures.

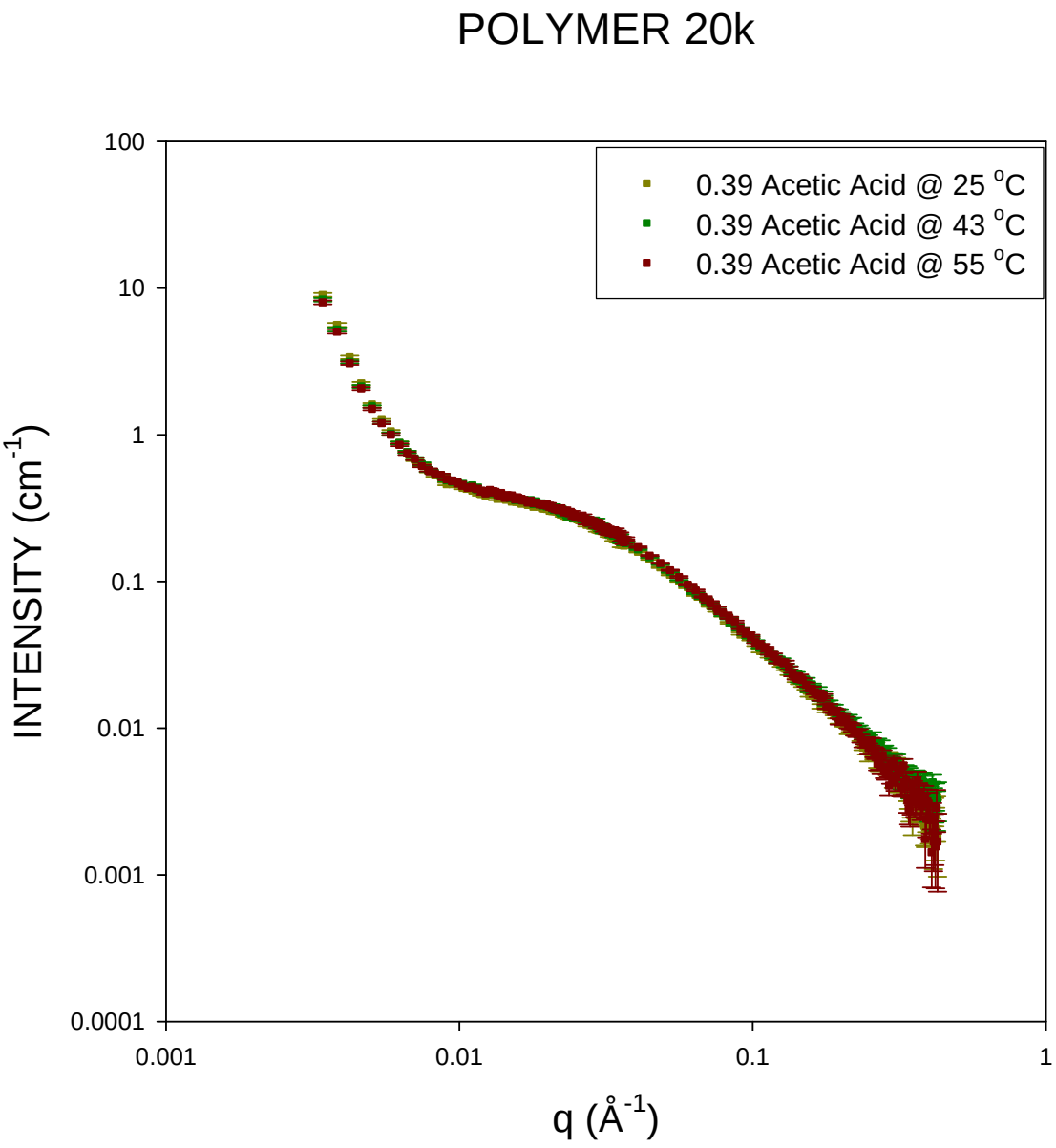

Figure 12. Neutron scattering data for Polymer 20k in a solution of D_2O and 0.39 IBA at three temperatures.

Figures 11 and 12 show Polymer 20k in pure and aqueous acetic acid solutions. Like the samples in Run 1, these samples showed an aggregation peak at low q and little temperature dependence for the conformation. These samples did, however, show free chains as evidenced by the mid-q slope less than -1, and do not show any signs of a Porod-like downturn, indicating a coil.

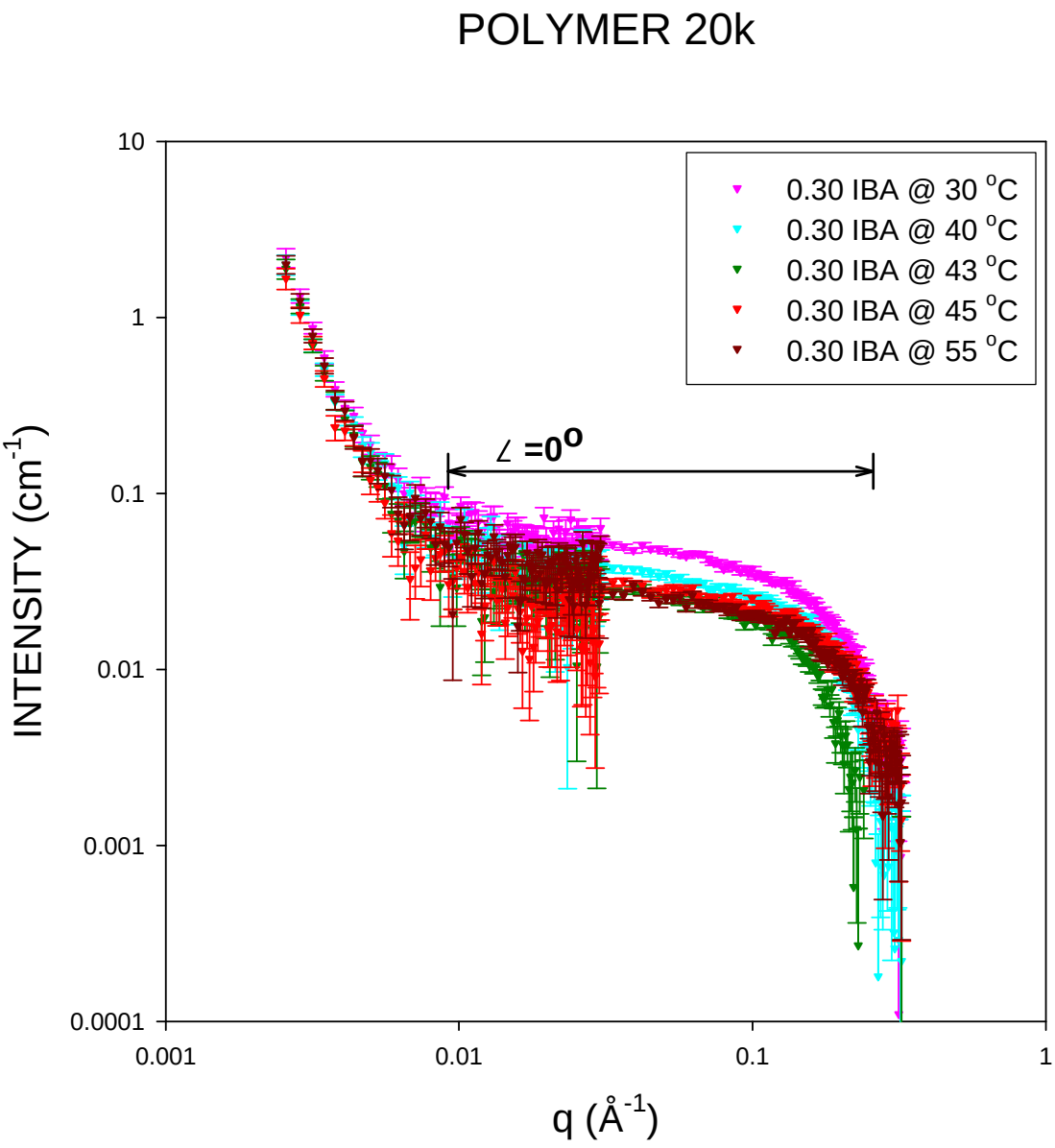

Figure 13. Polymer 20k in a solution with an IBA mass fraction of 0.30 at five temperatures, showing a very flat mid-q range.

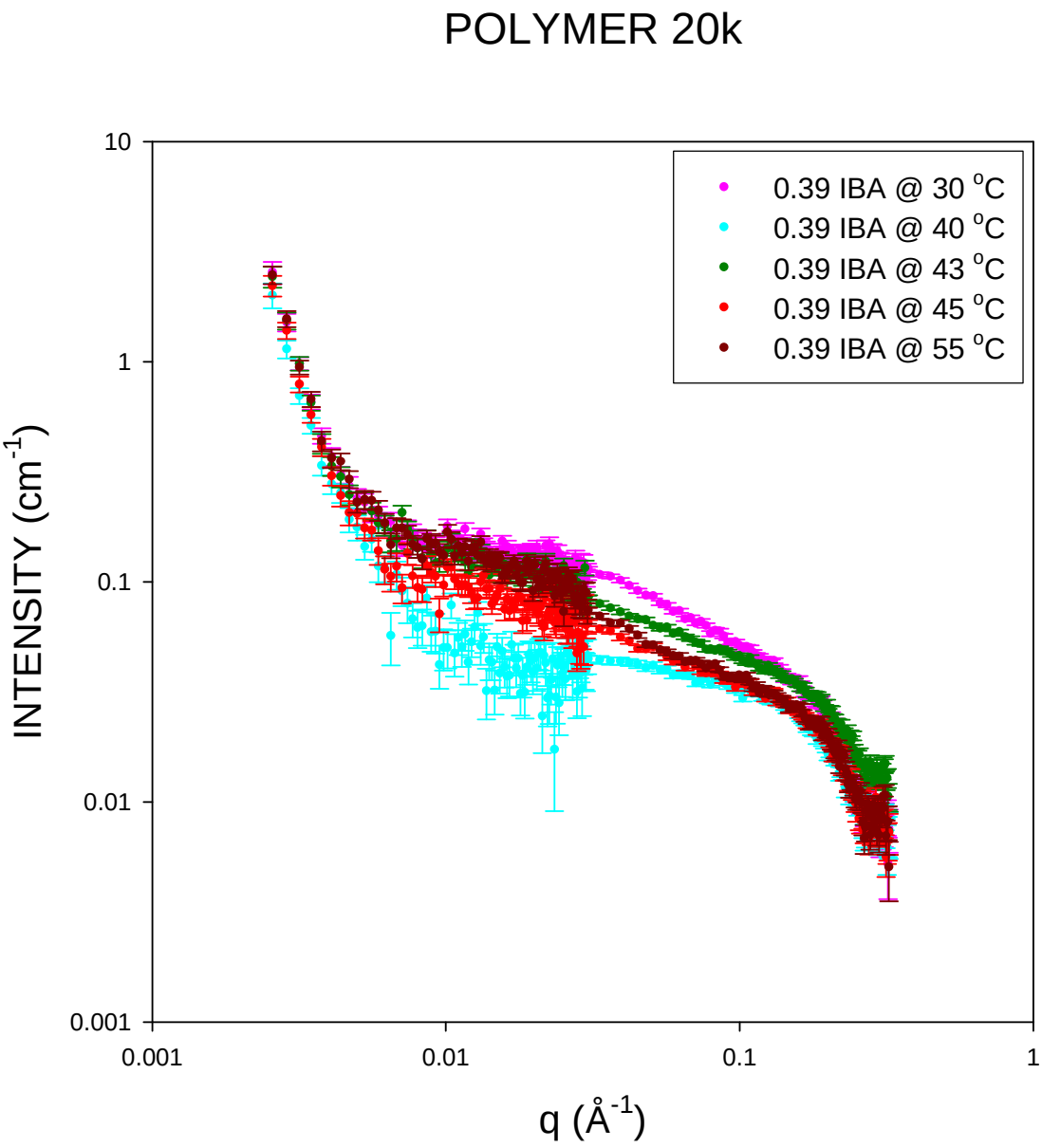

Figure 14. Polymer 20k in a solution with a critical mass fraction of isobutyric acid (x_m=0.39) at five temperatures.

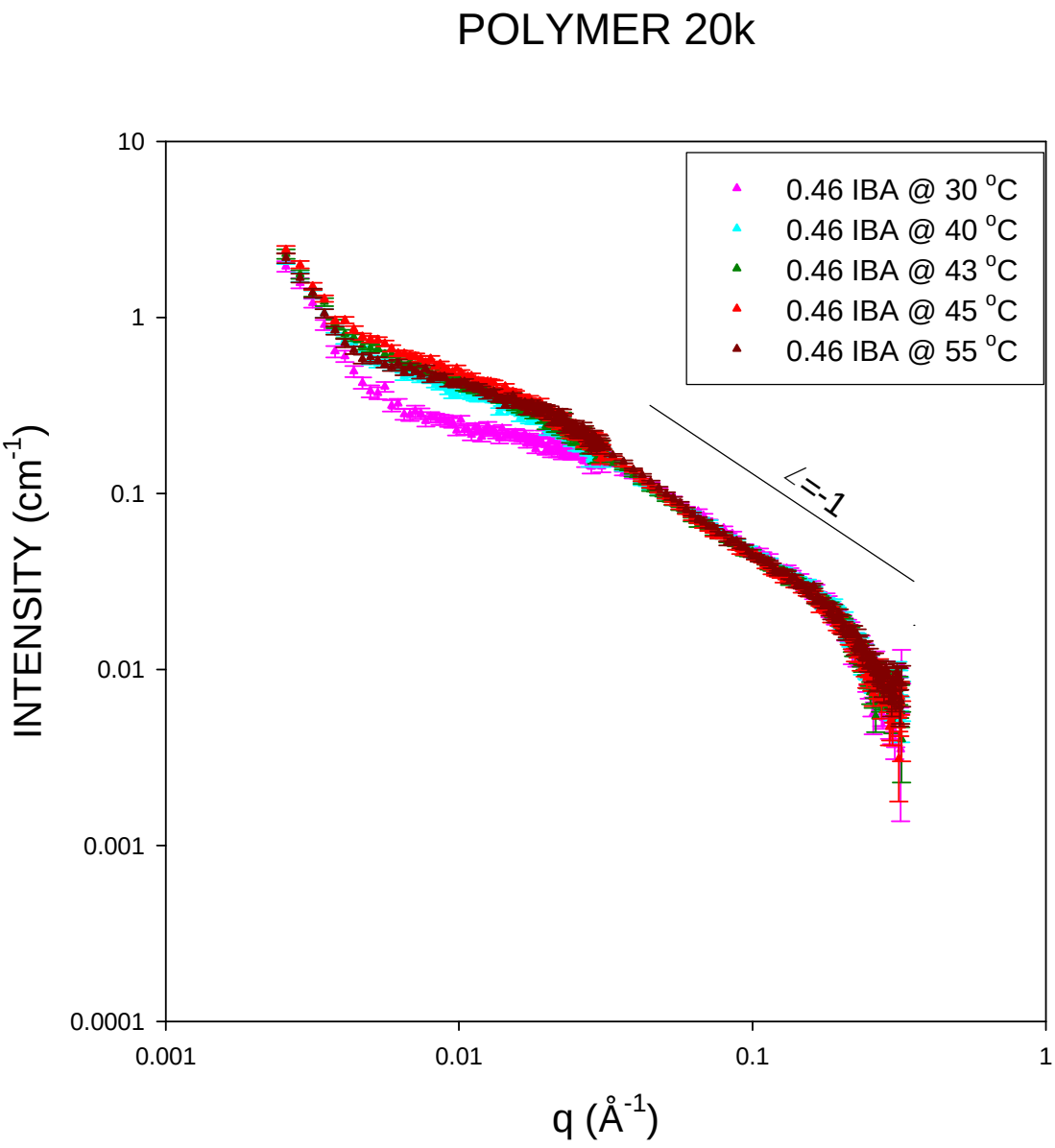

Figure 15. Polymer 20 in a solution with a mass fraction of IBA of 0.46 at five temperatures.

Figures 13 and 14, unfortunately both showed a relatively flat mid-q range, indicating a lack of free chains for observation. The slope in Figure 14 (~-0.8) was larger than that shown in Figure 13, which may show better PEO solubility in the higher IBA concentration solutions. Figure 15 showed an aggregation upturn, had a reasonable slope in the mid-q range, and showed the appearance of a Porod downturn (slope ~ -4) in the high q range.

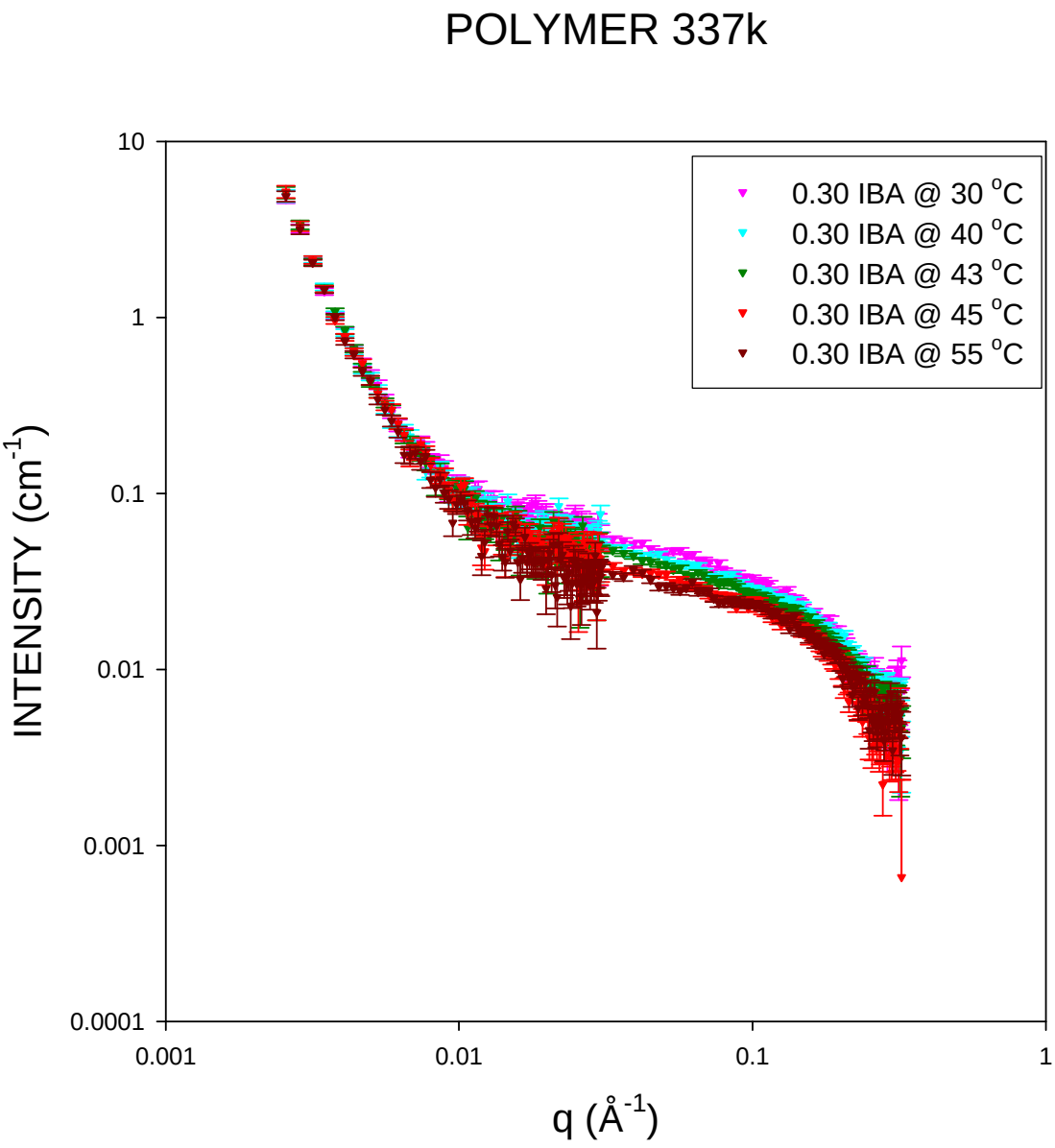

Figure 16. Polymer 337k in a solution with a 0.30 mass fraction of IBA at five temperatures.

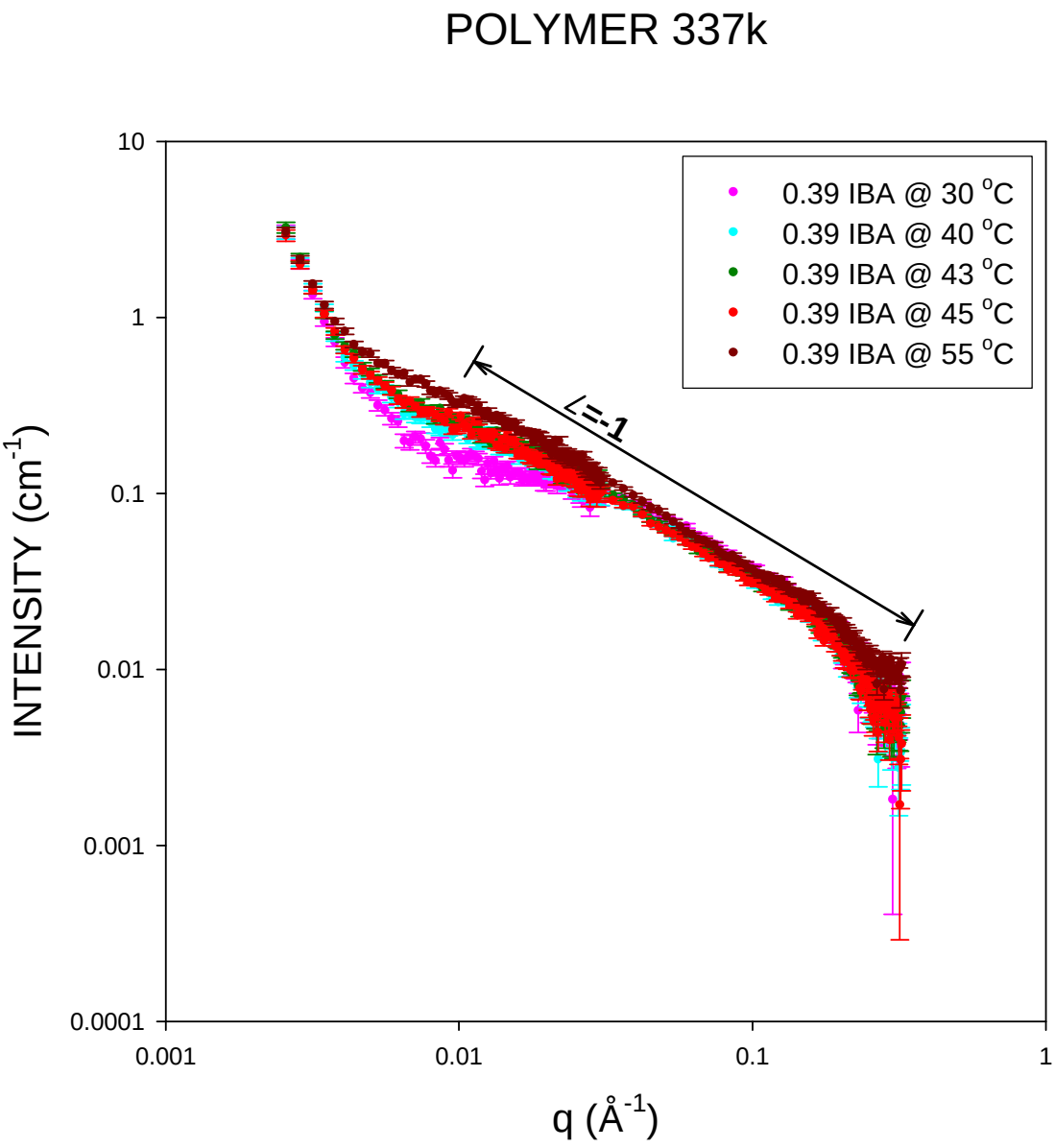

Figure 17. Polymer 337k in a critical solution of D_2O and d-IBA at five temperatures. Notice the mid-q range slope.

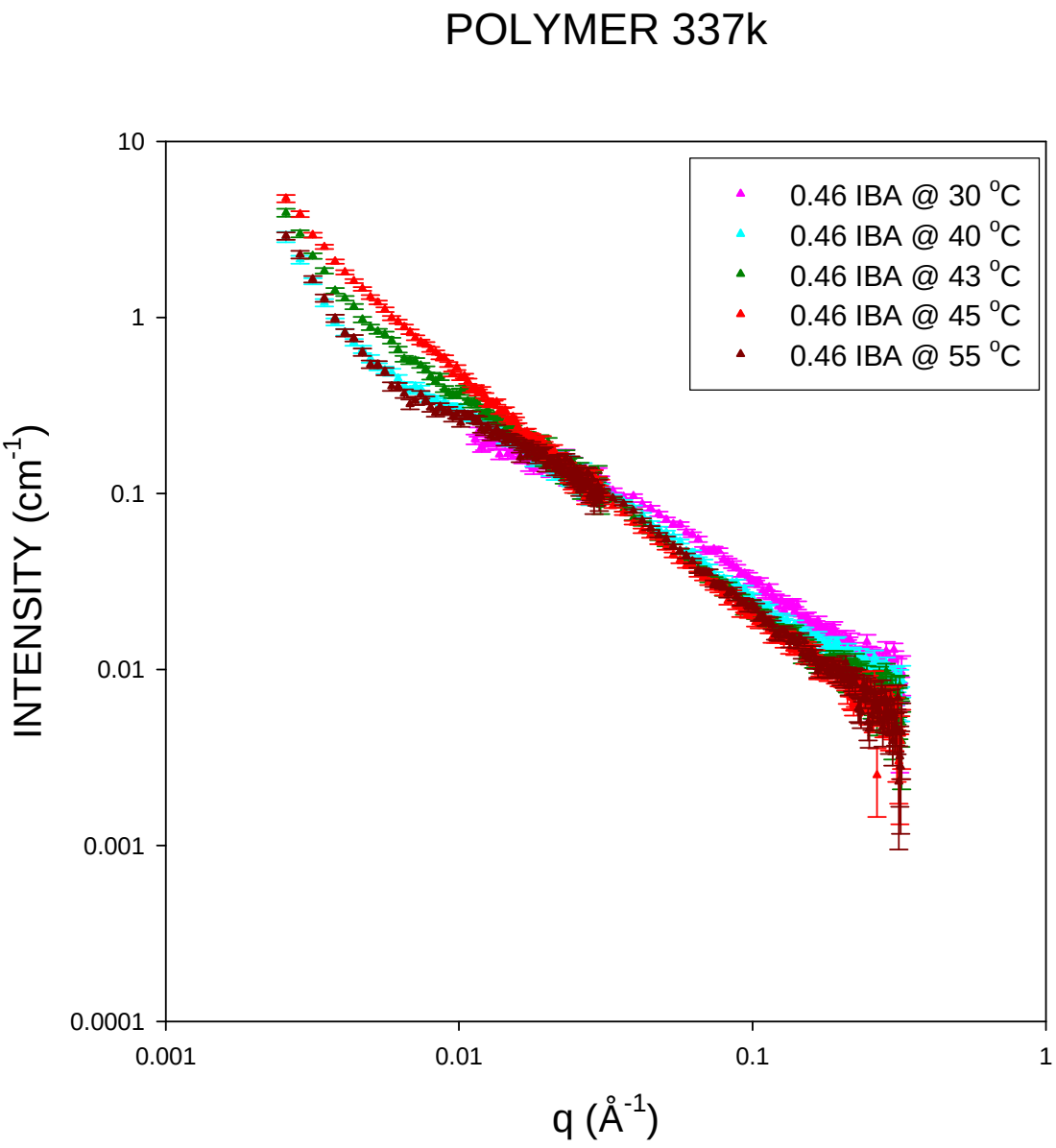

Figure 18. Polymer 337k in a solution with a mass fraction of d-IBA 0.46 at five temperatures.

As Figure 16 shows, the solution with the lowest concentration of IBA does not have many free chains and mostly aggregations, irrespective of temperature. Figures 17 and 18 have more free chains, but Figure 18 does not show the high-q downturn seen in Figure 17.

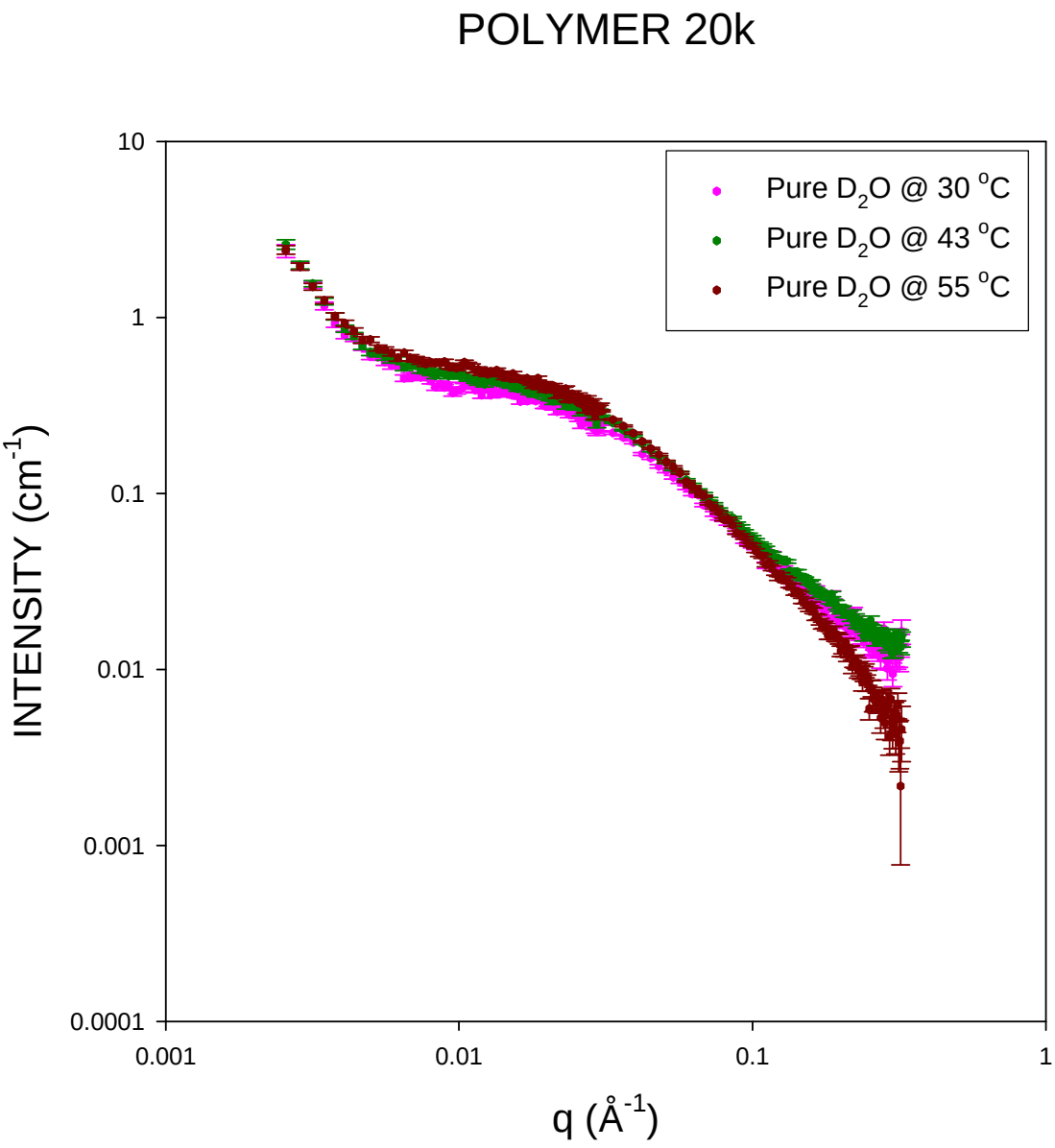

Figure 19. Polymer 20k in pure D_2O at three temperatures.

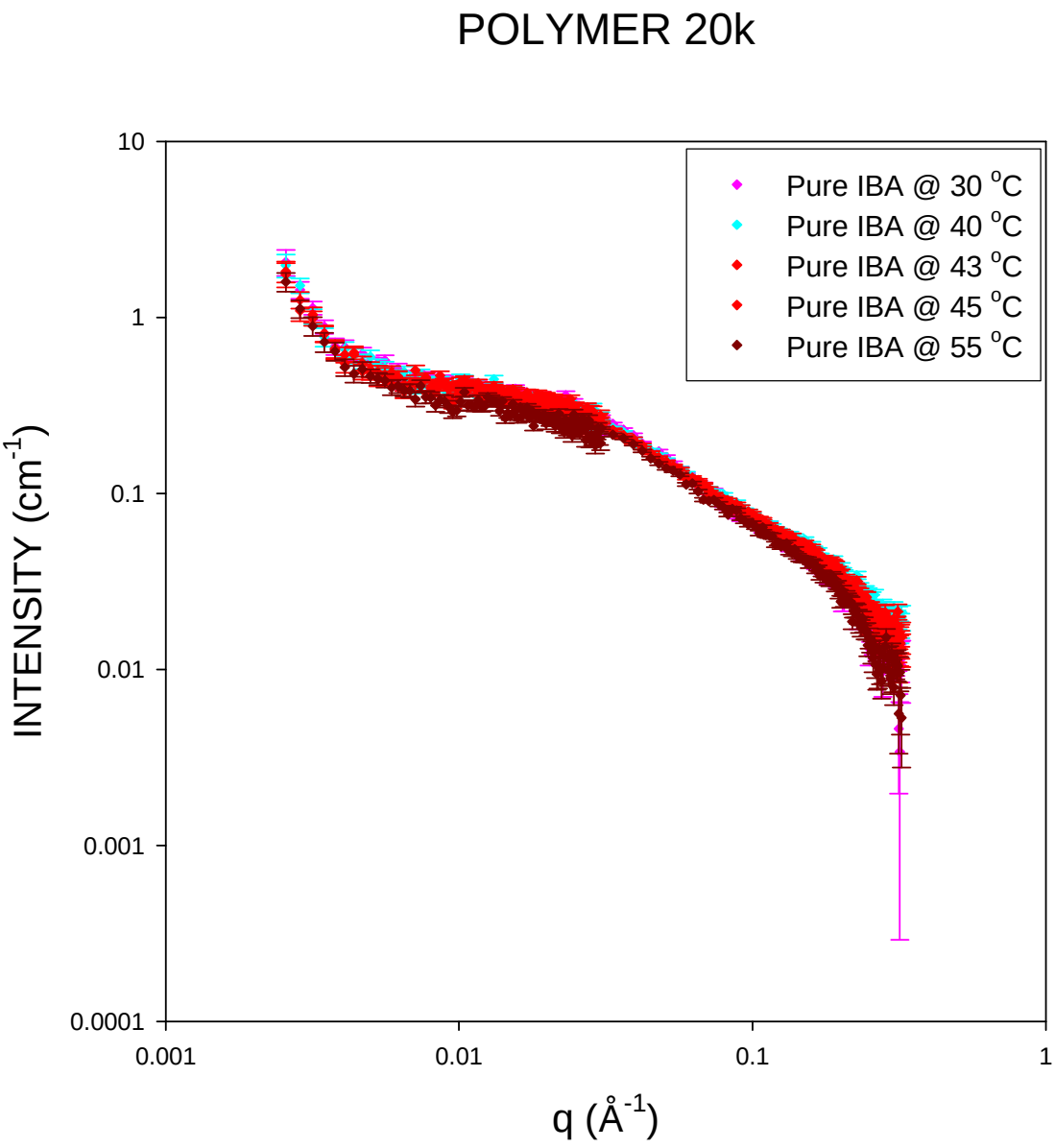

Figure 20. Polymer 20k in pure d-IBA at three temperatures.

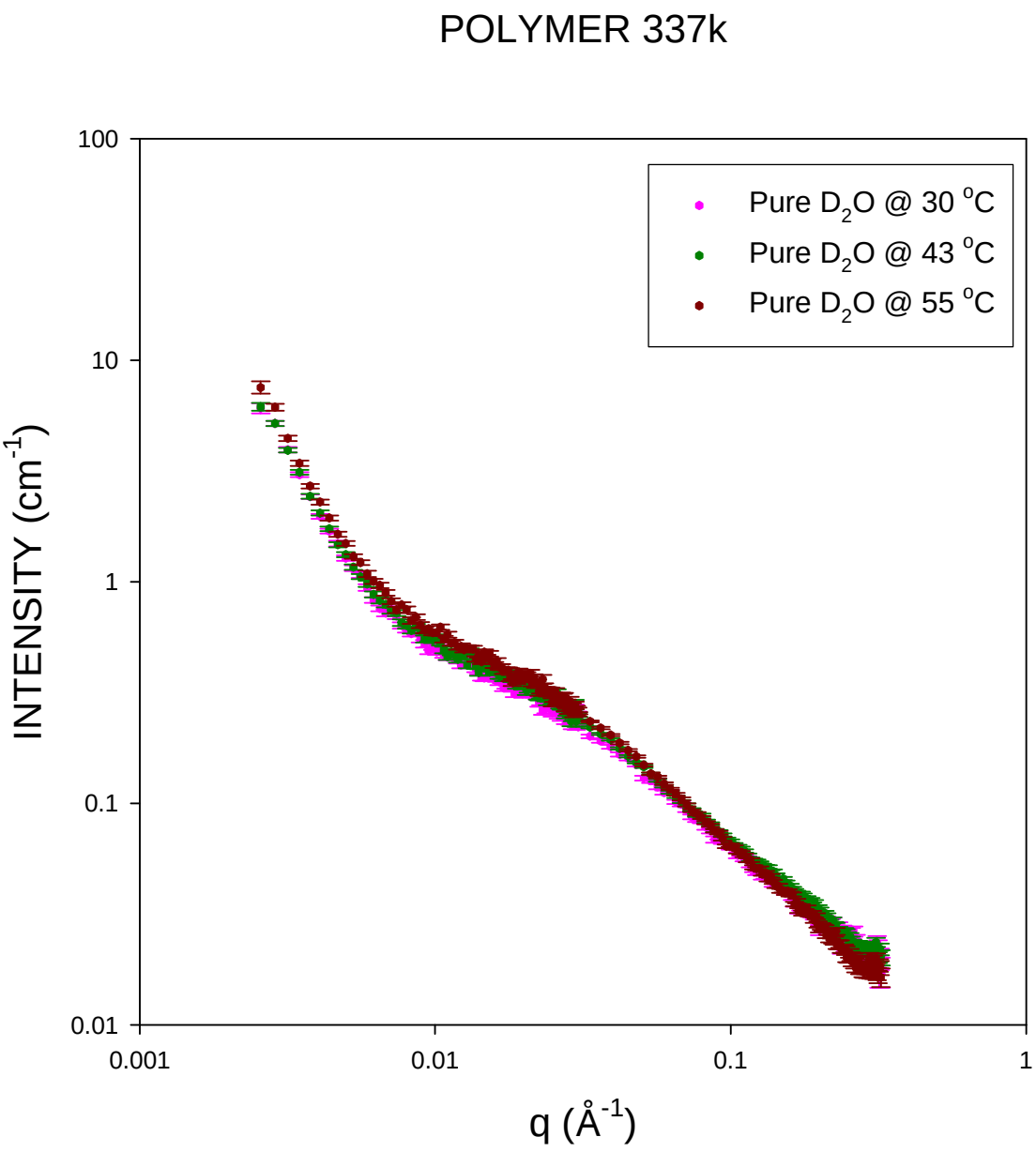

Figure 21. Polymer 337k in pure D_2O at three temperatures.

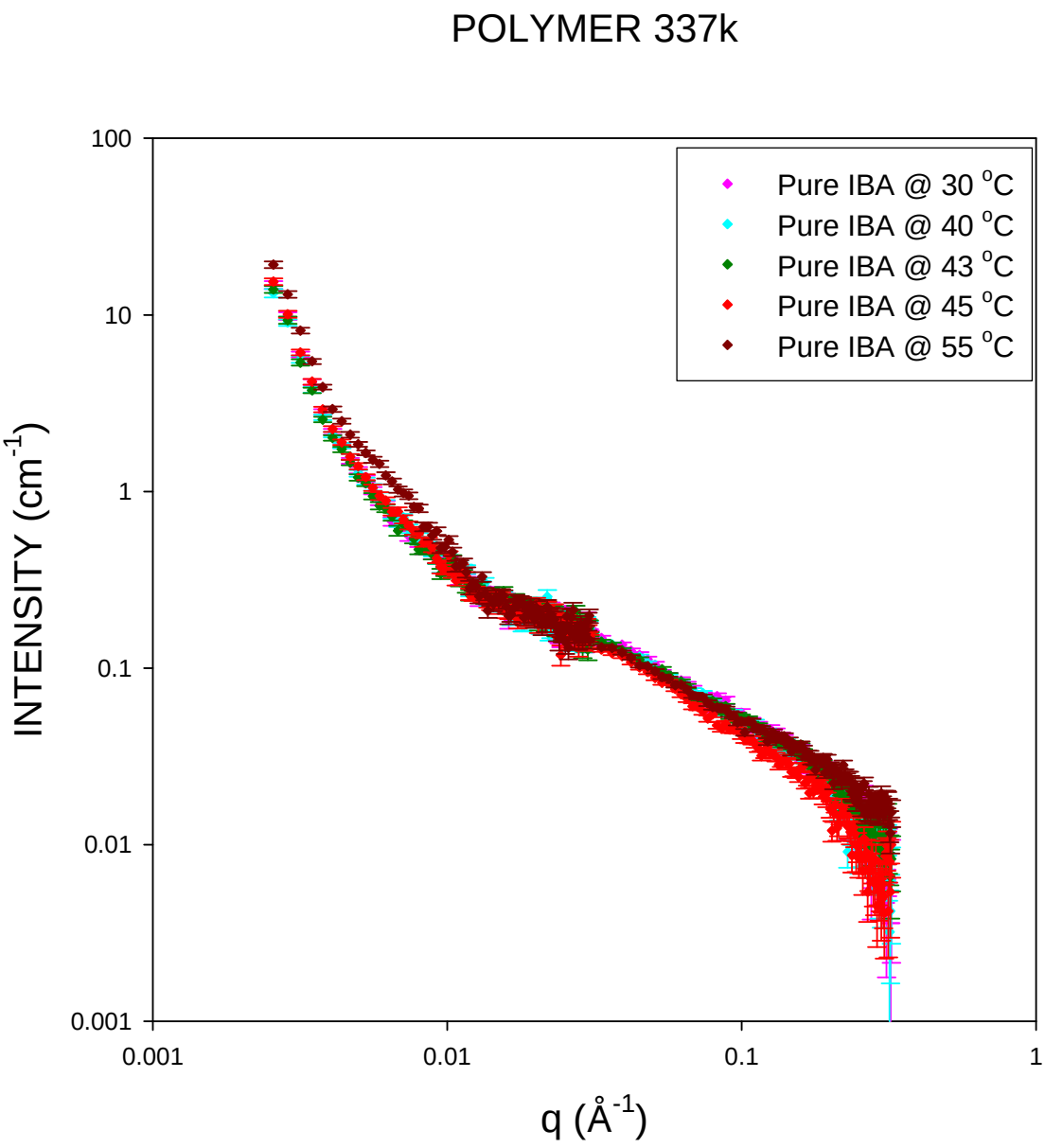

Figure 22. Polymer 337k in pure d-IBA at three temperatures.

Figures 19 and 21 show Polymer 20k and 337k in pure D_2O at several temperatures. Both of the curves showed the typical upturn due to aggregations, a slope that indicated adequate free chains for analysis, and no significant changes with temperature. Figures 20 and 22 are solutions consisting of pure IBA. Both of these runs show, like the D_2O runs, a combination of large aggregates and free chains. The figures also showed the Porod downturn in the high q region. Figure 22 shows a stronger aggregation upturn, which indicates the stronger tendency to aggregate of the higher molecular weight polymer.

Run 2 is an improvement over Run 1 in that there were no sample leaks and a wider temperature and composition range was covered. Like Run 1, the concentration of Polymer 337k is above the c^* calculated using the newer relation for R_g. This complicates the amount of analysis that can be carried out on these data and may be responsible for the low R_g values found by fitting Run 1 (see Analysis section). The most important result of Run 2 was the observation of rod-like scattering of PEO in pure IBA versus a standard Gaussian coil in pure D_2O, indicated by the slope in the mid-q range. This slope can be used as a measure of chain stiffness (rod-like character), even if the individual molecular dimensions cannot be found by fitting the data to a model.

Run 3

Since the rod-like behavior was observed in an acidic solution, it was decided to further investigate the effect of pH on the chain conformation by using strong and weak acids and bases in addition to the earlier measurement in Run 2a of PEO in a weak acid (d-acetic acid). In addition to looking at acidic and basic solutions of Polymer 20k, other molecular weight polymers were studied: Polymer 252k in d-IBA/D_2O solutions and pure d-acetic acid, and Polymer 4k in pure acetic acid. The samples were mixed on the benchtop in 2 mm pathlength quartz banjo scattering cells.

The solvents used in this experiment included the same D_2O, d-acetic acid, and d-IBA used in Run 2 and 35 wt % deuterium chloride, Sigma-Aldrich Batch # 18614AB 99% D enrichment, and 40 wt % sodium deuteroxide, Sigma-Aldrich Batch # 09701MA 99.9% D enrichment, with an approximate polymer concentration of 12 mg/mL. After the samples were mixed they were stored an oven set to 60 ^oC to heat the samples into the one-phase region and to help solubilize the larger polymer molecules. The detector was set to 3 and 15 meters to cover a q range of 0.00327-0.3622 $Å^{-1}$ using 8 Å neutrons. The Polymer 252k samples were studied at 43 and 55 ^oC, while the pH runs (samples 1-5) were studied at 25 ^oC. The sample compositions are listed below.

Table 6. Sample compositions used in SANS Run 3.

Sample	Polymer	Mass Polymer (grams)	Polymer Concentration (mg/mL)	Solvent Composition (Mass Fraction)
1	20k	0.0060	11	Pure DCl
2	20k	0.0062	11	0.001 DCl
3	20k	0.0067	12	NaOD
4	20k	0.0062	11	0.001 NaOD
5	20k	0.0067	12	D_2O + 0.0067 mg NaCl
7	252k	0.0070	13	0.46 $_{d-}$IBA
8	252k	0.0061	11	D_2O
9	252k	0.0062	11	$_{d-}$Acetic Acid
10	252k	0.0061	11	0.30 $_{d-}$IBA
11	252k	0.0065	12	0.39$_{d-}$ IBA
12	4k	0.0065	12	$_{d-}$Acetic Acid

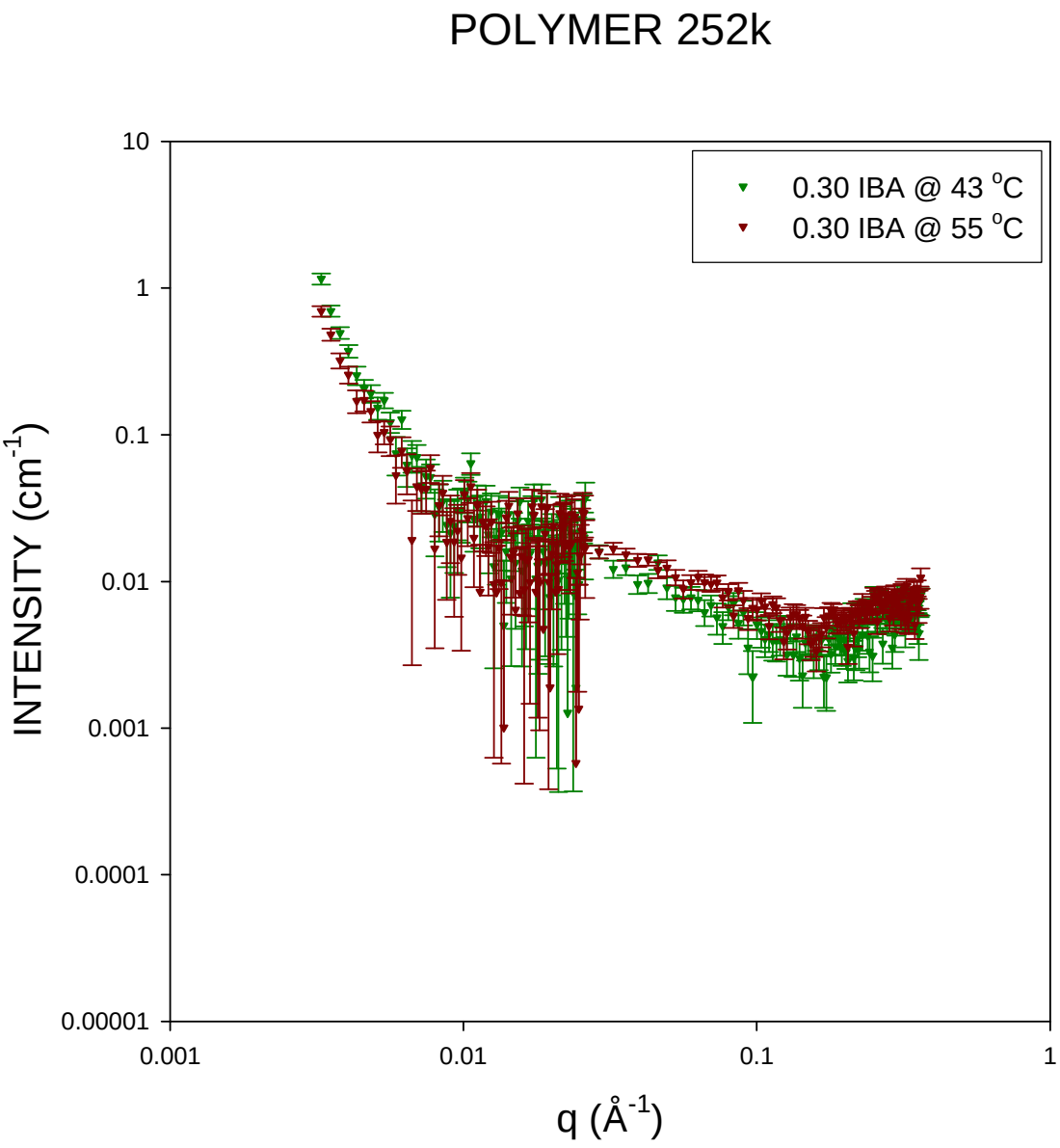

Figure 23. Polymer 252k in a solution with an IBA mass fraction of 0.30.

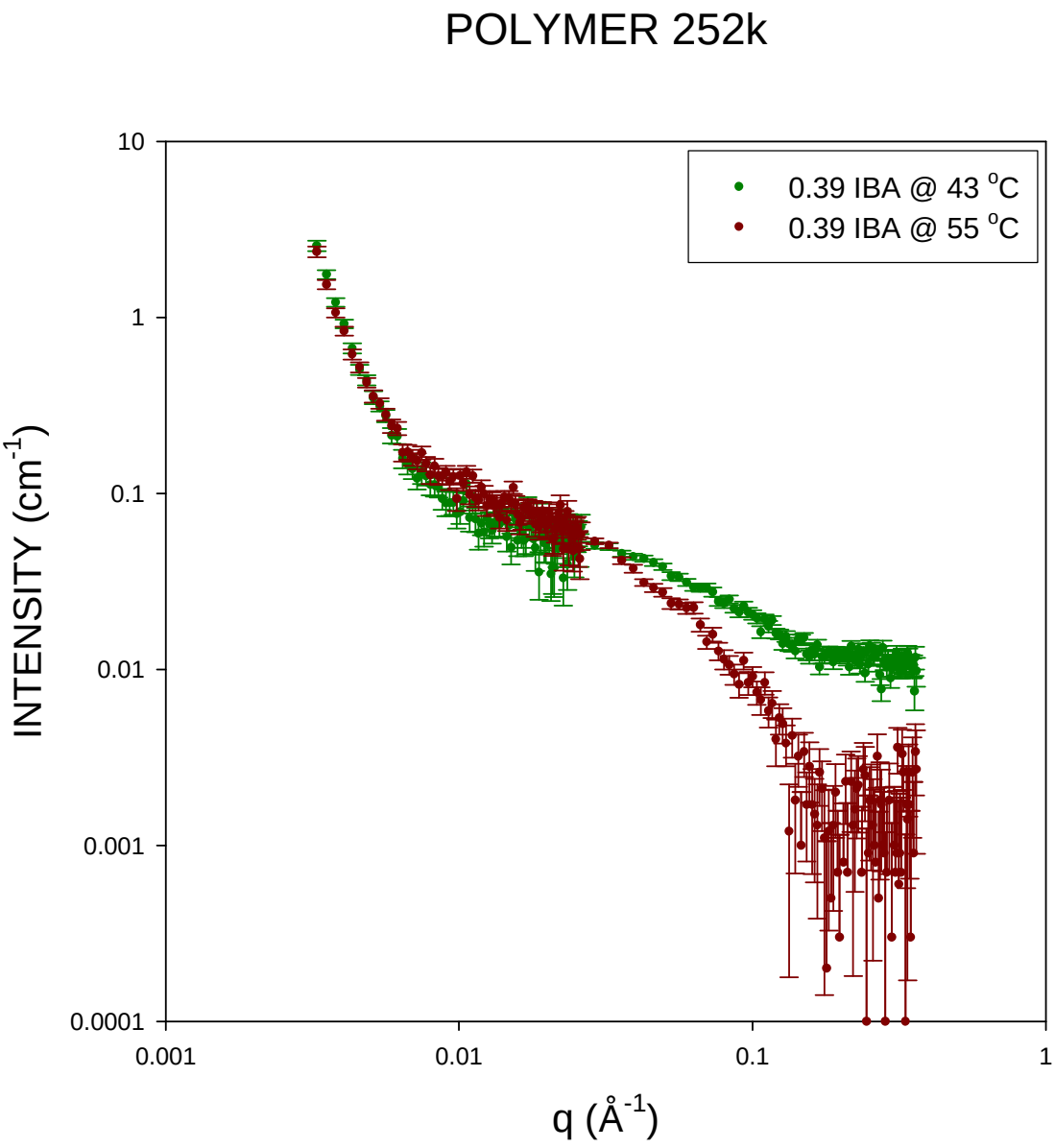

Figure 24. Polymer 252k in a solution of critical concentration of d-IBA in D_2O at two temperatures.

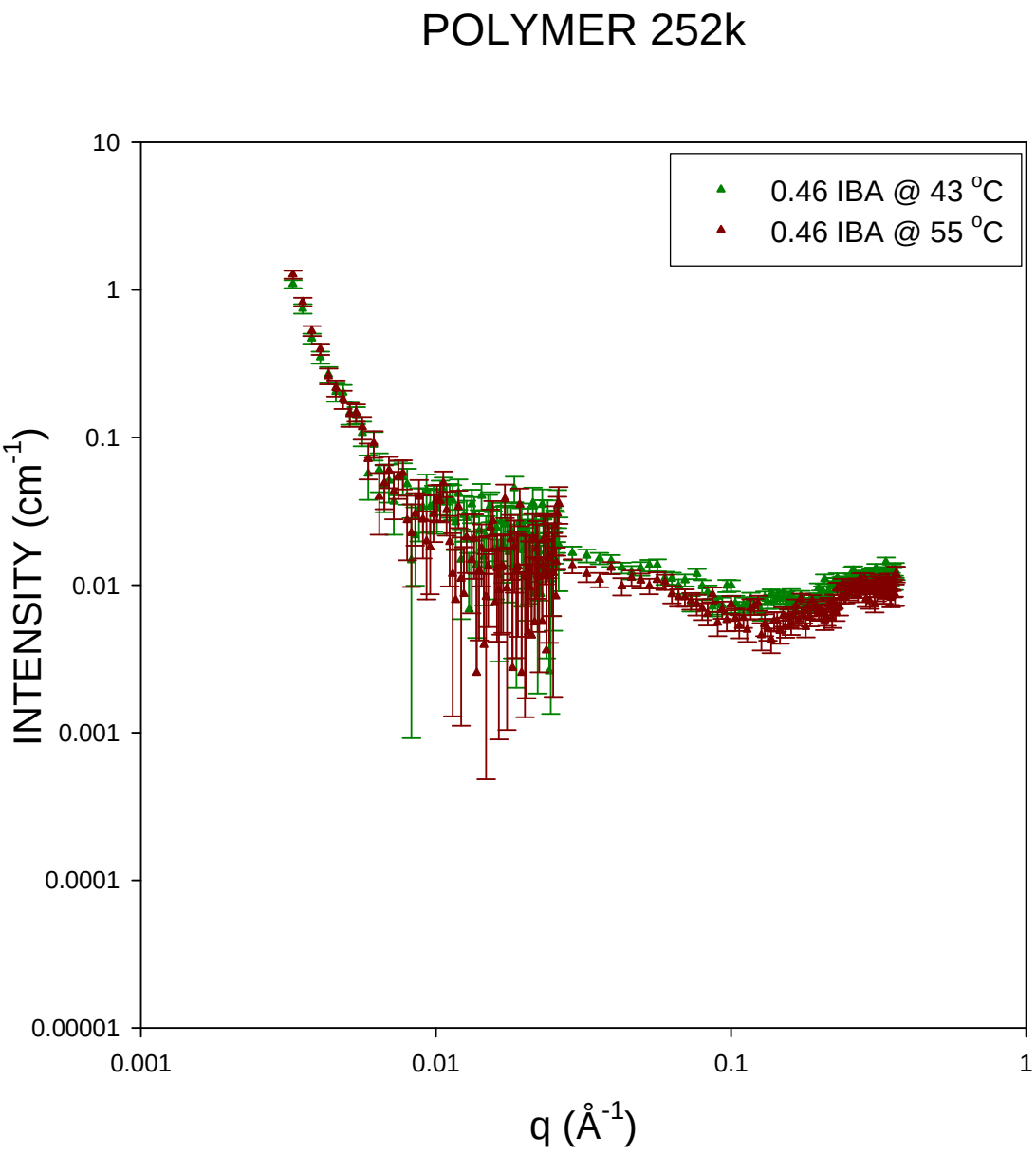

Figure 25. Polymer 252k in a solution with an IBA mass fraction of 0.46 at two temperatures.

Figures 23-25 show Polymer 252k in varying concentrations of IBA/D_2O solutions. The only effect of temperature on the samples is seen in Figure 24, in which the higher temperature run (55 ^oC) shows free chains, as evidenced by the slope > 1.0 ($0.01<q<0.1$), which is not seen in the other compositions or temperatures. The other main feature of these curves is the appearance of a peak in the high-q area. A possible explanation of this peak will be discussed in the Analysis section. In Figure 26, Polymer 252k in D_2O, we see a standard scattering curve for a Gaussian coil with large aggregations and no high-q downturn or conclusive peak.

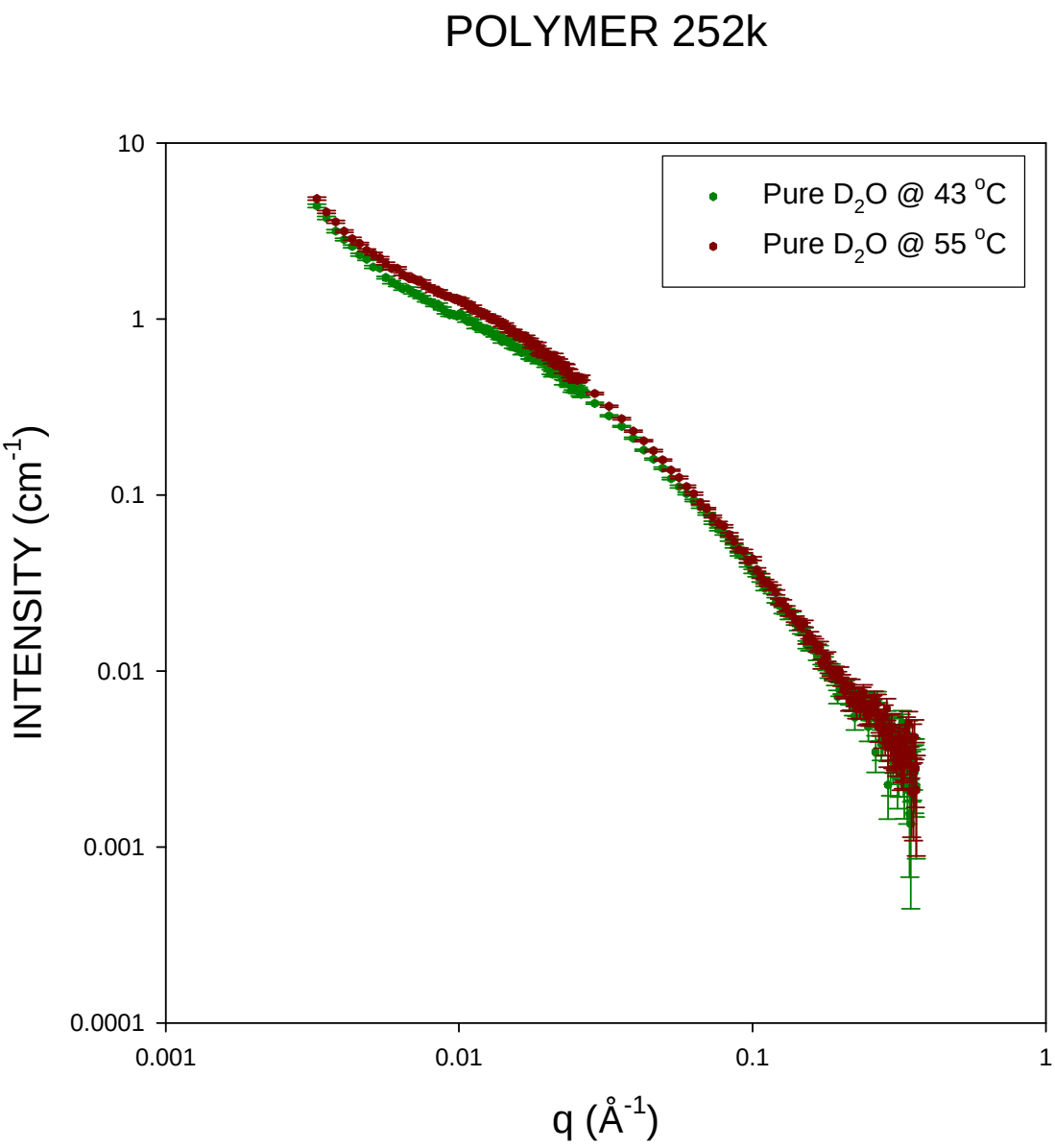

Figure 26. Polymer 252k in pure D_2O at two temperatures.

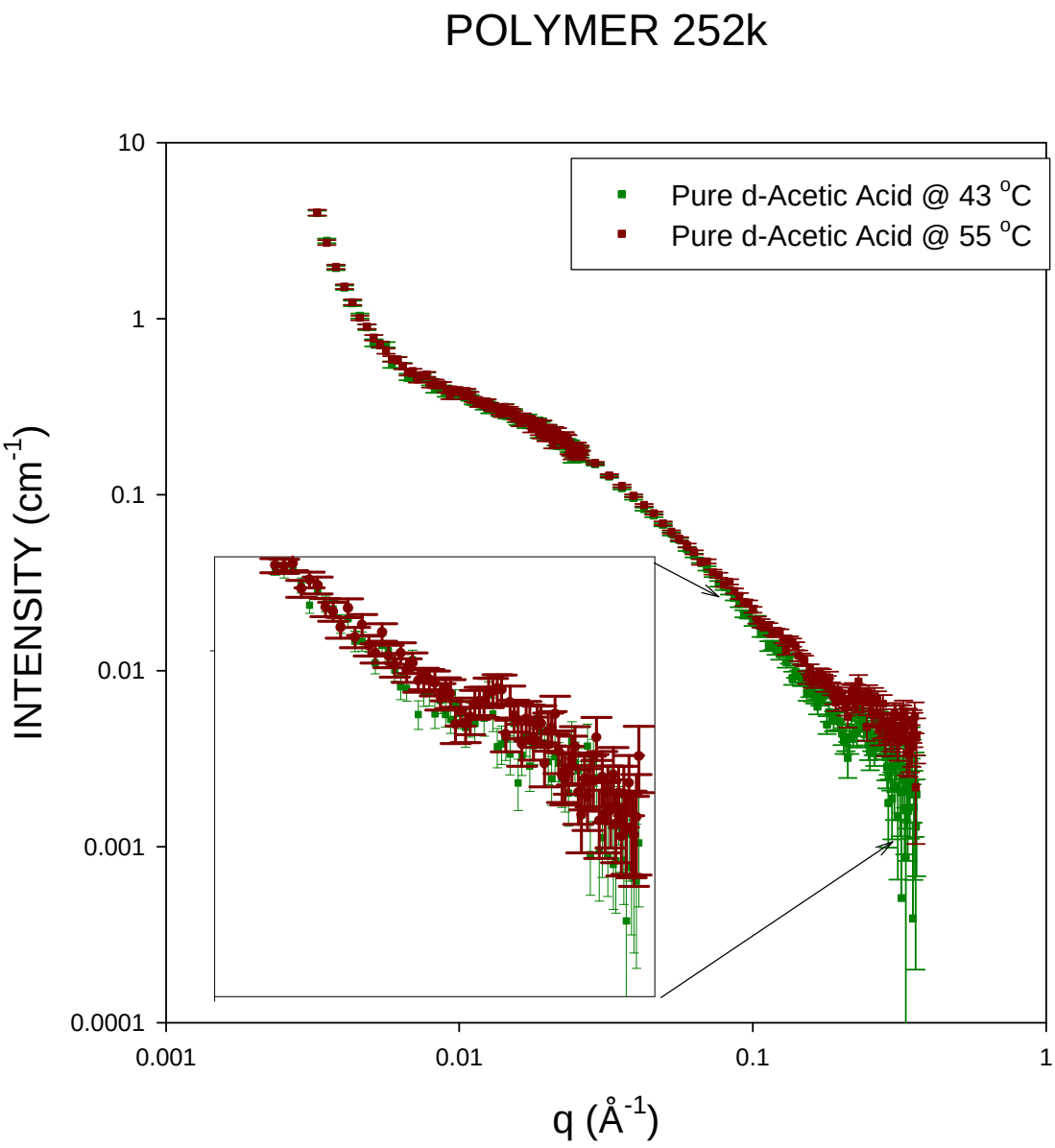

Figure 27. Polymer 252k in pure deuterated acetic acid at two temperatures. The inset shows a close up of the high-q area indicated by the arrows.

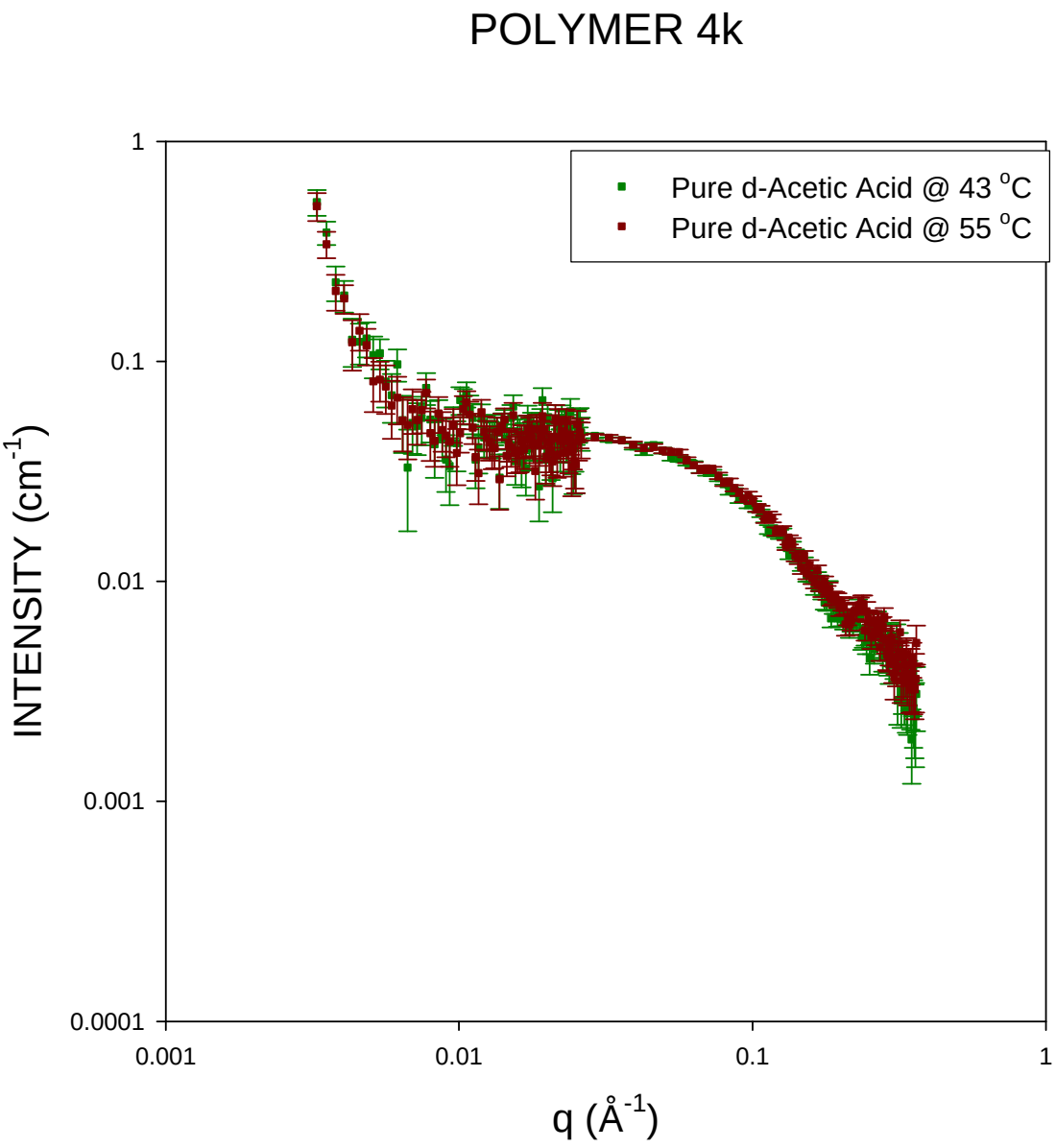

Figure 28. Polymer 4k in pure deuterated acetic acid at two temperatures.

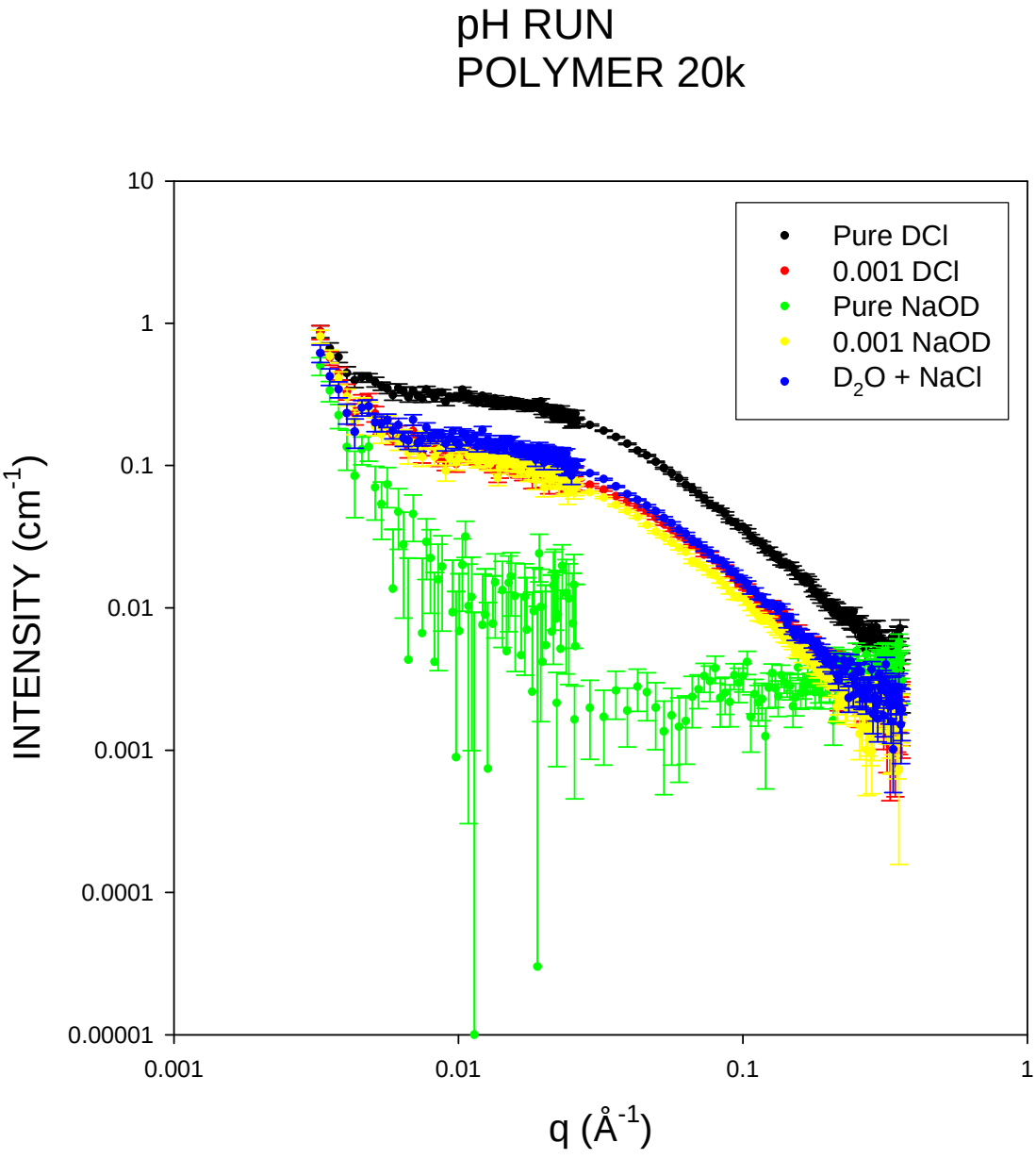

Figure 29. Polymer 20k in solutions of strong deuterated acids and bases. All were run at 25 °C.

Figures 27 and 28 show Polymer 252k and Polymer 4k in solutions of deuterated acetic acid at 43 and 55 ^{o}C. Both of these figures show no real temperature dependence between runs, as can be seen by the parallel slopes in the mid-q range. The samples showed an aggregation peak in the low-q range. The mid-q range of Polymer 252k and Polymer 4k had similar slopes that indicate a coil-like conformation for the chains. In the high-q region, there is no strong downturn as seen in the IBA samples, but there is a small hitch that is not as obvious as seen in Figures 23-25, but may be indicative of a systematic problem. The inset in Figure 27 shows the region a bit more clearly. The appearance of the hitch will be discussed in the Analysis section.

Figure 29 shows Polymer 20k in five different solutions of varying pH. With the exception of the pure NaOD run, all of the runs showed free chains and very low aggregation peaks. The sample in pure NaOD showed almost no free chains, indicating insolubility. This effect could be seen visually by the appearance of undissolved polymer floating in the solution. None of the samples seemed to show a strong temperature dependence.

Run 4

Run 4 was the final set of neutron runs carried out. Since temperature did not show a very strong effect, it was decided that the molecular weight would be varied and the temperature held constant. A number of solvents were used for each molecular weight polymer, D_2O, d-IBA, and deuterated n-butyric acid. The butyric and isobutyric acids were custom synthesized by Isotec. The solvent information is listed in the table below.

Table 7. Solvent information used in SANS Run 4.

Solvent	Manufacturer	Lot #	Deuterium Enrichment
Deuterated Isobutyric Acid	Isotec Custom Synthesis, 2004	IS0050	98%
Deuterium Oxide	Isotec	IG0056-2	99.999%
Deuterated Butyric Acid	Isotec Custom Synthesis, 2004	IS0135	98%

The samples were mixed in 2 mm quartz banjo cells on the benchtop. The cells were sealed with Teflon plugs and additional Teflon tape. Once mixed, the samples were placed in the oven at 65 ^{o}C for several hours to dissolve the polymer. The sample block holder was set to a constant temperature of 60 ^{o}C. The detector was set to cover a q range from 0.003796-0.378 Á. These samples were made with lower polymer concentrations in order to remain below c^* for both of the relationships used for R_g.[14,17] One sample of Polymer 20k was studied in n-butyric acid instead of D_2O, since several runs had already been carried out with Polymer 20k in D_2O.

Samples L and K were noted to have some entrained air bubbles in the samples. The samples were warmed in the oven and placed into a sonicator to remove the bubbles.

Table 8. Sample compositions for SANS Run 4.

Sample	Polymer	Mass Polymer (g)	Polymer Concentration (mg/mL)	Solvent
A	4k	0.0307	56	Pure d-IBA
B	20k	0.0061	11	Pure d-IBA
C	252k	0.0034	6	Pure d-IBA
D	337k	0.0018	3	Pure d-IBA
E	4k	0.0310	57	0.39 d-IBA
F	20k	0.0062	11	0.39 d-IBA
G	252k	0.0037	7	0.39 d-IBA
H	337k	0.0016	3	0.39 d-IBA
I	4k	0.0334	61	Pure D_2O
K	252k	0.0030	6	Pure D_2O
L	337k	0.0021	4	Pure D_2O
M	20k	0.0065	12	Pure d-Butyric Acid

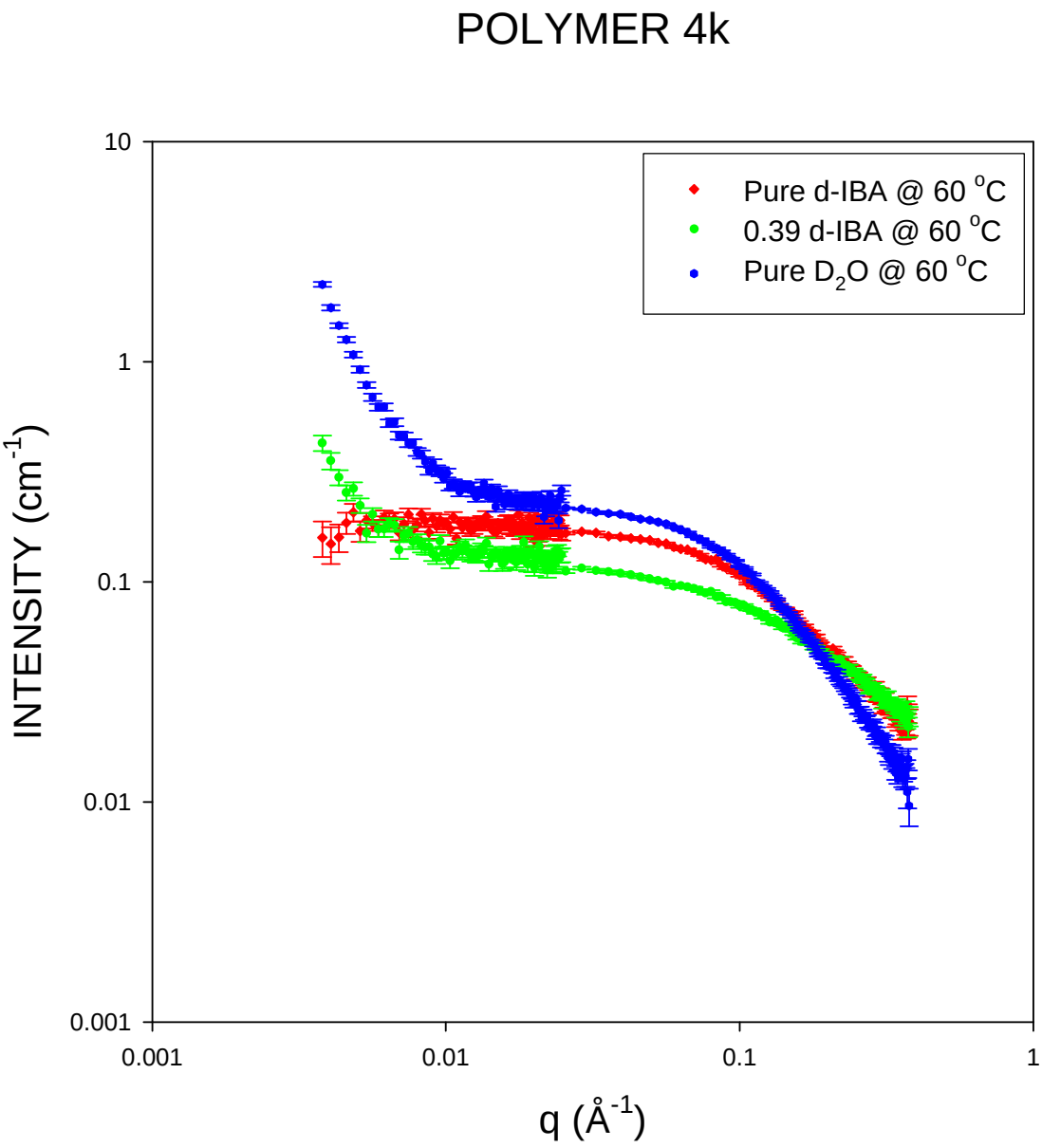

Figure 30. Polymer 4k in solutions with three different compositions at 60 °C.

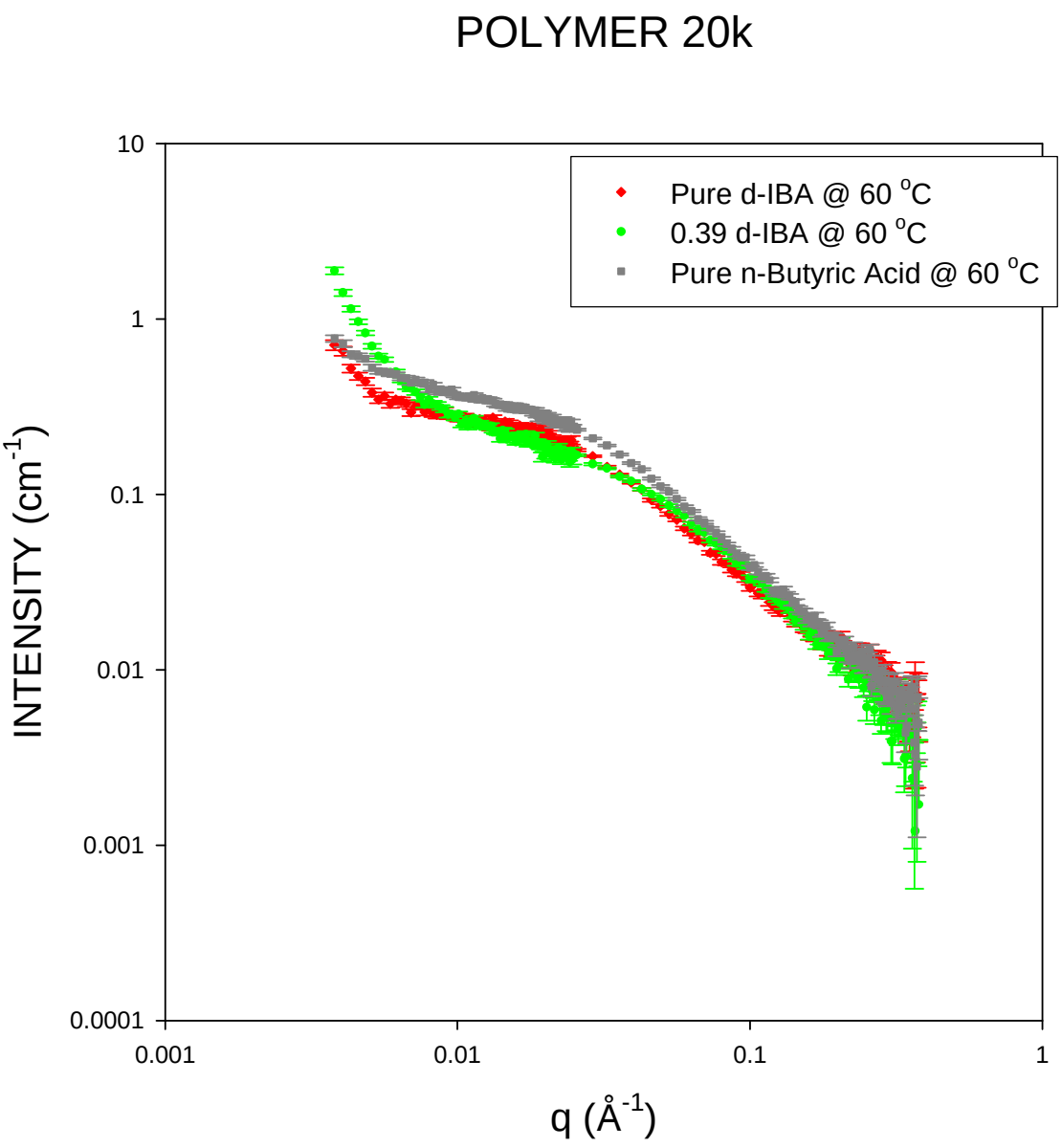

Figure 31. Polymer 20k in solutions of isobutyric and butyric acid at 60 °C.

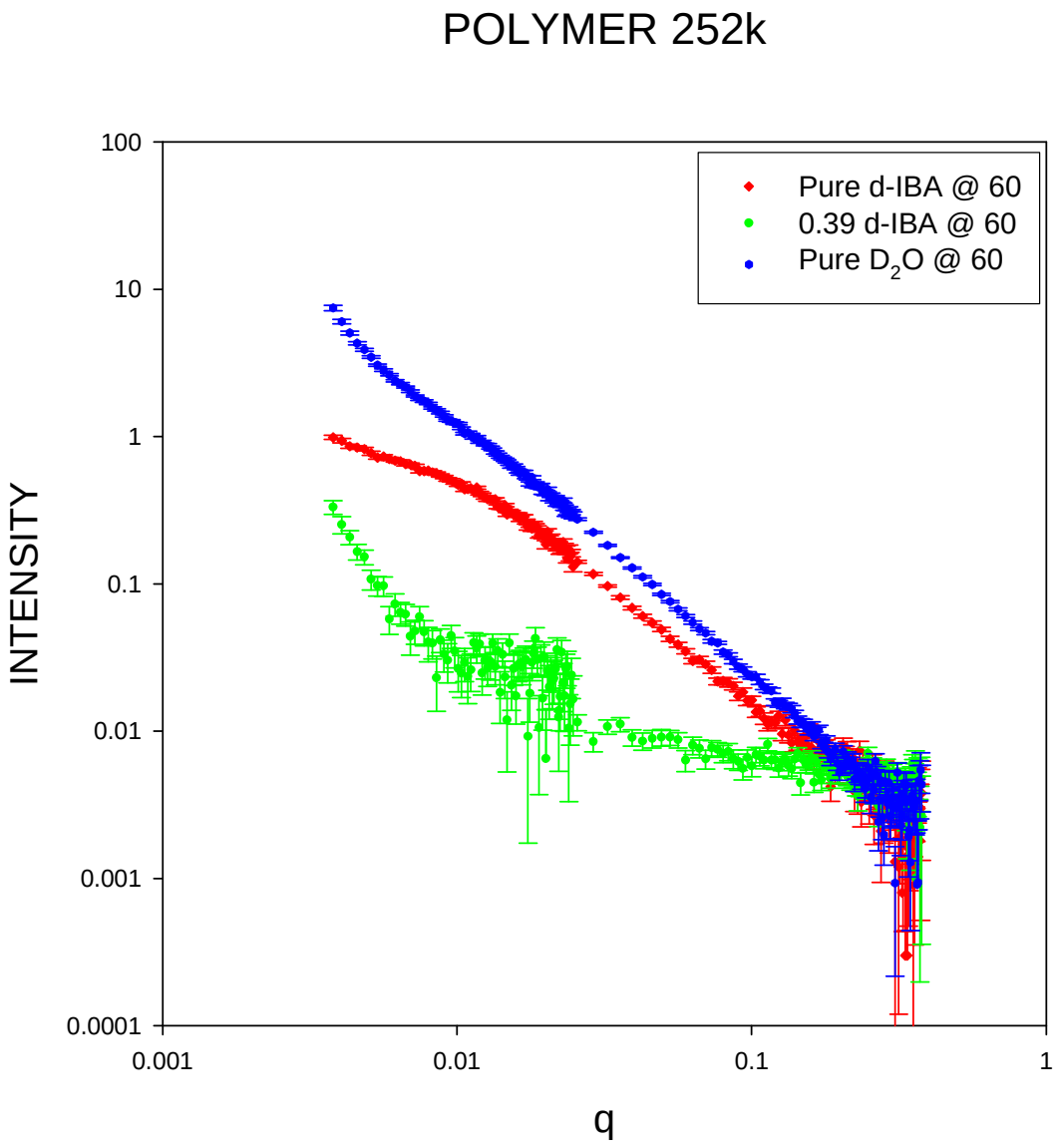

Figure 32. Polymer 252k in solutions of varying $_{d}$-IBA mass fraction at 60 ^{o}C.

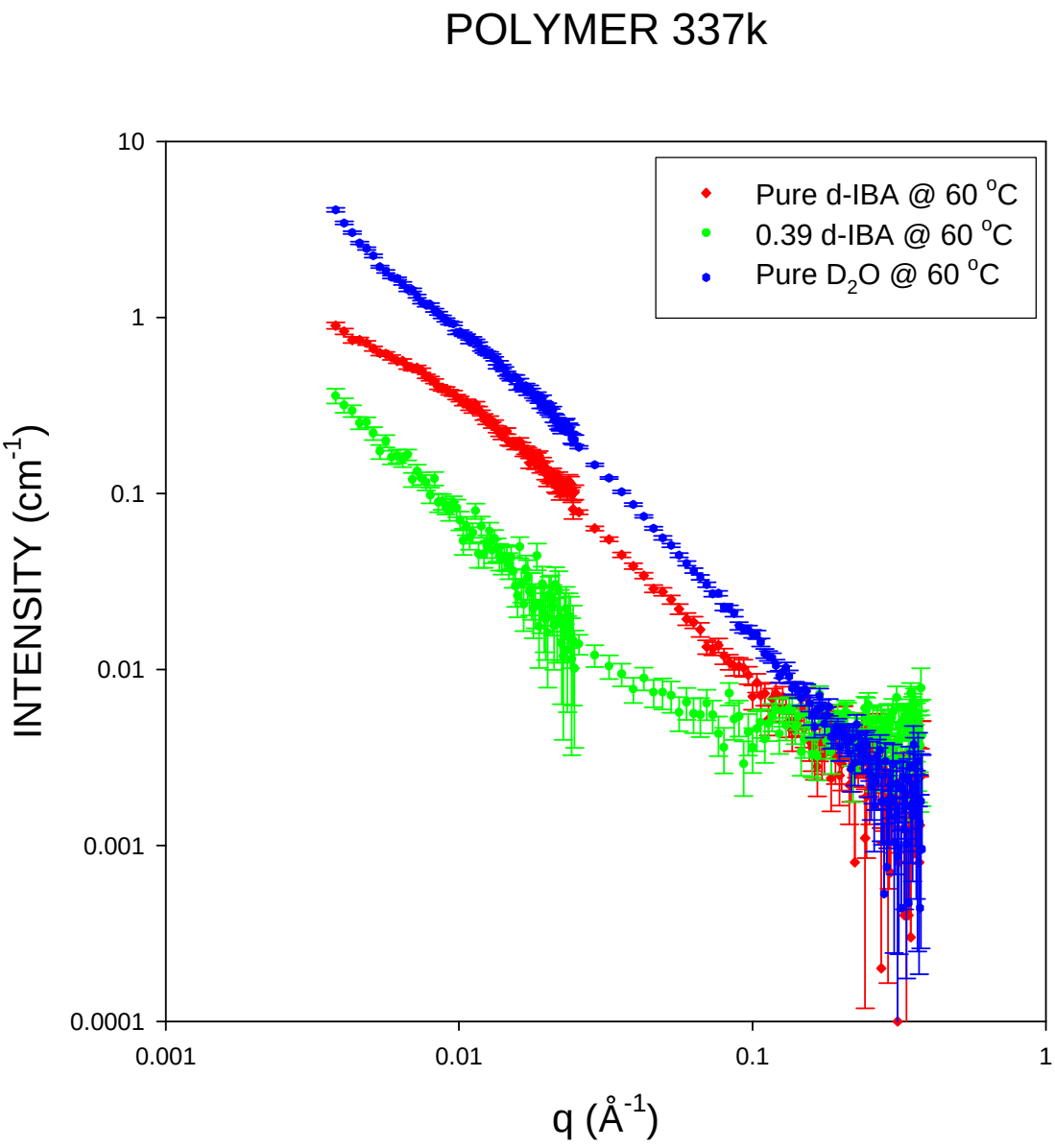

Figure 33. Polymer 337k in solutions of varying deuterated isobutyric acid.

Figures 30-33 show the neutron scattering intensity versus wave vector for Run 4. Unlike the previous figures, which showed each polymer in a solution of constant composition at several temperatures, these figures show each polymer in a number of solution concentrations at a single temperature. Figure 29 shows Polymer 4k in pure D_2O, pure d-IBA, and a binary solution with a mass fraction of d-IBA of 0.39. All of the solutions showed no sign of a high-q turndown and had sufficient free chains to have a slope in the mid-q range. The amount of aggregation shown by the low-q regime does seem to have a strong compositional dependence. The pure d-IBA sample shows no aggregation peak, while increasing the D_2O content increases the aggregation peak. Figure 31 shows Polymer 20k in the critical mixed solvent, pure d-IBA, and pure d-butyric acid. All of the samples show very similar slopes in the mid-q range, no high-q downturn, and aggregation peaks in the low-q regime. Figure 32 shows Polymer 252k in pure D_2O, d-IBA, and a mixed solvent. There was no sign of a high-q turndown in the runs and all three showed an aggregation peak in the low-q regime. The two pure solvents showed a slope indicative of free chains. The critical mixed solvent did not, however, show free chains in the mid-q region. Figure 33 shows Polymer 337k in the pure and mixed solvents. Like Figure 32, the pure solvent samples show free chains and the mixed solvent sample does not show many free chains in the mid-q range. Both Figures 32 and 33 show strong aggregation peaks that almost create a straight line with no discernable Guinier region.

Polarimetry

In an effort to ascertain the helical nature of the rod-like PEO molecules, polarimetry measurements were made of PEO solutions. There are a number of methods of observing a helix at the molecular level. These include: Circular Dichroism, Infrared Spectroscopy, NMR Spectroscopy, and Polarimetry. One of the most popular methods in biology of measuring the appearance of helices is circular dichroism (CD). Circular dichroism is a type of UV absorption spectroscopy that measures the difference in absorption of left and right hand polarized light. Chiral bonds absorb left polarized light more strongly than right polarized light. The difference in absorption is converted into a standardized unit referred to as ellipticity. Different structures produce characteristic curves which are shown below[50]

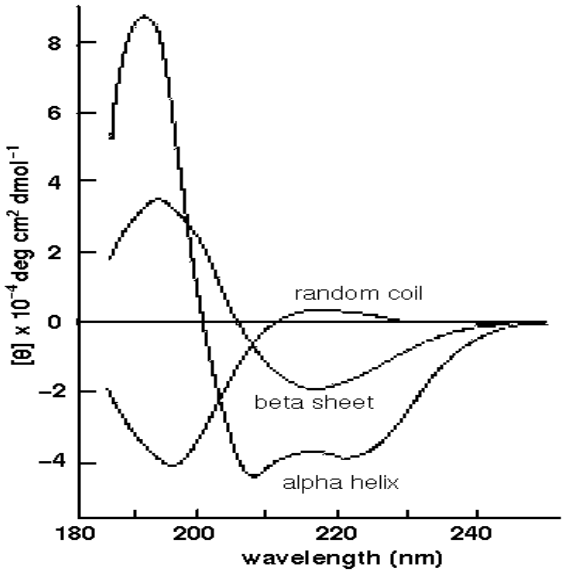

Figure 34. Standard curves for circular dichroism.

The measured curve is then fitted to these standard curves to get a measure of the conformation of the molecule. This is a powerful technique that can reliably identify helical structures in solution, but PEO does not have a UV active chromophore. This would necessitate using what are known as "reporter molecules," which are UV active molecules which associate with the polymer. This technique was not attempted because of the added complexity of another chemical species that might alter the polymer conformation. Adding a new chemical species would have required further neutron studies to ensure that the reporter molecules did not change the conformation of the PEO.

Infrared and NMR spectroscopy have also been used to study the conformation of PEO in solution.[37,51-56] These studies have shown an increase in the local helical structure of PEO in aqueous solutions. The global structure has not, however, been found to be helical in any solvent prior to our work. Infrared and Raman spectroscopy was attempted on our solutions, but there is a difficulty in both assigning peaks to certain bond angle combinations and separating out the effect of global structure and the local helical structure. These difficulties were sufficient to make these techniques unsuitable for observing the conformation of PEO in IBA.

With all of the difficulties with the previous methods, it was decided that the most effective method of determining whether PEO forms a helix in IBA solutions was to use polarimetry. Polarimetry passes plane polarized light through a sample and measures the rotation of that light. The plane polarized light actually consists of two superimposed beams of circularly polarized light (left and right). Chiral molecules lack a plane of symmetry. An everyday example of this is human hands,

which cannot be superimposed on each other. The left- and right-handed chiral molecules interact differently with the left- and right-handed light, causing a net rotation. Because helical molecules can be left or right handed, they are chiral and will rotate the plane of polarized light. Unfortunately, there is no specific reason for the PEO to favor a specific chirality, which should result in a racemic mixture that will have a net rotation (α) of 0^o. It is, however, possible that the mixture may have a slight bias that will push the mixture to an off-racemic ratio, resulting in a small signal.

Enantiomeric amplification is a not very well understood phenomenon in which chiral "impurity" molecules can influence the stereochemistry of the products of organic synthesis. In addition to influencing the chirality of synthesis products, other authors have found the so-called "sergeants and soldiers" effect of chiral monomers on polymer conformation.[57] Relatively small numbers of chiral monomers can have a large influence on the conformation and chiral signal of a polymer, much as a sergeant can affect a large number of soldiers. With this in mind, it was decided to attempt to influence the sign and strength of the signal in our helices by adding chiral impurities.

Measurements were carried out on a Jasco P1010 polarimeter, Serial # B019260637, using a 10 cm pathlength glass cell with an interior volume of 8 mL. The P1010 uses a halogen lamp with a wavelength of 589 nm selected by a filter and has an accuracy of 0.002^o with a reproducibility of $\pm$ 0.002 or better for measurements less than 1^o. The instrument was first blanked for solvent effect and then run with the polymer in the solvent. Each run was carried out by making

repeated integrations of the signal to improve the statistics of the run. Polarimetry results are usually corrected for concentration and reported as a specific rotation using the following equation:

$$[\alpha] = \frac{\alpha}{pathlength(dm) * concentration(g/mL)} \quad (26)$$

The polarimetry runs were carried out in three runs, the first with the polymer in neat IBA and the later two using chiral impurities in an effort to influence the ratio of left-handed to right-handed helices through enantiomeric multiplication.[58-64]

Run 1

The first run was carried out using Polymer 20k in neat IBA as received. This sample of IBA was not, unfortunately, well characterized. For later IBA samples, the lot numbers were more carefully noted. Samples of varying molecular weight were made on the bench top with a PEO concentration of approximately 12 mg/mL, to correspond to the concentration used for Polymer 20k in the neutron scattering aspect of the experiment. The samples studied are listed in the table below. Samples II and III were made with IBA from Sigma Aldrich, Lot # 01821LI. Sample I may have been made with the same batch of solvent, but this is not known for certain since another, much older bottle of IBA was open in the lab at the same time. Once the samples were mixed, the vials were heated on the bench using a hotplate to help solubilize the PEO. The temperature was difficult to control in this type of setup, so the actual temperature that the samples reached in this run is not certain.

Table 9. Sample compositions for polarimetry. Run 1.

Sample	Polymer	M_n	Mass (g)	Volume (mL)	Concentration (mg/mL)	Solvent
I	Polymer 20k	18,900	0.1090	8.0	13.6	IBA
II	Polymer 4k	4,080	0.0950	8.0	11.9	IBA
III	Polymer 252k	252,000	0.084	8.0	10.5	IBA
IV	Polymer 20k	18,900	0.1269	10.0	12.7	H_2O

The first set of experiments showed a rotation (see Results), but the sign of the rotations was not consistent. Sample I had a negative rotation, while Samples II and III showed positive rotations. This was taken to mean that we were seeing a signal because of a slight random bias in the handedness of the helices.

Run 2

The next series of measurements was carried out using IBA from a new lot, Sigma-Aldrich Lot # 07710PB. This series showed no sign of the rotations seen in Run 1. The different signs of the rotation and the effect of changing the lot number of solvent indicated that the handedness of the helix was capable of being influenced. It was decided to introduce a known chiral impurity or dopant to influence the signal of the rotation through a "sergeant and soldiers" effect.

The first dopant used was L-phenylalanine (PHL) purchased from Lancaster, ($[\alpha] = -34^o$). 0.0217 grams of phenylalanine were mixed with 25 mL of IBA. The phenylalanine was not very soluble in the IBA so the entire solution was heated to 52

^{o}C in an oven. The low solubility was not considered a problem since the "sergeants and soldiers" effect showed that small amounts of chiral molecules can have a large effect. A single sample using this solvent was with Polymer 20k. At this point of the experiment the instrument began to exhibit some long-term drift and needed to be serviced by the Jasco engineer. While this happened, tartaric acid (TA) ([α] = +12^{o}) and aspartic acid ([α] = +24.6^{o}) were obtained from Aldrich. Both tartaric acid and aspartic acid showed a low solubility in pure IBA. In an attempt to dissolve the tartaric acid, 5 mL of IBA were combined with 0.5 mL of H_2O and 1.005 g of tartaric acid. The water formed a second liquid phase. The solution was left overnight, the IBA phase was then decanted off for use as a doped solvent for polarimetry. Samples were also made of other molecular weights in pure H_2O and in H_2O with tartaric acid added to ensure there was no rotation of PEO in water. The samples for Run 2 are listed in the table below.

Table 10. Sample compositions for polarimeter, Run 2.

Sample	Polymer	M_n	Mass (g)	Volume (mL)	Concentration (mg/mL)	Solvent
V	Polymer 20k	18,900	0.0120	10.0	1.2	IBA
VI	Polymer 20k	18,900	0.0505	10.0	5.1	IBA
VII	Polymer 20k	18,900	0.1512	10.0	15.1	IBA
VIII	Polymer 20k	18,900	0.2012	10.0	20.1	IBA
IX	Polymer 20k	18,900	0.2514	10.0	25.1	IBA
X	Polymer 20k	18,900	0.1018	10.0	10.2	IBA + PHL
XI	Polymer 252k	252,000	0.1219	10.0	12.2	H_2O
XII	Polymer 4k	4,080	0.1226	10.0	12.3	H_2O

Sample	Polymer	M_n	Mass (g)	Volume (mL)	Concentration (mg/mL)	Solvent
XIII	Polymer 20k	18,900	0.1219	10.0	12.2	H_2O +TA
XIV	Polymer 20k	18,900	0.1220	10.0	12.2	IBA + TA
XV	Polymer 252k	252,000	0.1026	10.0	10.3	IBA + TA

Run 3

The third and final run was the most successful round of polarimetry. Run 2 showed (see Results) that adding a chiral dopant had an effect upon the rotation of the PEO in IBA. Run 3 tested whether the handedness of the helix could be controlled by changing the type of dopant used. Since tartaric acid and phenylalanine were only sparingly soluble in IBA and left and right handed pairs were not available, another molecule, 1,2-propanediol, was chosen. R and S enantiomers of 1,2-propanediol (98%) were purchased from Lancaster Research Chemicals for use with IBA Lot # 07710PB. The samples in this run were heated in the oven to dissolve the polymer, in order to provide better control of the temperature during sample preparation. Temperature effects, dopant concentration, a wider array of molecular weights, and the effect of termination groups were also examined in this run. It was noticed that the maximum temperature to which the sample was heated could have an effect upon the signal. When the samples were heated to above 90 ^{o}C, the polarimeter signals became more consistent, explaining some of the inconsistency in the results from Run 2. The polymer and solvent compositions are listed in the tables below.

Table 11. Solvent compositions used to make samples for polarimetry, Run 3. The rotation sign indicates the enantiomer of propanediol used. + corresponds to S(+)1,2-propanediol and – corresponds to R(-)1,2-propanediol.

Sample	Mass Propanediol	Mass IBA	Mass Fraction Propanediol	Rotation Sign
1	0.0524	56.5414	9.27e-4	+
2	0.0483	56.1684	8.60e-4	-
3	0.0470	28.2902	1.67e-3	+
4	0.0428	28.3930	1.51e-3	-
5	0.0148	28.2919	5.23e-4	+
6	0.0230	27.8590	8.26e-4	-

Table 12. Sample compositions for polarimetry, Run 1. See Table 11 for the solvent compositions.

Sample	Polymer	M_n	Mass (g)	Volume (mL)	Concentration (mg/mL)	Solvent
XVI	Polymer 20k	18,900	0.1266	10.0	12.3	1
XVII	Polymer 20k	18,900	0.1252	10.0	12.5	2
XVIII	Polymer 252k	252,000	0.1220	10.0	12.2	1
XIX	Polymer 252k	252,000	0.1110	10.0	11.1	2
XX	Polymer 10kM	12,000	0.1157	10.0	11.6	1
XXI	Polymer 10kM	12,000	0.1164	10.0	11.6	2
XXII	Polymer 4k	4,080	0.1256	10.0	12.6	1
XXIII	Polymer 4k	4,080	0.1253	10.0	12.5	2
XXIV	Polymer 2kH	2,000	0.1252	10.0	12.5	1
XXV	Polymer 2kH	2,000	0.1232	10.0	12.3	2
XXVI	Polymer 337k	337,000	0.1185	10.0	11.9	1
XXVII	Polymer 337k	337,000	0.1229	10.0	12.3	2
XXVIII	Polymer 10kH	10,500	0.1186	10.0	11.9	1
XXIX	Polymer 10kH	10,500	0.1167	10.0	11.7	2
XXX	Polymer 10kM	12,000	0.1131	10.0	11.3	1
XXXI	Polymer 10kM	12,000	0.1155	10.0	11.6	2
XXXII	Polymer 10kH	12,000	0.1230	10.0	12.3	3
XXXIII	Polymer 10kH	12,000	0.1260	10.0	12.6	4
XXXIV	Polymer 10kH	12,000	0.1229	10.0	12.3	5
XXXV	Polymer 10kH	12,000	0.1238	10.0	12.4	6

Chapter 4: Results

Neutron Scattering

Neutron scattering data are generally analyzed through fitting models to the data. The analysis of the neutron data was carried out using Wavemetrics Igor Pro software with macros developed and released by NCNR.[65] These macros allow the neutron data to be reduced and fitted to model functions, also available through NCNR. These models are used to obtain molecular parameters by fitting the model using Igor's non-linear fitting function. Three main models were used for the data analysis. The simplest was a Debye model used for coils that will provide a fitted value for R_g. The appearance of stiffened molecules also led to the use of two more complicated models, the worm-like polymer and the core-cylinder polymer.

The worm-like model, listed as FlexExclVolCyl on the NCNR website,[65] is a model function for the scattering of a flexible cylinder with excluded volume. This model was based upon off-lattice Monte Carlo simulations.[66] Polymer molecules can exist between two extremes: a soft coil and a hard rigid rod. The authors created a scattering function that was a linear combination of the scattering functions of a chain and a rod, with a function to account for the crossover between the two behaviors. The model function provides a measure of the contour length, the Kuhn length and the radius of the particle.

The core shell cylinder model was also used to study the data. This model function provides for the scattering of a hollow, right-handed cylinder.[6] The hollow model was developed as the difference between the scattering of two cylinders, i.e. the

scattering of a solid cylinder composed of the solvent subtracted from the scattering of a solid cylinder composed of the polymer. This model can be used to find the radius of the core, the radius of the shell, and the length of the cylinder.

The use of model fitting to neutron data provides a powerful technique for characterizing polymer molecules. The model functions can now incorporate instrument details to account for "smearing" due to real world conditions. The primary, and largest, drawback of this technique is the large number of fitting parameters. For a non-linear fit, the large number of fitting parameters opens the door for unrealistic results that have no connection to reality. The number of fitting parameters can be decreased by holding some of the parameters to known values. The fitting was done with fixed values for the volume fraction of polymer and for the scattering length densities of the solvents, which are known.

Other methods of analysis were also used, when possible, to avoid the sensitivity of non-linear fitting. This includes attempting to correlate the apparent stiffness of the chain to the mid-q slope, and estimating the dimensions of the rod-like structures by relating the position of the slope changes to 1/Length and 1/Diameter. Wherever possible, these methods were compared to the fitting results to see if they provide a reasonable approximation.

An example of this is shown in Figure 34, where the transition from the Guinier to fractal region corresponds to the inverse of the rod length and the transition from the fractal region to the Porod downturn corresponds to the inverse of the rod diameter. An analysis shows these points correspond to q values of about 0.013 for L^{-1} and about 0.15 $Å^{-1}$ for D^{-1}. These would correspond to rod 77 Å long with a diameter of 7 Å. The core

shell model was fitted to these data and gave rod dimensions of 130 Å long and 14 Å in diameter. While not perfect, the uncertainty inherit in nonlinear fitting means that using the slope changes could be more effective for comparing the basic sizes of the rods among runs. For Sample C, Polymer 20k in solution with d-IBA x_m=0.46, the downturns indicate a rod about 86 Å long and 6 Å in diameter. Using the core-shell model gave dimensions of 140 Å long and 18 Å in diameter. Since the dimensions found using the method of slope changes are within an order of magnitude of the fitting results, this indicates that this technique could be used to analyze the rod dimensions if non-linear fitting is unsuccessful.

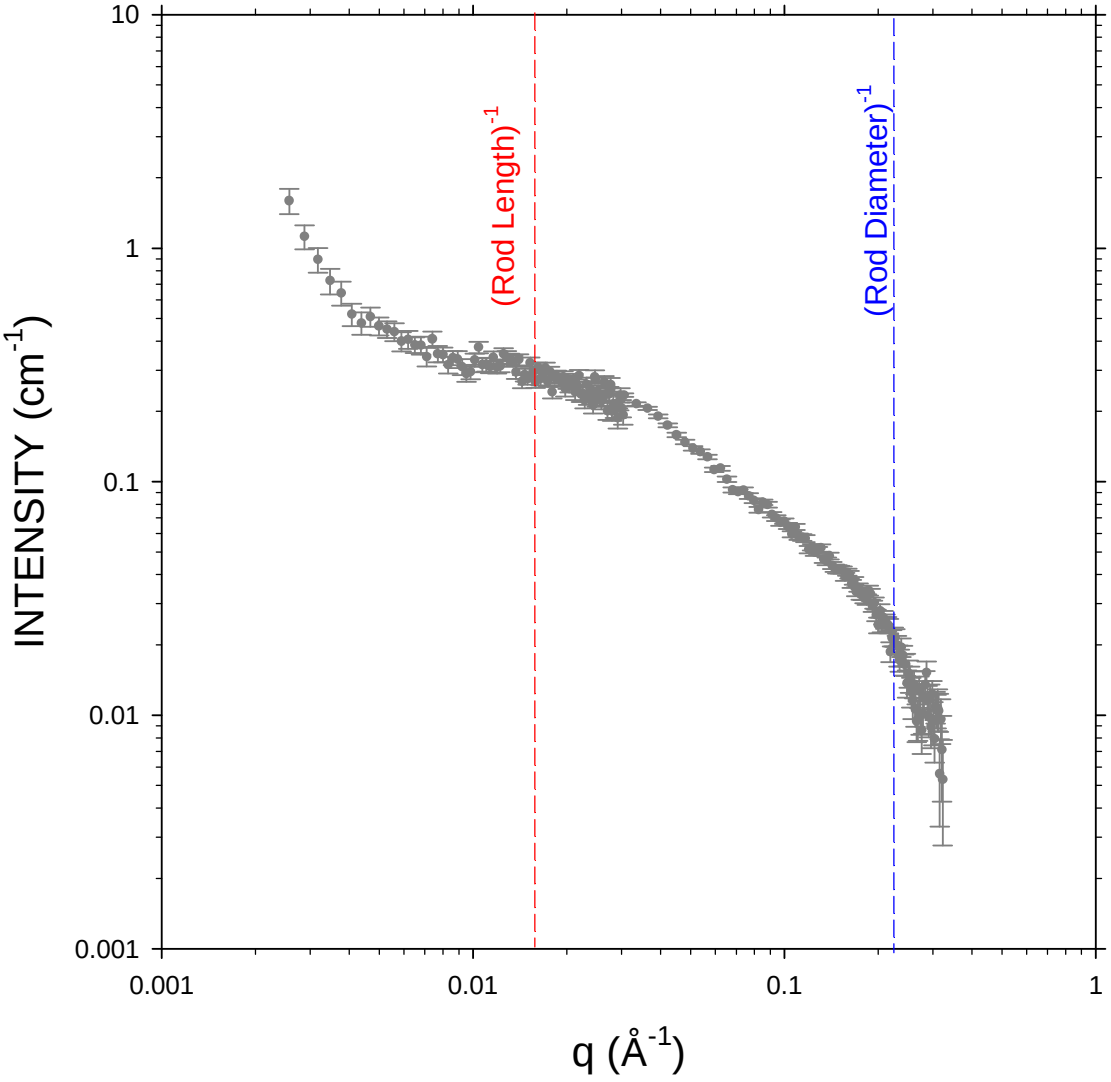

Figure 35. Intensity versus q for Polymer 20k in pure d-IBA at 55 °C. The red and blue dashed lines correspond to the inverse of the length and diameter of the rod, respectively.

The apparent stiffness of a polymer chain can be characterized by the ratio of the Kuhn length (b) to the contour length (L). The Kuhn length is defined as twice the persistence length of the polymer chain,[67] which is an intrinsic stiffness of the molecule. The contour length represents the maximum end-to-end distance of the polymer chain. A metal link chain is often used as an easily visualized example of these distances. The individual metal links would be the Kuhn length and the contour length would be the total chain length. When $b \approx L$, the chain behaves as a rigid rod and when $b/L \approx 0$ the polymer chain can be considered a coil. Between these two extremes, polymers exist as wormlike molecules, visualized as soft cylinders with varying stiffness. This behavior can be visualized as the difference between fishing line and cotton thread. Cotton thread has a low stiffness and forms a coil. Fishing line is still soft, but has more intrinsic stiffness than the thread and is a good example of a wormlike model. Figures 36 and 37 show plots of the ratio of b/L to the slope of the mid-q region. The figures show that an inference about the stiffness of the chains can be made by looking at the slope instead of only fitting a model to the data, which is problematic at times.

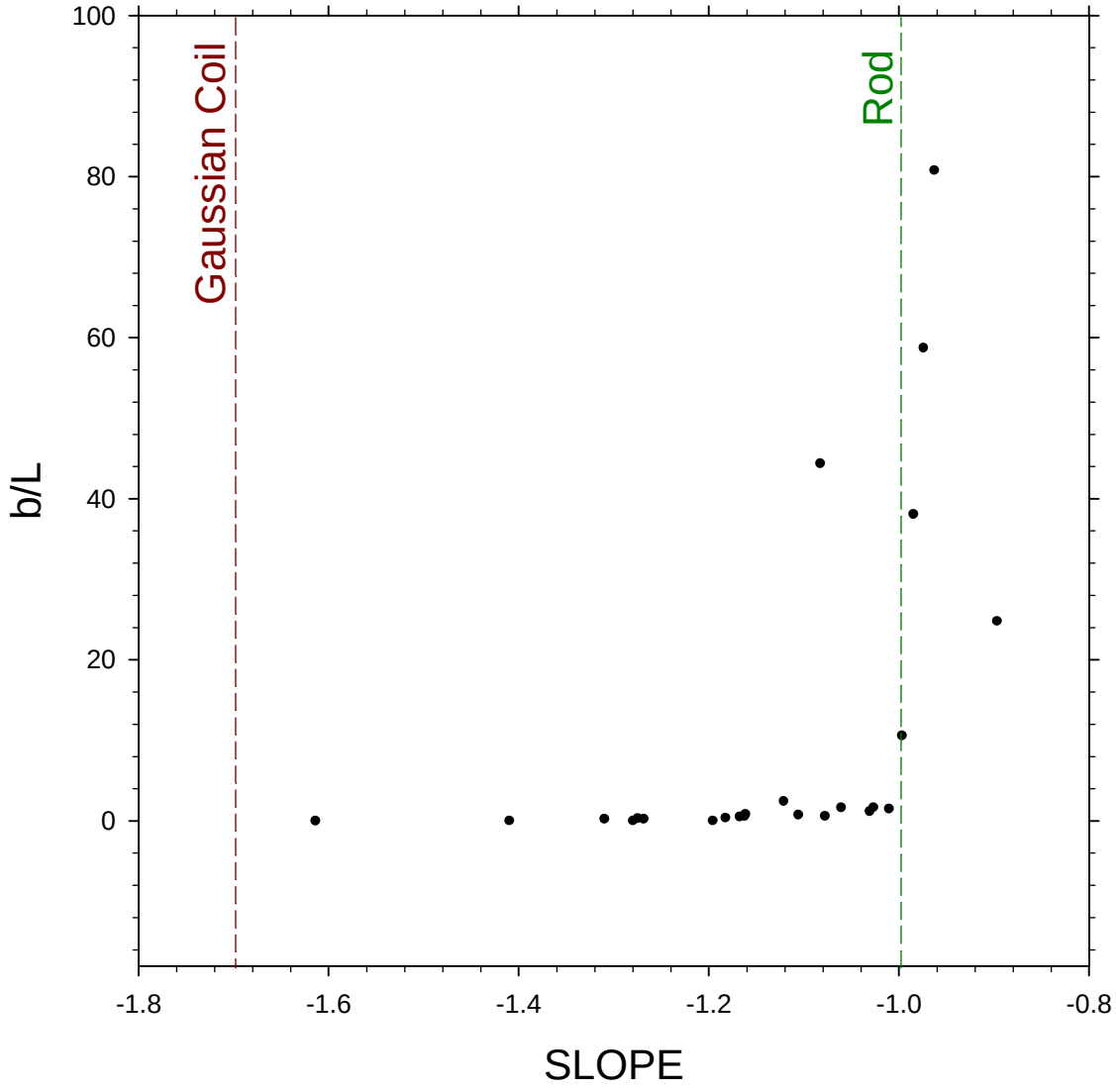

Figure 36. Graph showing the stiffness of a polymer chain compared to the slope in the fractal region of the scattering curve. These points are from fitting to the worm-like chain model carried out on Run 2 for Polymer 20k and Polymer 337k.

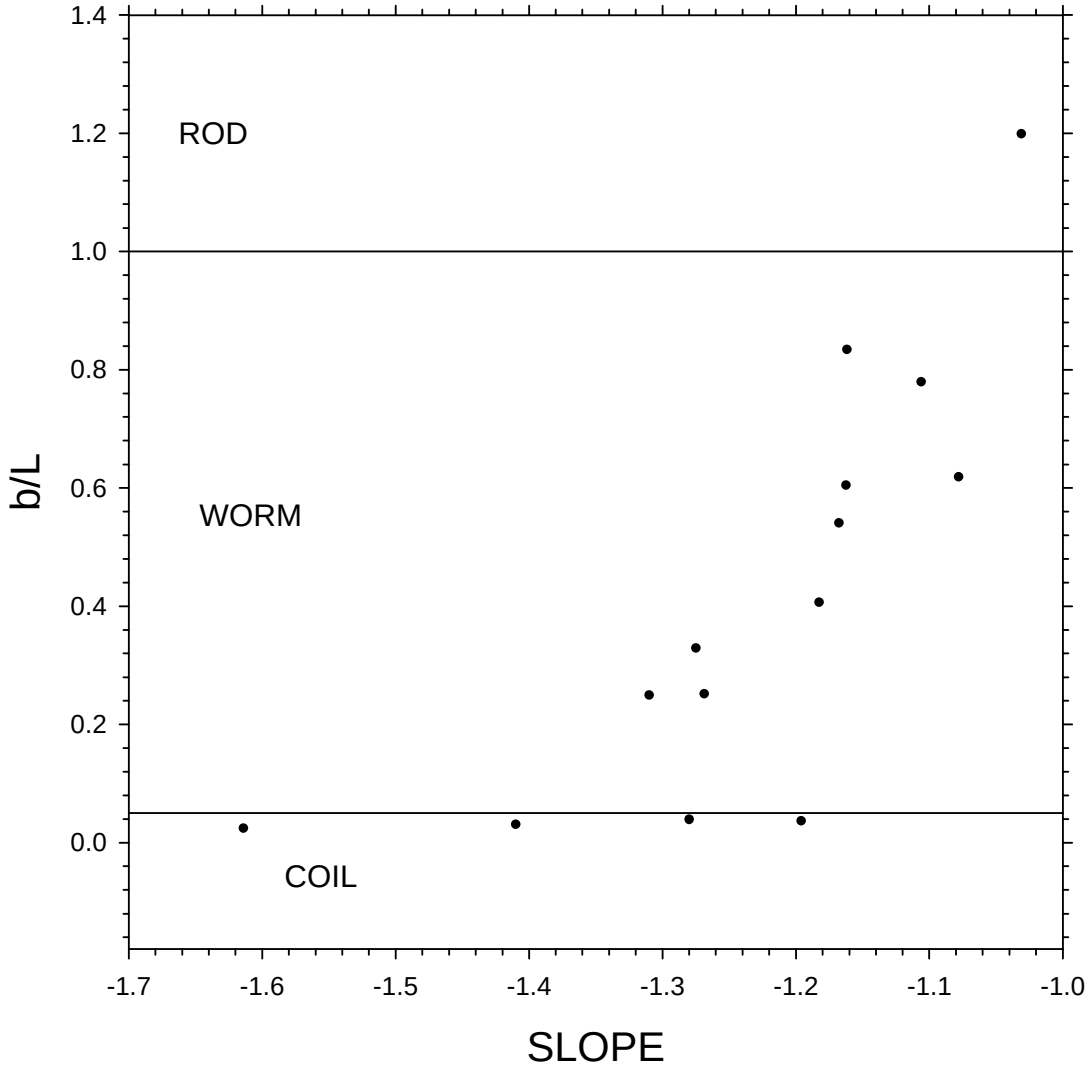

Figure 37. Graph of b/L versus slope showing only the region of b/L < 1.2 for Polymer 20k and Polymer 337k. General classifications are listed at the left of the curve.

Scattering curves can also be analyzed by carefully plotting the scattering data in such a way that it forms a straight line and using the slope or intercept of the line to obtain molecular parameters. A commonly used example of this technique is Guinier analysis.[68] The scattering intensity is plotted in terms of log[I(q)] versus q^2. The slope of this line is equivalent to $R_g^2/3$. This technique, however, requires that the molecules be dilute and non-interacting.

Run 1

Run 1 was analyzed using Guinier fits to measure the radius of gyration of the molecules in solution. The R_g values are listed in the following table. In addition to the Guinier fits, the slopes of the mid-q range were measured as well, and the q ranges and the chi-squared values of the fits are given in the table. Because of the problems with this run, as mentioned in the experimental section, further analysis of these data was not attempted.

Table 13. Radius of gyration of polymer and mid-q slope for SANS, Run 1. Samples are described in Table 3. Uncertainties are given as one standard deviation.

Sample	Temp (°C)	R_g (Å)	qR_g	Slope	q Range	X^2
>C1	43	32.8 ± 0.7	0.70-1.55	-1.1806 ± 0.01	0.021-0.1595	6.5
>C1	45	32.6 ± 0.6	0.69-1.54	-1.267 ± 0.009	0.0278-0.2957	8
>C1	49	33.0 ± 0.7	0.7-1.56	-1.175 ± 0.01	0.017-0.2236	8
<C1	43	10.1 ± 0.4	0.61-1.51	-0.67 ± 0.02	0.0376-0.2817	1.45
<C1	45	10.7 ± 0.6	0.85-1.47	-0.72 ± 0.01	0.02127-0.2817	4.7
<C1	49	9.8 ± 0.5	0.82-1.50	-0.77 ± 0.02	0.02127-0.331	4
C1	45	22.6 ± 0.5	0.48-1.59	-1.08 ± 0.01	0.0377-0.33613	1.9
C1	49	23.4 ± 0.5	0.50-1.56	-1.06 ± 0.01	0.0278-0.2675	3.8
>C2	43	77.8 ± 2.5	0.78-1.45	-1.39 ± 0.01	0.0278-0.2675	1.9
>C2	45	88.6 ± 2.3	0.89-1.66	-1.18 ± 0.02	0.0278-0.3012	1.2
>C2	49	93.0 ± 2.3	0.94-1.64	-1.23 ± 0.01	0.0278-0.3012	1
<C2	43	10.3 ± 3.6	0.32-0.82	-0.48 ± 0.04	0.0278-0.3012	1
<C2	45	19.4 ± 2.7	0.60-1.55	-0.039 ± 0.04	0.0278-0.3012	1
<C2	49	25.1 ± 4.7	0.53-1.43	-0.49 ± 0.05	0.0278-0.3012	0.8
C2	45	43.6 ± 6.1	0.93-1.64	-0.45 ± 0.02	0.0278-0.3012	1.1
C2	49	29.7 ± 8.7	0.63-1.12	-0.62 ± 0.04	0.0278-0.3012	0.9

Run 2

The scattering data were fitted to the worm-like model, the results of which are shown below in Table 14. The slope of the mid-q region for each run was also measured and listed in Table 15. As shown in Figure 35, a correlation between the slope and the stiffness of the chain from model fitting can be used to characterize the stiffness of the molecules directly. The data shows a dramatic stiffening of the PEO with increasing IBA content. Two samples were also studied in a weak acid (deuterated acetic acid) and showed no signs of stiffness.

Table 14. Fitting parameters from the worm-like model for SANS, Run 2. The samples are described with the abbreviation P20k meaning Polymer 20k etc. The uncertainties are given as one standard deviation.

Sample	Temperature (°C)	Contour Length (L) (Å)	Kuhn Length (b) (Å)	Radius (Å)	I(0) (cm^{-1})
A P20k 0.30 IBA	55				
	45				
	43				
	40				
	30	52 ± 1	13 ± 1	3.3 ± 0.1	164 ± 35
B P20k 0.39 IBA	55				
	45				
	43				
	40				
	30				
C P20k 0.46 IBA	55	278 ± 3	168 ± 6	4.2 ± 0.1	61 ± 8
	45	344 ± 5	186 ± 6	4.2 ± 0.1	13 ± 4
	43	304 ± 5	237 ± 11	4.1 ± 0.1	10 ± 3
	40	248 ± 4	415 ± 32	4.3 ± 0.1	14 ± 5
	30	114 ± 12	1208 ± 155	4.7 ± 0.1	17 ± 5
D P337k 0.30 IBA	55				
	45				
	43				
	40				
	30				
E P337k 0.39 IBA	55				
	45				
	43				
	40				
	30				
F P337k 0.46 IBA	55	325 ± 6	107 ± 5	2.9 ± 0.1	20 ± 4
	45	505 ± 19	126 ± 5	2.9 ± 0.1	5 ± 1
	43	473 ± 12	119 ± 4	2.9 ± 0.1	8 ± 1
	40	342 ± 7	139 ± 6	3.0 ± 0.1	11 ± 2
	30	181 ± 4	112 ± 9	3.3 ± 0.1	20 ± 4

Sample	Temperature (°C)	Contour Length (L) (Å)	Kuhn Length (b) (Å)	Radius (Å)	I(0) (cm^{-1})
G P20k D_2O	55	616 ± 9	15 ± 1	2.9 ± 0.1	19 ± 6
	45				
	43				
	40				
	30	519 ± 12	16 ± 1	2.8 ± 0.1	35 ± 15
H P20k IBA	55	127 ± 2	314 ± 55	5.2 ± 0.1	6 ± 3
	45	161 ± 2	247 ± 22	5.2 ± 0.1	228 ± 15
	43	155 ± 2	261 ± 27	5.2 ± 0.1	10 ± 2
	40	161 ± 2	193 ± 15	5.1 ± 0.1	15 ± 3
	30	163 ± 3	136 ± 11	5.1 ± 0.1	7 ± 4
I P337k D_2O	55	461 ± 6	17 ± 1	2.8 ± 0.1	11 ± 1
	45				
	43				
	40				
	30	433 ± 8	17 ± 1	2.7 ± 0.1	15 ± 1
J P337k IBA	55	218 ± 6	5412 ± 31	4.4 ± 0.1	80 ± 10
	45	177 ± 4	7857 ± 30	4.5 ± 0.1	96 ± 17
	43	149 ± 2	12039± 15	4.7 ± 0.1	140 ± 30
	40	123 ± 1	4685 ± 95	4.9 ± 0.3	29 ± 6
	30	128 ± 3	7522± 236	5.0 ± 0.1	130 ± 26
1 P20k Acetic Acid	55	310 ± 4	31 ± 1	2.9 ± 0.1	3 ± 1
	45				
	43	322 ± 3	29 ± 1	2.9 ± 0.1	3 ± 1
	40				
	25	311 ± 4	29 ± 1	2.9 ± 0.1	5 ± 1
2 P20k 0.39 Acetic Acid	55	407 ± 3	24 ± 1	3.3 ± 0.1	45684 ±
	45				
	43	408 ± 3	25 ± 1	3.3 ± 0.1	40054 ±
	40				
	25	390 ± 9	25 ± 3	3.3 ± 0.1	2968 ± 97

Table 15. Mid-q slopes and R_g values for SANS, Run 2. Samples are described in Table 14 of this chapter. R_g was calculated using Guinier fits where applicable. Blanks indicate no Guinier region or a slope, indicating no free chains. Uncertainties are given as one standard deviation.

Sample	Temperature (^oC)	Slope	q range	χ^2	R_g (Å)
A	30	-0.314 ± 0.008	0.0297-0.143	2.6	
	40	-0.30 ± 0.01	0.1676-0.1562	1.7	
	43	-0.31 ± 0.01	0.1676-0.1562	2.3	
	45	-0.25 ± 0.01	0.1676-0.1562	2.5	
	55	-0.37 ± 0.01	0.1676-0.1562	1.3	
B	30	-0.722 ± 0.005	0.02189-0.1919	3.2	
	40	-0.29 ± 0.01	0.02189-0.1919	1.3	
	43	-0.555 ± 0.005	0.01857-0.1783	1.3	
	45	-0.531 ± 0.007	0.01857-0.1783	1.5	
	55	-0.653 ± 0.006	0.01857-0.1783	2.1	
C	30	-0.997 ± 0.007	0.0228-0.1865	2.6	44 ± 1
	40	-1.061 ± 0.005	0.02280-0.1865	1.1	60 ± 1
	43	-1.106 ± 0.005	0.02069-0.1865	1.7	51 ± 1
	45	-1.1678 ± 0.005	0.02069-0.1865	1.4	51 ± 1
	55	-1.1625 ± 0.005	0.02069-0.1892	1.6	49.2 ± 0.6
D	30	-0.53 ± 0.01	0.01797-0.1475	1.5	
	40	-0.52 ± 0.01	0.01797-0.1475	1.6	
	43	-0.51 ± 0.01	0.01797-0.1475	1.7	
	45	-0.51 ± 0.01	0.01797-0.1475	1.3	
	55	-0.43 ± 0.01	0.01797-0.1475	1.3	

Sample	Temperature (^{o}C)	Slope	q range	χ^2	R_g (Å)
E	30	-1.00 ± 0.01	0.03343-0.2135	2.6	
	40	-0.976 ± 0.005	0.01767-0.2081	1.8	
	43	-0.998 ± 0.006	0.01767-0.1783	1.4	
	45	-0.981 ± 0.006	0.01767-0.1783	1.4	
	55	-1.009 ± 0.005	0.01767-0.1617	1.3	
F	30	-1.078 ± 0.008	0.0231-0.2108	2.1	101 ± 5
	40	-1.183 ± 0.007	0.01857-0.1783	1.6	104 ± 3
	43	-1.269 ± 0.008	0.01857-0.1783	1.3	100 ± 2
	45	-1.310 ± 0.008	0.01857-0.1783	0.9	114 ± 2
	55	-1.275 ± 0.008	0.01857-0.1783	1.5	77 ± 2
G	30	-1.41 ± 0.01	0.03923-0.1783	1.4	43 ± 1
	43	-1.64 ± 0.01	0.02343-0.1783	8	43.2 ± 0.6
	55	-1.614 ± 0.006	0.02343-0.1783	5	45.7 ± 0.6
H	30	-1.162 ± 0.008	0.03343-0.2188	1.4	42.4 ± 0.9
	40	-1.031 ± 0.006	0.02853-0.2188	1.3	40.6 ± 0.9
	43	-1.027 ± 0.005	0.0231-0.1865	1.5	42.3 ± 0.8
	45	-1.011 ± 0.005	0.02038-0.2081	1.8	41.1 ± 0.8
	55	-1.122 ± 0.006	0.02974-0.2268	2.3	38 ± 1
I	30	-1.28 ± 0.01	0.02612-0.2733	1.4	
	43	-1.20 ± 0.01	0.02612-0.2733	1.8	
	55	-1.196 ± 0.003	0.02974-0.2733	1.8	
	30	-0.97 ± 0.01	0.02552-0.2001	1.5	101 ± 5

Sample	Temperature (°C)	Slope	q range	χ^2	R_g (Å)
J	40	-0.985 ± 0.008	0.02552-0.2215	1.9	92 ± 2
	43	-0.963 ± 0.008	0.02552-0.2215	1.5	120 ± 7
	45	-1.083 ± 0.009	0.02552-0.2215	1.5	109 ± 7
	55	-0.897 ± 0.007	0.02431-0.2425	1.5	102 ± 6
1	25	-1.440 ± 0.006	0.03483-0.3944	1.7	43.4 ± 0.7
	43	-1.343 ± 0.005	0.03641-0.3845	1.1	43 ± 1
	55	-1.452 ± 0.006	0.0407-0.3977	1.5	45 ± 1
2	25	-1.699 ± 0.005	0.0407-0.401	3.4	43.7 ± 0.7
	43	-1.645 ± 0.005	0.0407-0.3845	1.8	44.5 ± 0.5
	55	-1.701 ± 0.005	0.0407-0.3805	3.5	42.0 ± 0.3

Run 3

Run 3 was analyzed using the worm-like and Debye models to find the stiffness and R_g of the polymer molecule. Additional Guinier fits were also used to find R_g. The method of analysis used is listed in the table. The results are listed in Table 16 below. Samples 1-5, the pH runs, all show coil-like behavior. This indicates that the stiffness seen in scattering Run 2 was not caused by a pH change. Model equations could not be fitted to Polymer 252k in the binary IBA solutions.

Table 16. Fitting parameters from SANS Run 3. Blank lines indicate no model could be fitted to the data. Guinier fits were attempted for runs at 43 °C. Uncertainties are given as one standard deviation.

Sample	Temperature (°C)	Contour Length (Å)	Kuhn Length (Å)	Radius (Å)	R_g (Å)	Mid-q Slope	Model Used
1 P20k DCl	25	713 ± 67	9.7 ± 1.3	3.4 ± 1.5	41.7 ± 0.2	-1.7	Worm and Debye
2 P20k 0.001 DCl	25	846 ± 50	6.3 ± 1.1	3.0 ± 1.3	39.6 ± 0.4	-1.7	Worm and Debye
3 P20k NaOD	25					-0.3	N/A
4 P20k 0.001 NaOD	25	520 ± 14	18.5 ±0.5	2.4 ± 0.4	48 ± 1	-1.4	Worm and Guinier
5 P20k D_2O + NaCl	25	885 ± 36	8.4 ± 0.4	5.6 ± 1.7	45.2 ± 0.4	-1.84	Worm and Debye
7 P252k 0.46 IBA	43					-0.60	N/A
	55					-0.62	N/A
8 P252k D_2O	43	2100 ± 200	10 ± 1	8.4 ± 0.4	90 ± 1	-1.95	Worm and Guinier
	55	2349 ± 285	8.9 ± 0.5	9.4 ± 0.5	81.7 ±0.04	-2.0	Worm and Debye
9 P252k Acetic Acid	43	1400 ± 200	10 ± 2	5.8 ± 0.4	62 ± 1	-1.65	Worm and Guinier
	55	1745 ± 229	7.7 ± 0.6	3.6 ± 1.5	62.8 ± 0.4	-1.7	Worm and Debye
10 P252k 0.30 IBA	43				56 ± 5	-0.9	Guinier
	55				49 ± 5	-0.77	Guinier
11 P252k 0.39 IBA	43					-0.92	

Sample	Temperature (°C)	Contour Length (Å)	Kuhn Length (Å)	Radius (Å)	R_g (Å)	Mid-q Slope	Model Used
	55				71 ± 4	-1.45	Guinier
12 P4k Acetic Acid	43	184 ± 32	8 ± 18	5.7 ± 4.8	16.1 ± 0.4	-1.65	Worm and Guinier
	55	196 ± 19	7.0 ± 0.9	3.8 ± 1.8	17.5 ± 0.2	-1.62	Worm and Debye

Run 4 is significant in that, for the first time, a strong temperature dependence was seen. All of the molecular weights showed small b/L ratios except for Sample E, which had a low mid-q slope (<1.0) which may indicate that the fit was not reliable.

Table 17. Fitting parameters from SANS Run 4. Uncertainties are given as one standard deviation.

Sample	Temperature (^{o}C)	Contour Length (Å)	Kuhn Length (Å)	Radius (Å)	R_g (Å)	Mid-q Slope	Model Used
A P4k IBA	60	187 ± 15	12.0 ± 0.3	1.4 ± 0.4	13.6 ± 0.1	-1.21	Worm-like and Debye
B P20k IBA	60	672 ± 10	13.2 ± 0.2	1.5 ± 0.5	45.7 ± 0.3	-1.32	Worm-like and Debye
C P252k IBA	60	3629 ± 27	126 ± 0.6	1.5 ± 0.6	117.7 ± 0.8	-1.56	Worm-like and Debye
D P337k IBA	60	5695 ± 74	13.0 ± 0.3	1.7 ± 0.4	160.4 ± 0.6	-1.5	Worm-like and Debye
E P4k 0.39 IBA	60	33.8 ± 0.8	530 ± 6	3.3 ± 0.2	13.9 ± 0.6	-0.95	Worm-like and Guinier
F P20k 0.39 IBA	60	367 ± 1	12.9 ± 0.7	1.3 ± 0.4	34.4 ± 0.2	-1.47	Worm-like and Debye
G P252k 0.39 IBA	60					-0.44	N/A
H P337k 0.39 IBA	60					-1.49	N/A
I P4k D_2O	60	105 ± 1	13.3 ± 0.1	3.0 ± 0.1	15.9 ± 0.1	-1.73	Worm-like and Debye
K P252k D_2O	60	5127 ± 188	19.0 ± 0.4	4.2 ± 0.1	148.3 ± 0.8	-1.8	Worm-like and Debye
L P337k D_2O	60	5689 ± 194	20.5 ± 0.5	4.2 ± 0.1	200.4 ± 0.9	-1.8	Worm-like and Debye
M P20k Butyric Acid	60	571 ± 14	12.3 ± 0.4	1.3 ± 0.3	44.5 ± 0.2	-1.4	Worm-like and Debye

Temperature Effects

Temperature often plays a major role in the behavior of polymer solutions. The following figures show the effect of temperature upon the molecular parameters of the PEO molecules in solution. Figure 38 shows the ratio of Kuhn length to contour length for Polymer 20k and Polymer 337k in pure D_2O and d-IBA as a function of temperature (data from Runs 2 and 3). Because of the scale difference, Polymer 337k in d-IBA is plotted against the axis on the right. As mentioned earlier, a ratio of Kuhn length to contour length greater than one indicates a rigid polymer that acts as a rod. In D_2O, both polymers showed a very small b/L ratio, which indicates that the molecule is the soft coil expected in water. In the IBA, however, the ratio of b/L is much higher. Polymer 20k is within two standard deviations of 1.0 at 30 ^oC and appears to increase in stiffness with temperature up to 55 ^oC, with a maximum ratio of 2.4. Polymer 337k had a much higher b/L ratio; the low temperature data were noisy but appear to be decreasing in the temperature range of 30-55 ^oC. All of the points in this range were, however, well above 1.0, indicating a rod.

The most striking feature of the figure is seen at 60 ^oC. The D_2O samples maintained a low ratio consistently through the entire temperature range. The d-IBA samples, however, showed a dramatic decrease in their b/L ratios at 60 ^oC. Polymer 20k and Polymer 337k showed a decrease of over 99% between their value at 55 and 60 ^oC, from 2.5 to 0.02 and 25 to 0.003, respectively. These numbers compare well with the ratio found for the polymer in pure D_2O at the same temperature of 0.024 for Polymer 20k at 55 ^oC (this sample was not studied in D_2O at 60 ^oC) and 0.0036 for

Polymer 337k in D_2O at 60 ^oC. This decrease indicates that the polymer undergoes a rod to coil transition between 55 and 60 ^oC. Polymers 4k and 252k showed similar ratios expected for a coil in pure d-IBA at 60 ^oC. They were not included in Figure 38 because there were not enough data to observe a trend.

Figure 37 above showed a correlation between the slope of the fractal regime and the behavior of the molecule. Figure 39 shows the slope of Polymer 337k and Polymer 20k versus temperature. When compared to Figure 38 it can be seen that using only the value of the slope to measure the stiffness of the polymer does not appear to hold rigorously. Both polymer samples in pure IBA have slopes near that expected of a rod (-1), but Polymer 337k had a surprisingly high slope in D_2O. All of the samples, with the exception of Polymer 20k in D_2O, which was not studied at 60 ^oC, showed a decrease in slope at 60 ^oC, indicating a relative decrease in chain stiffness, as seen in Figure 38.

Another parameter available from fitting the worm-like model to the data is the radius of the worm-like particle. Figure 40 shows the radius of the "worm" as a function of temperature for Polymer 20k and Polymer 337k in D_2O and d-IBA, as a function of temperature. Both samples showed a lower radius in D_2O than they did in d-IBA, about 2.8 versus 5 in d-IBA. Interestingly, at 60 ^oC, the radius for both polymer samples in d-IBA showed a dramatic decrease to a radius of approximately 1.5.

Polymer 337k in D_2O showed an increase in radius at 60 ^0C. Similar behavior was also seen in Polymer 4k and Polymer 252k in D_2O at this temperature (Run 4). All of the polymer samples in D_2O at 60 ^oC also showed a slope lower (<-1.81) than

that expected of a normal chain with excluded volume (-1.67) (see Figure 39). Polymer chains in a theta solvent will have a slope of -2.0, and the lower slope may indicate that the solvent quality was changing with temperature.

The cylinder model[6,65] was used to find the dimensions of the rod in pure d-IBA. This method was used to find the rod length instead of using the location of the turndown as described earlier, because the logarithmic scale made the uncertainties in the "turndown method" too large to use for comparison, since the dimensions for these samples are not greatly different for different molecular weights. The model could not be fitted to the data from the mixed solvent samples, thus allowing the effects of temperature and molecular weight to be observed, but not the effect of concentration. Figure 41 shows the length of the rod as a function of temperature. In this case the error bars represent a 95% confidence interval (1.95 standard deviations), unlike all of the other figures which show only one standard deviation. As expected, Polymer 337k has a longer rod length than Polymer 20k, about 190 Å versus 150 Å. There was no obvious variation of rod length with temperature when the uncertainties are taken into account.

The measured radius of the worm-like molecule was also seen to change drastically with the stiffness ratio (see Figure 43), while the PEO samples in D_2O showed a small increase in radius at 60 ^oC when compared to their values below 60 ^oC. It is apparent that as the molecule becomes stiffer, the radius of the wormlike molecule increases. This further supports the assertion that the polymer is forming a helix in IBA, since the rod formation coincides with a thickening that could be caused by the "winding" of the helix.

In summary, the system has shown no significant temperature effects in the range of 30-55 ^{o}C. Above 60 ^{o}C, however, a significant change in the molecular behavior was observed. The PEO molecule undergoes what appears to be a rod to coil transition between 55 and 60 ^{o}C in d-IBA, with the stiffness ratio of the molecule approaching that seen in D_2O. Further evidence of the transition from a rod-like particle to a coil can be found by looking at the lack of a Porod turndown seen in the pure d-IBA samples below 60 ^{o}C in Runs 2 and 3, but not seen in Run 4 (see Figure 42). A Porod turndown occurs when there is a strong contrast between the solvent and the scattering particle; SANS does not reach a high enough q to probe the interface of a coil.

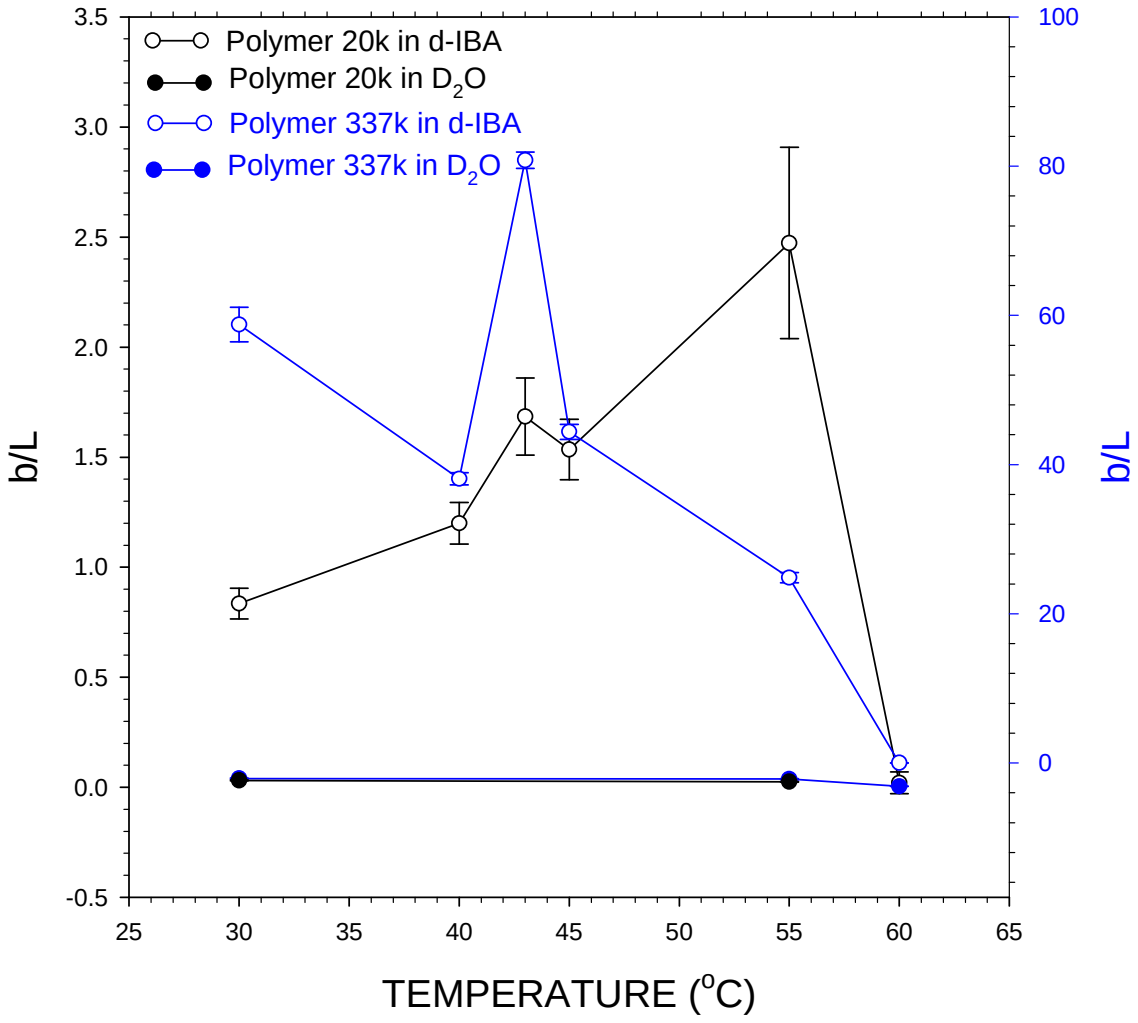

Figure 38. Ratios of Kuhn length to contour length of Polymer 20k and Polymer 337k as a function of temperature. Polymer 337k uses the right hand axis (blue) and the axis on the left is for Polymer 20k. Error bars are one standard deviation.

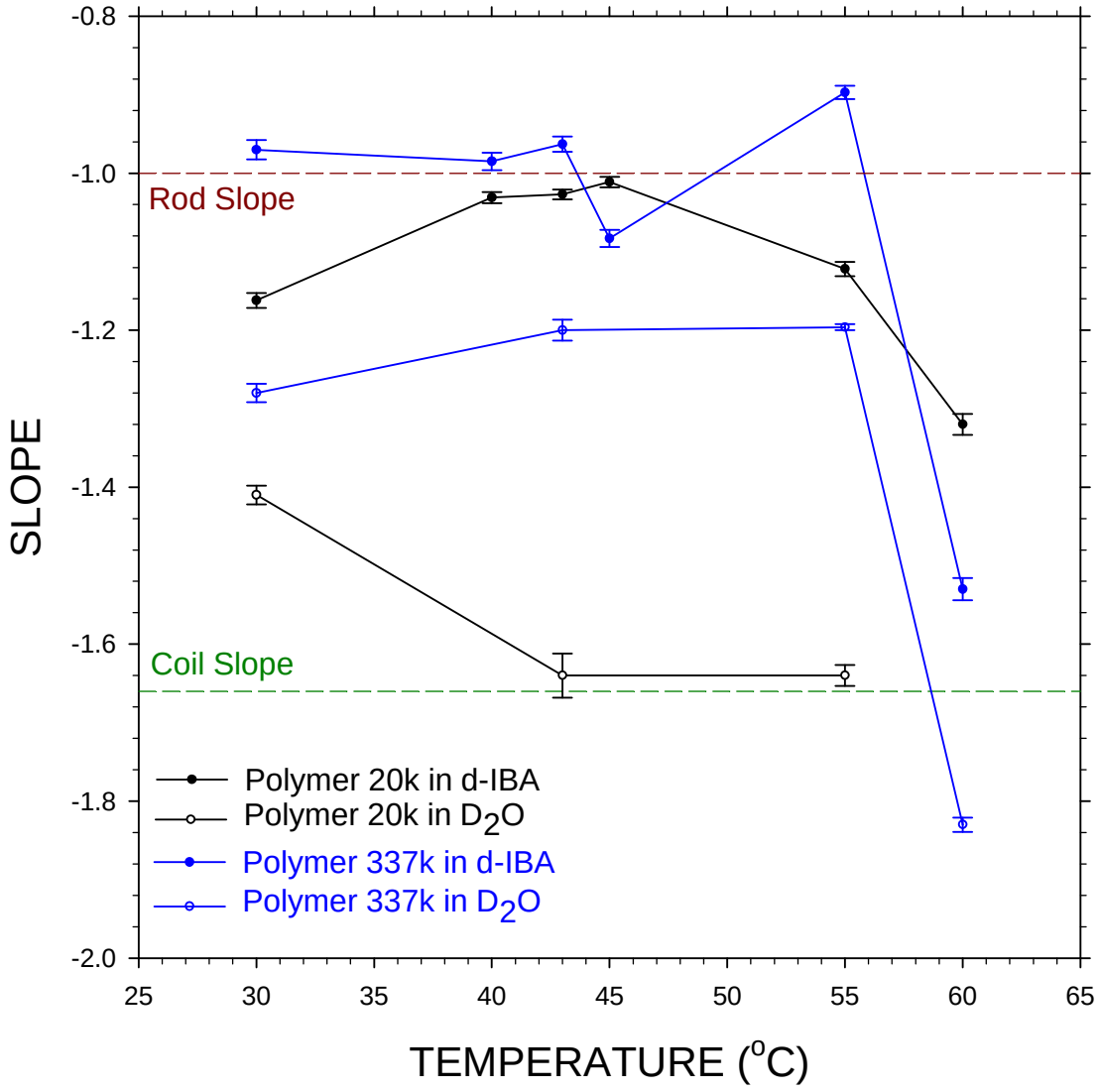

Figure 39. Slope of the mid-q region of the scattering curve as a function of temperature for Polymer 20k and Polymer 337k. Error bars represent one standard deviation.

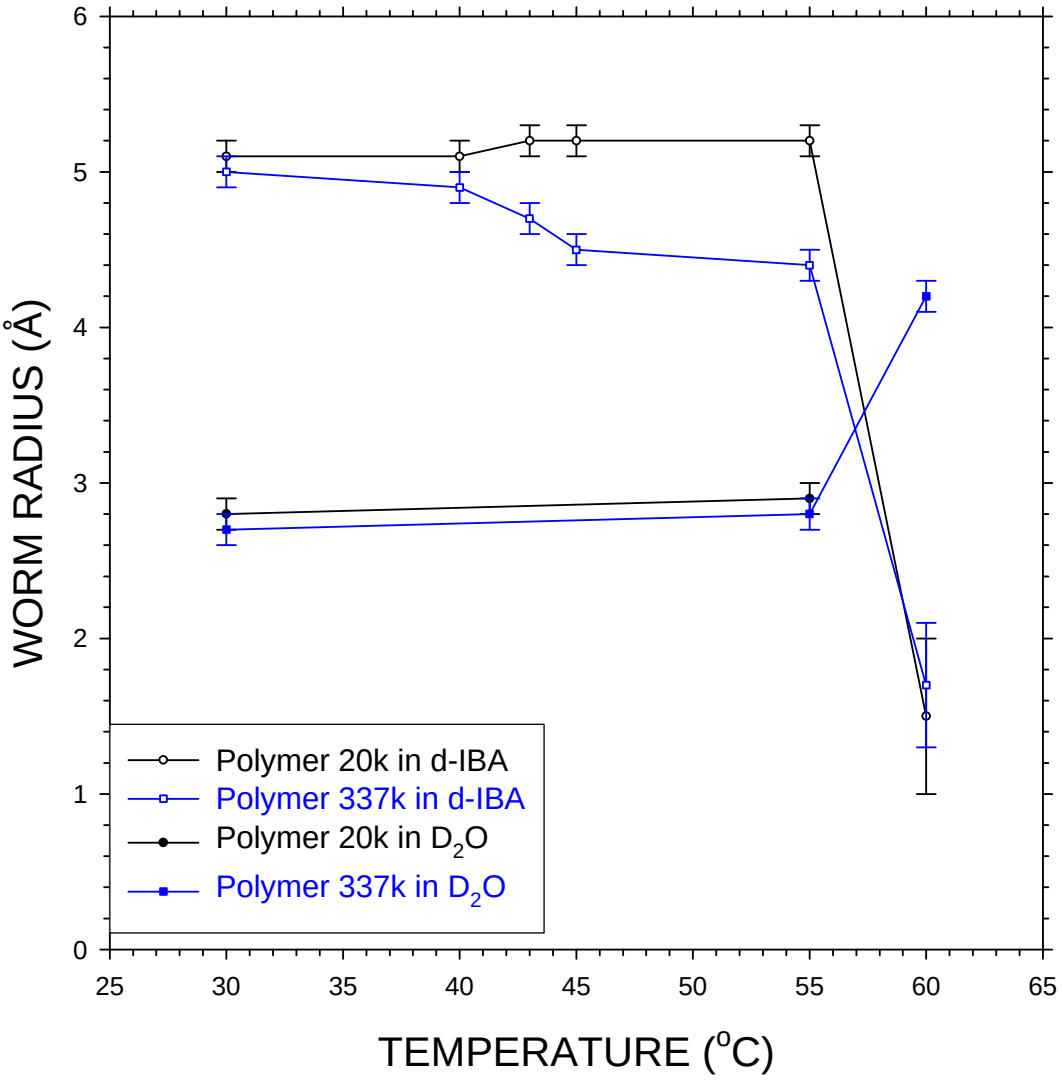

Figure 40. Radius of the worm-like molecule as a function of temperature for Polymer 20k and Polymer 337k in D_2O and d-IBA. Error bars are one standard deviation.

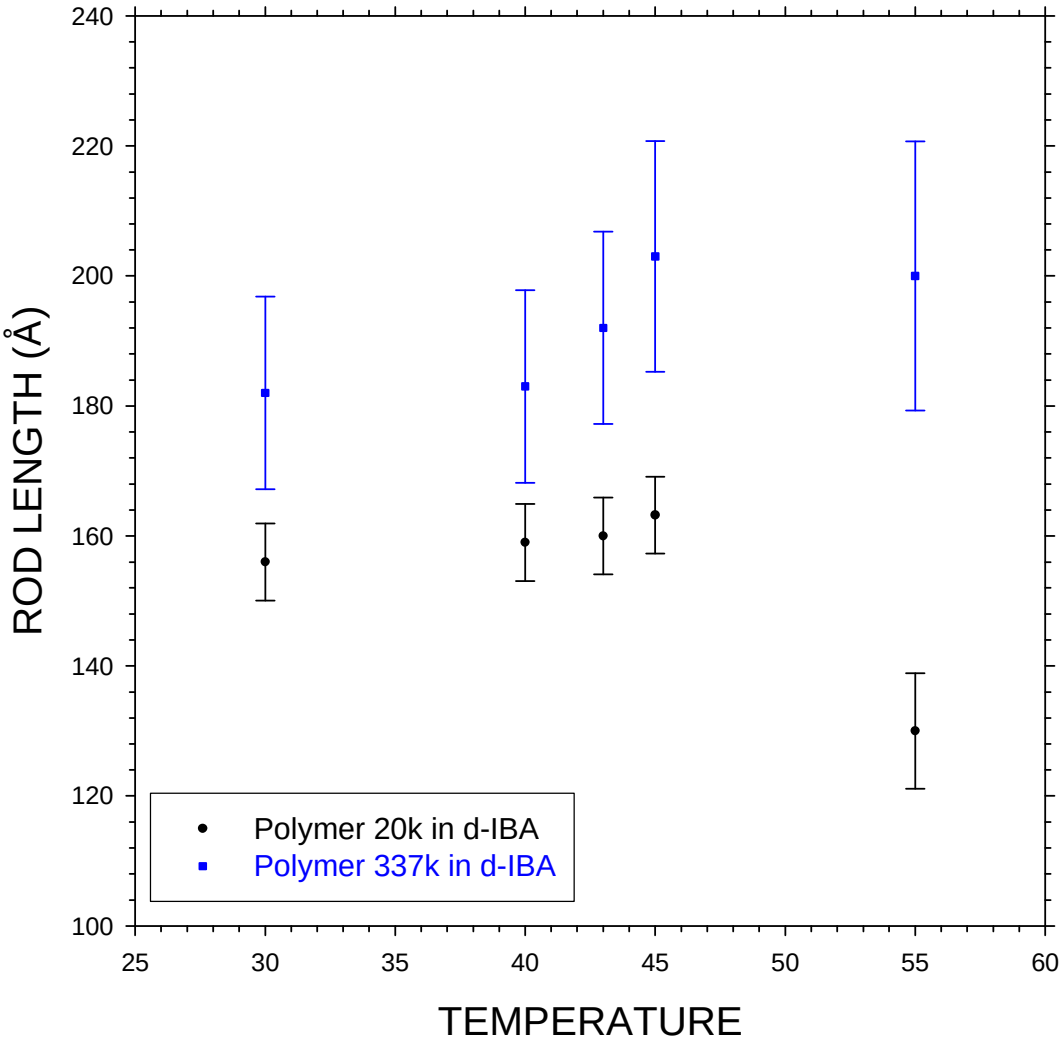

Figure 41. Rod length of Polymer 20k and Polymer 337k in d-IBA as a function of temperature. Error bars represent a 95% confidence interval.

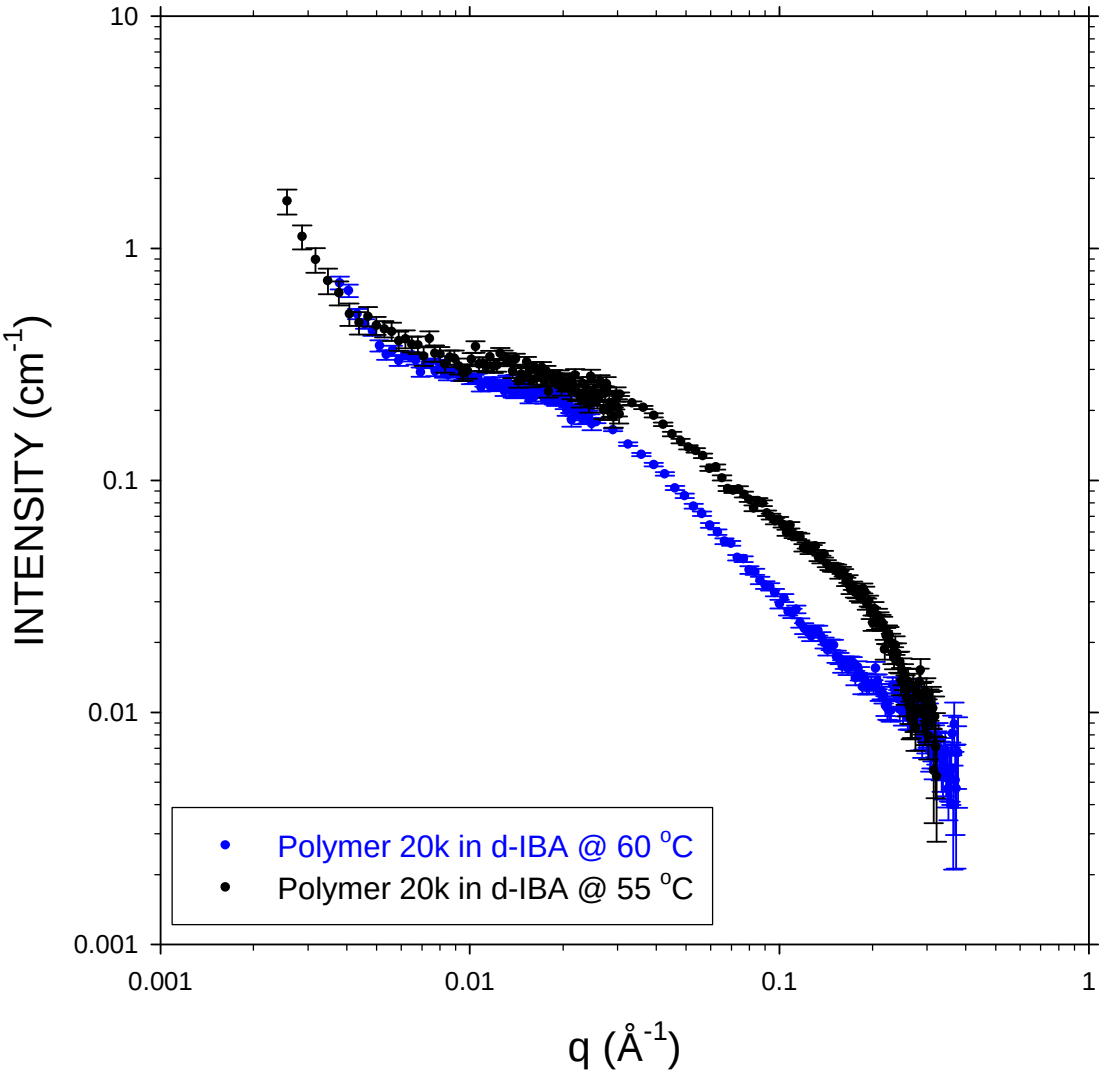

Figure 42. Scattering intensity curves for Polymer 20k in d-IBA. Note the Porod turndown at q = 0.11 Å^{-1} at 50 °C, but no turndown at 60 °C. The turndown indicates scattering from end features of a rod and the absence of a turndown indicates a coil configuration.

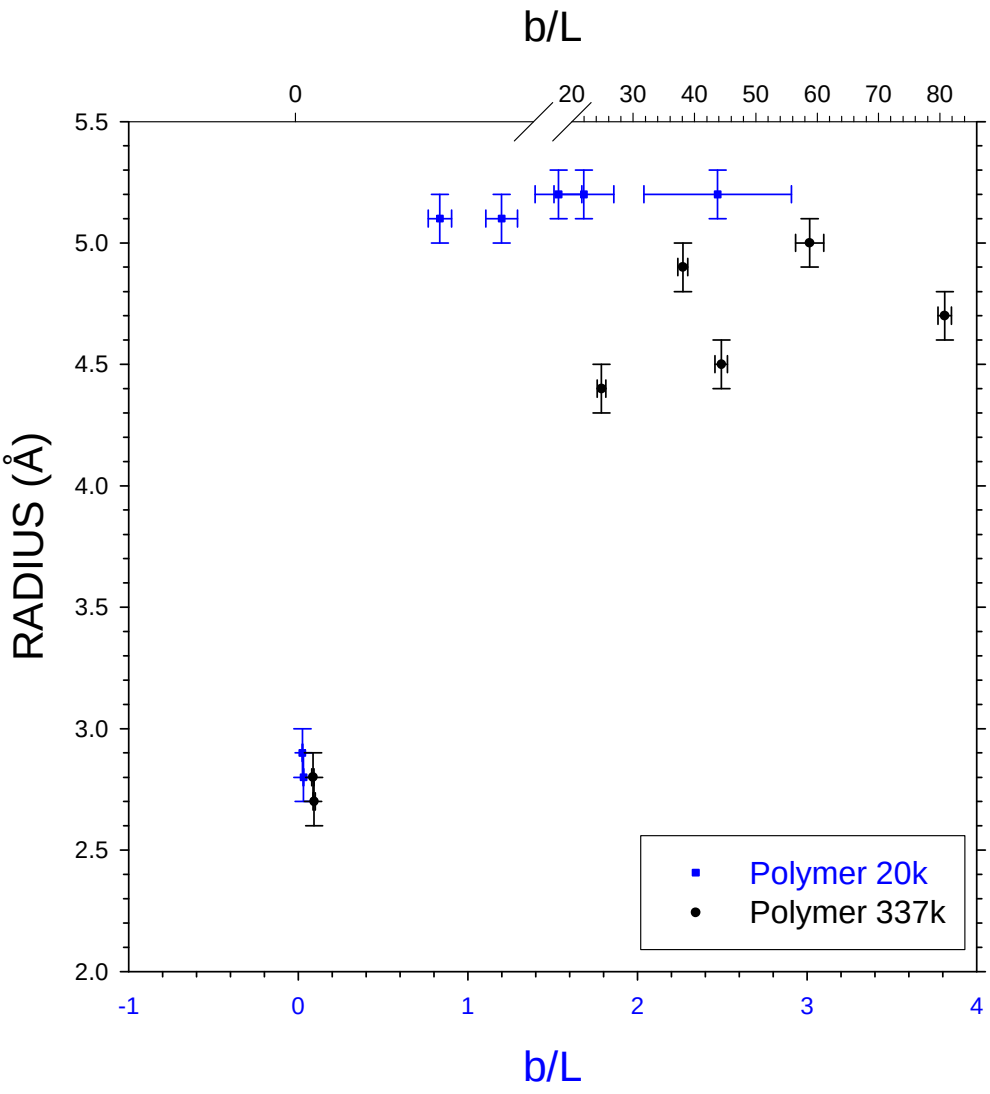

Figure 43. Radius as a function of stiffness ratio for Polymer 20k and Polymer 337k. In order to show both samples on the same graph Polymer 20k uses the bottom axis (blue) and Polymer 337k uses the top axis. Error bars indicated one standard deviation

Solvent Effects

The solvent composition was also varied to see the effect on the molecular behavior. Figure 45 shows the stiffness ratio as a function of IBA mass fraction for Polymer 20k and 337k at 30 and 55 ^{o}C. Because of the scaling, it is very difficult to see the trend clearly, so Figure 46 omits the point for Polymer 337k in pure d-IBA and the point for Polymer 20k in a solution with a mass fraction of 0.46 d-IBA, which appears to be an outlier. Clearly, the stiffness of the polymer chain increases linearly with increasing d-IBA content. A dramatic representation of this effect is seen in Figure 44, which shows Polymer 20k in pure D_2O and pure d-IBA at 43 ^{o}C. The polymer in pure d-IBA coincides almost perfectly with the line having a slope of -1. A Porod turndown is also seen in the d-IBA sample but not in the D_2O sample.

The radius of the worm-like particle was also plotted as a function of solvent composition for Polymer 337k and Polymer 20k at 30 ^{o}C in Figure 47. Figure 43 above, showed a decrease in worm radius for the polymers in d-IBA after the rod to coil transition. In Figure 47, a coil to rod transition is occurring, now driven by solvent composition instead of temperature. As the amount of d-IBA is increased, the radius of the worm-like particle increased to around 5 Å.

Figure 48 shows R_g values, found by non-linear fitting of the Debye model[6] as a function of molecular weight for D_2O, d-IBA, and a critical mixture (where possible), at 60 ^{o}C. At this temperature it has been shown that even in pure d-IBA, the polymer behaves as a coil and not a rod. Of particular note is the fact that R_g is higher in D_2O than in d-IBA, indicating that D_2O is a better solvent for PEO at this temperature. Only two points were able to be fitted for the mixed solvent, but the R_g

value for Polymer 20k in the binary solvent is less than R_g in either pure solvent. This behavior is not unexpected and could be explained by preferential adsorption, discussed in the Prior Work section on polymers in binary solvents.[43] A polymer can preferentially adsorb a solvent, creating a solvent shell. This solvent shell then attracts other monomers, leading to a net contraction.

In addition to d-IBA and D_2O, polymer samples were studied in Runs 2-4 in d-acetic acid and d-butyric acid, and in solutions of a strong acid (DCl) and a strong base (NaOD). As indicated in Tables 14, 16, and 17, these samples all behaved as standard coils, with none of the stiffness associated with the d-IBA solutions. However, for d-butyric acid the only measurement was made at 60 ^oC, above the observed rod to coil transition, so the behavior in d-butyric acid will need to be revisited at lower temperatures. The acidic and basic solutions appear to rule out conclusively that this effect is caused by a pH change, since a wide range of pH was covered with no sign of rod-like behavior.

As mentioned in the Introduction, the cause of PEO clustering is not well understood. Several authors contend that clustering is caused by impurities,[16] while others have seen the clustering regardless of water purity.[32] Figures 49 and 50 show the low-q region of the scattering curves for Polymer 4k and Polymer 20k. In Figure 49, the sample in pure d-IBA shows a flat low-q region, indicating a lack of aggregates. As the water concentration is increased, the low-q upturn signifying aggregation appears and becomes larger as the water increases. Figure 50 shows Polymer 20k in pure d-IBA, pure d-butyric acid, and a binary solvent of D_2O and a mass fraction of d-IBA of 0.39. In the pure d-IBA solution, there is an aggregation

upturn, indicating that some of the aggregation is inevitable with increasing molecular weight, but the aggregation upturn was smaller than that seen in the D_2O sample. These two figures strongly indicate that PEO aggregation in water is caused by water and not impurities.

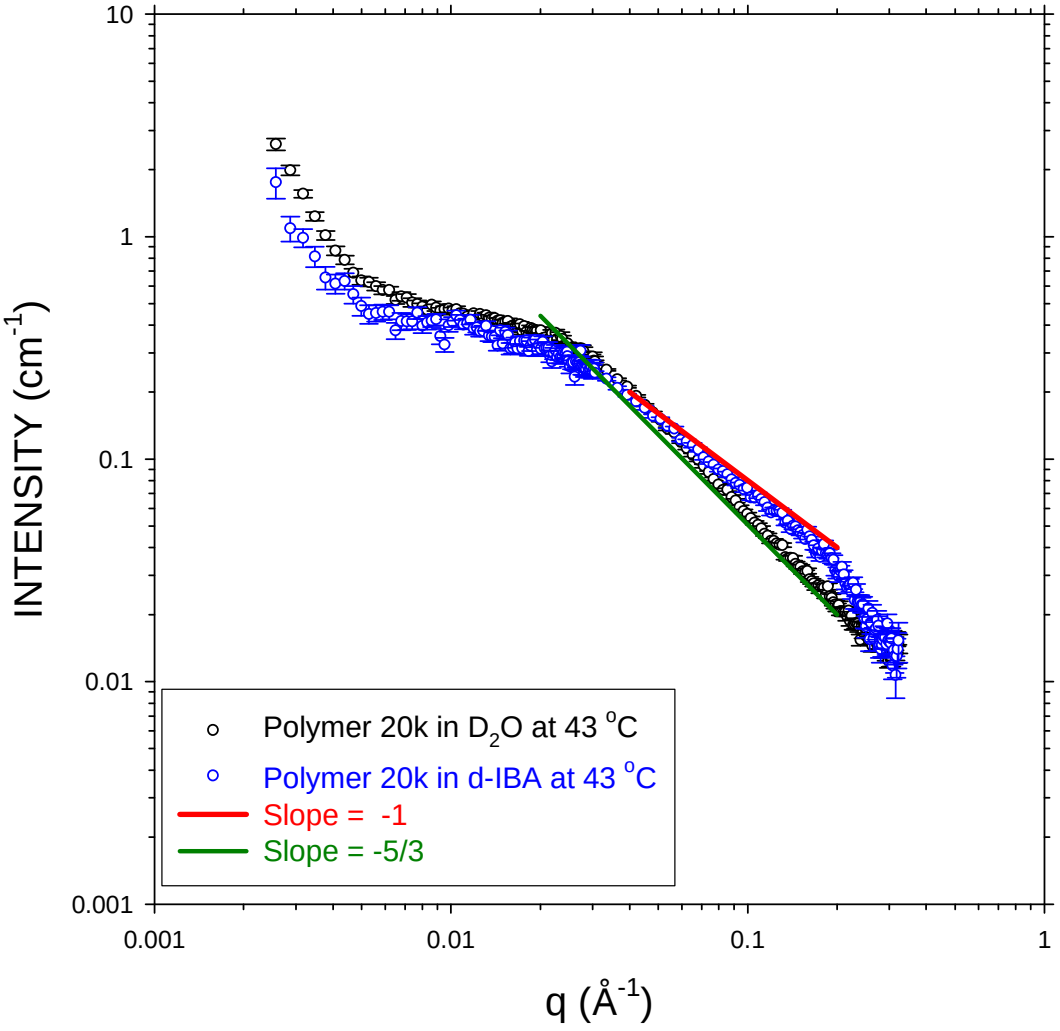

Figure 44. Polymer 20k in pure D_2O (black) and pure d-IBA (blue) with lines representing slopes of -1 (red) and -5/3 (green) overlaid on the scattering curves.

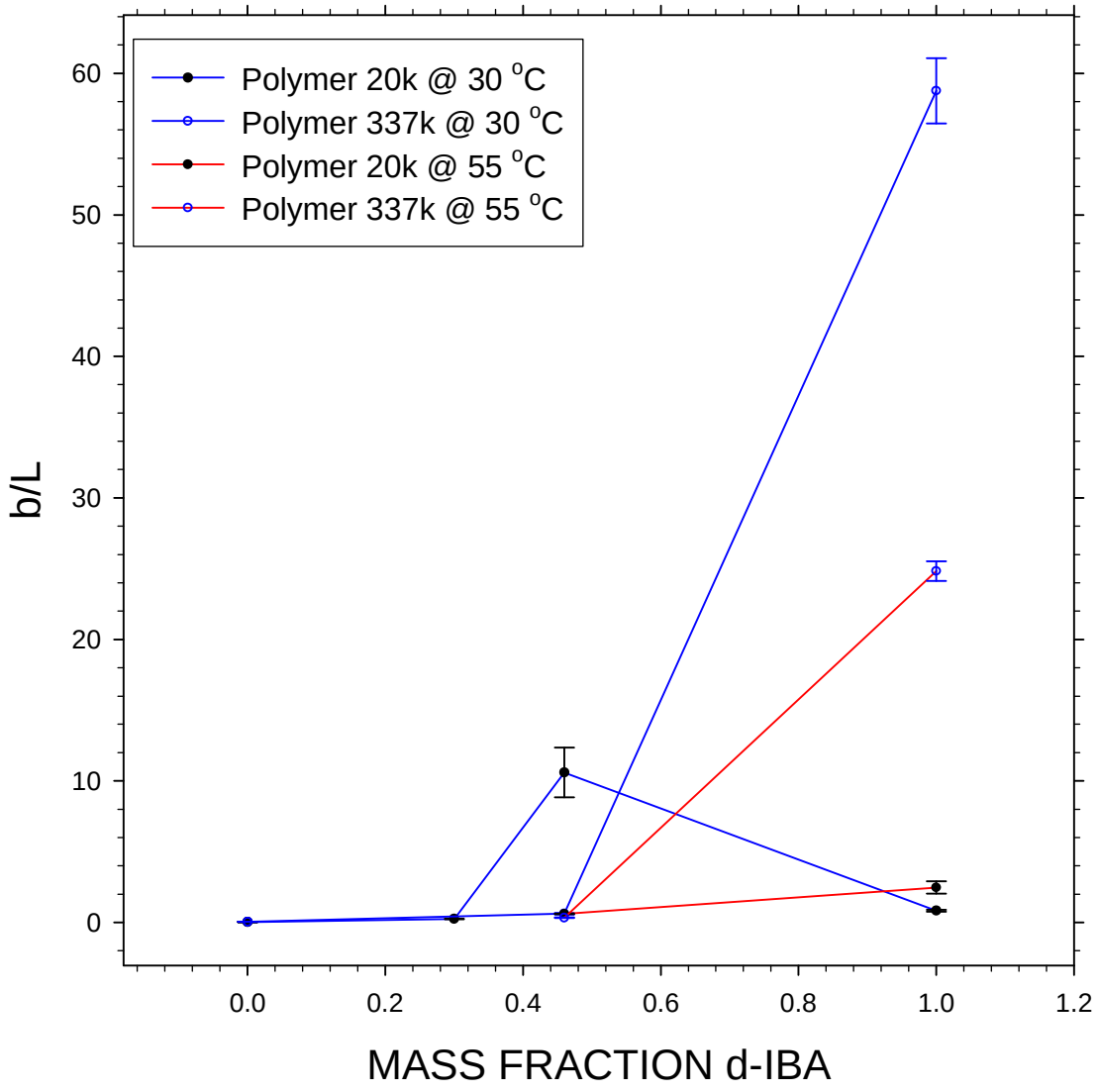

Figure 45. Stiffness ratio versus mass fraction of d-IBA for Polymer 20k and Polymer 337k at two temperatures. The error bars are one standard deviation.

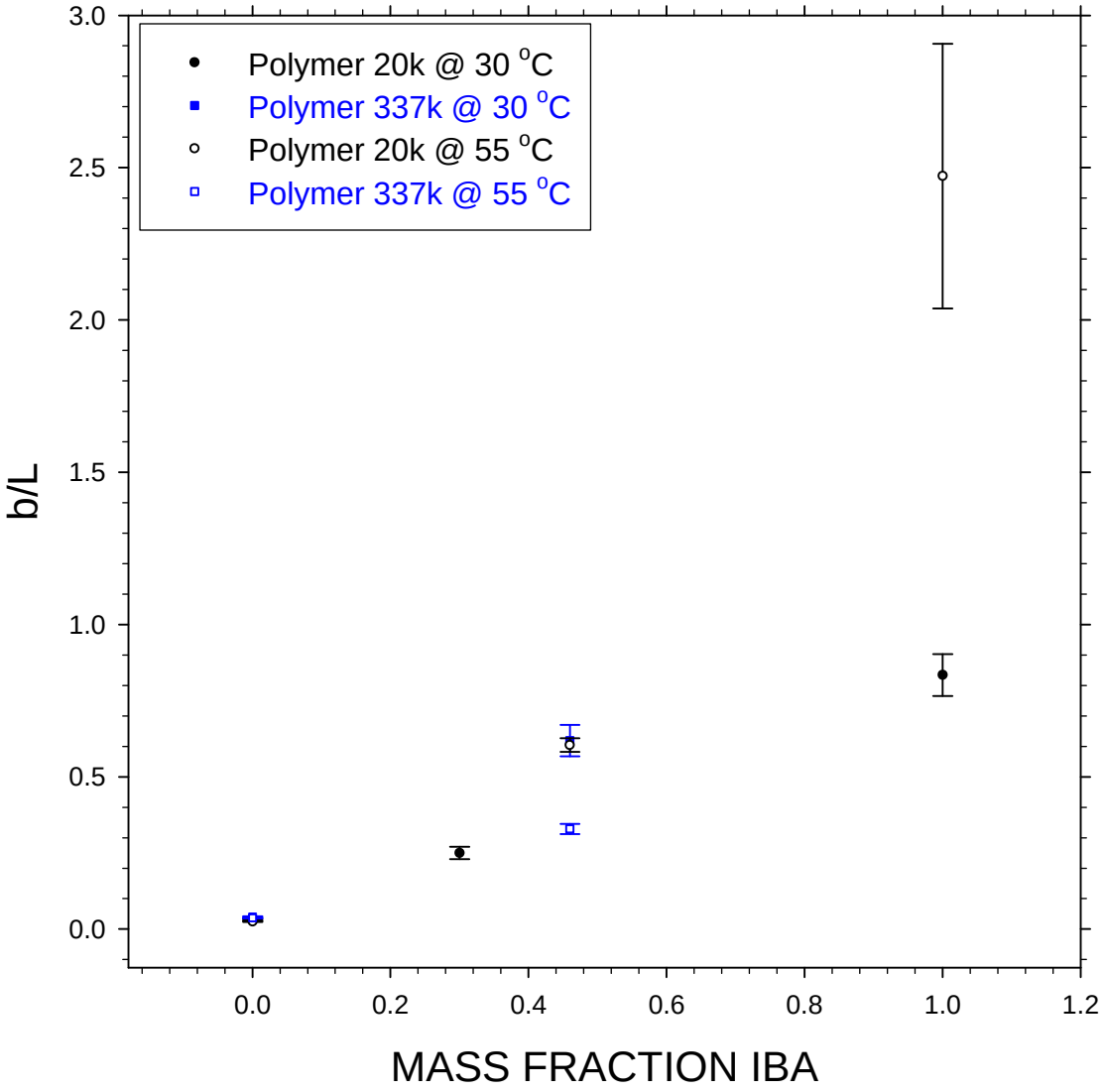

Figure 46. Stiffness ratio versus mass fraction of d-IBA for Polymer 20k and Polymer 337k at two temperatures, omitting points higher than 3.0 in order to show the trend more clearly. Error bars are one standard deviation.

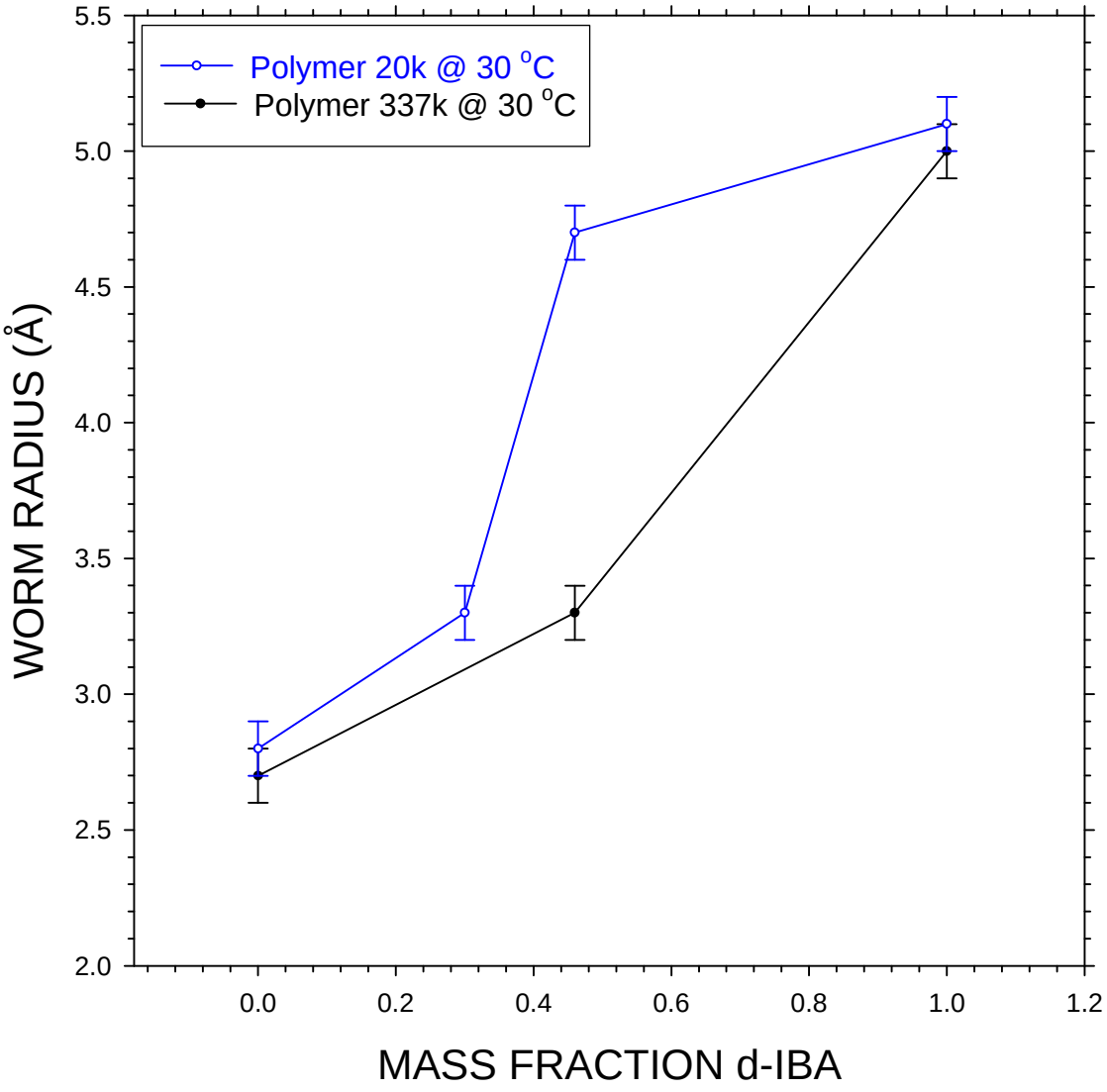

Figure 47. Radius of the worm-like molecule as function of mass fraction of d-IBA for Polymer 20k and Polymer 337k at 30 °C. Error bars are one standard deviation.

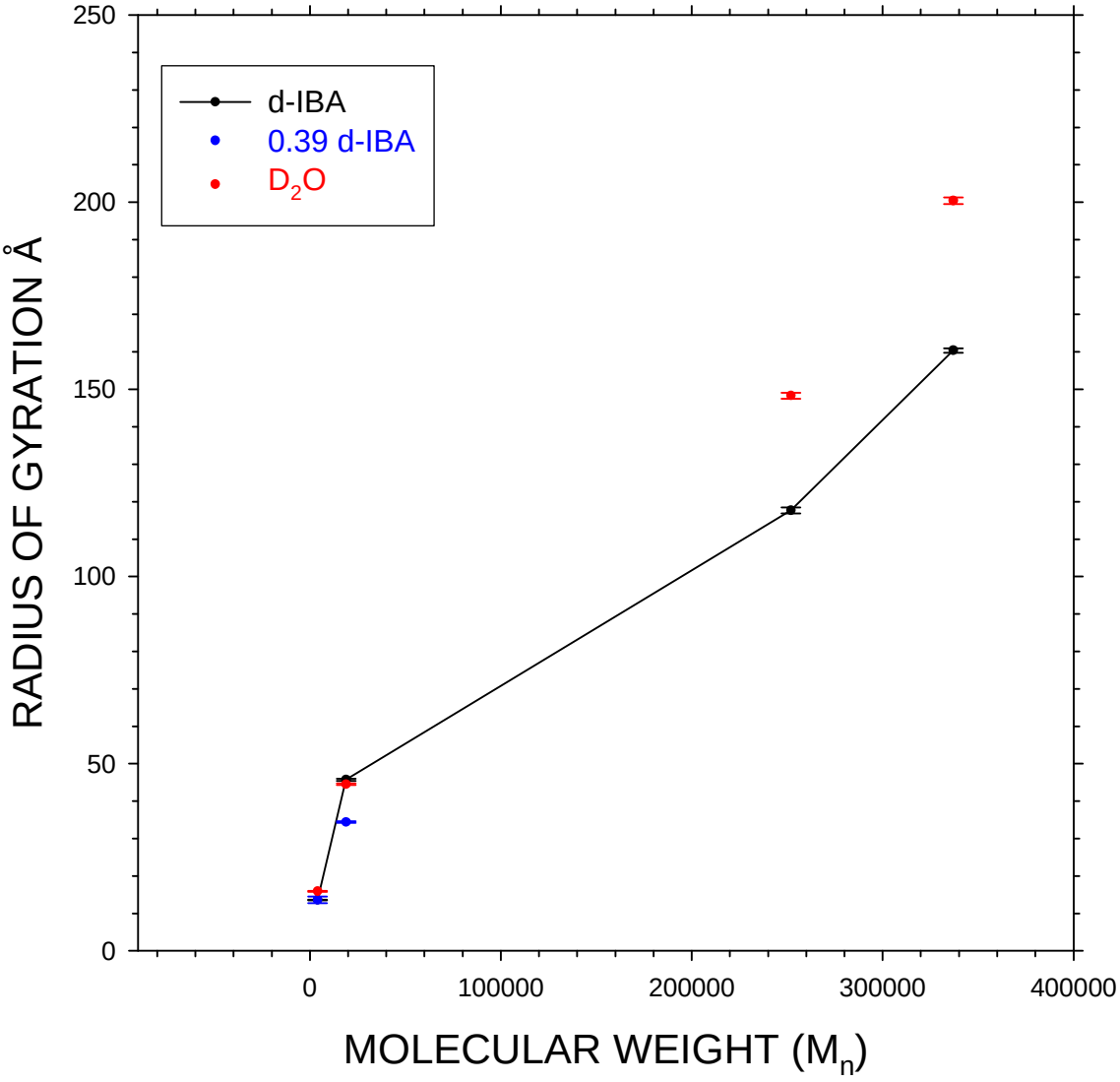

Figure 48. Radius of gyration versus molecular weight in D_2O, d-IBA, and a solvent of critical mass fraction at 60 °C. Error bars are one standard deviation.

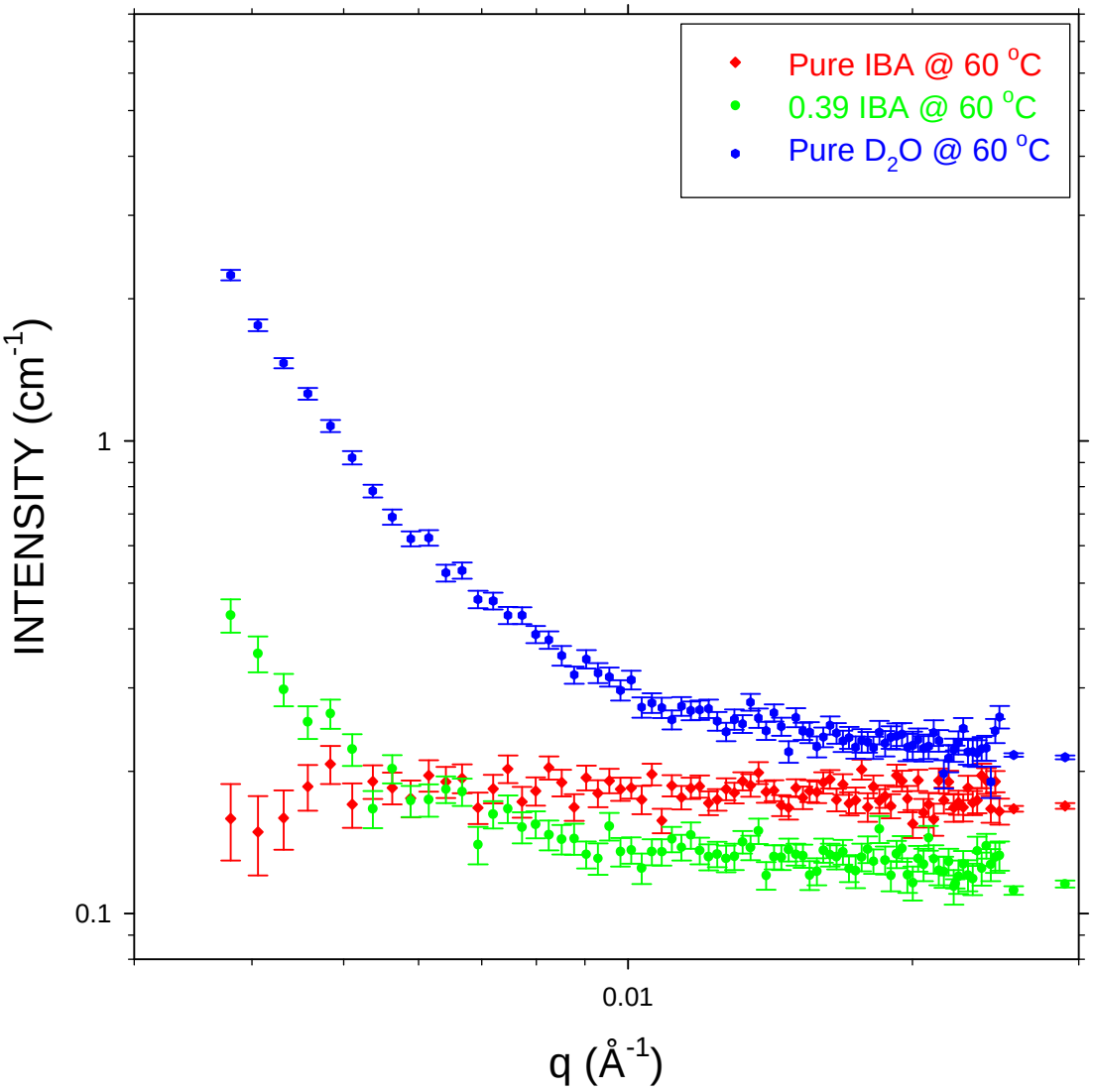

Figure 49. Low-q region of the scattering intensity curves for Polymer 4k showing the aggregation upturn.

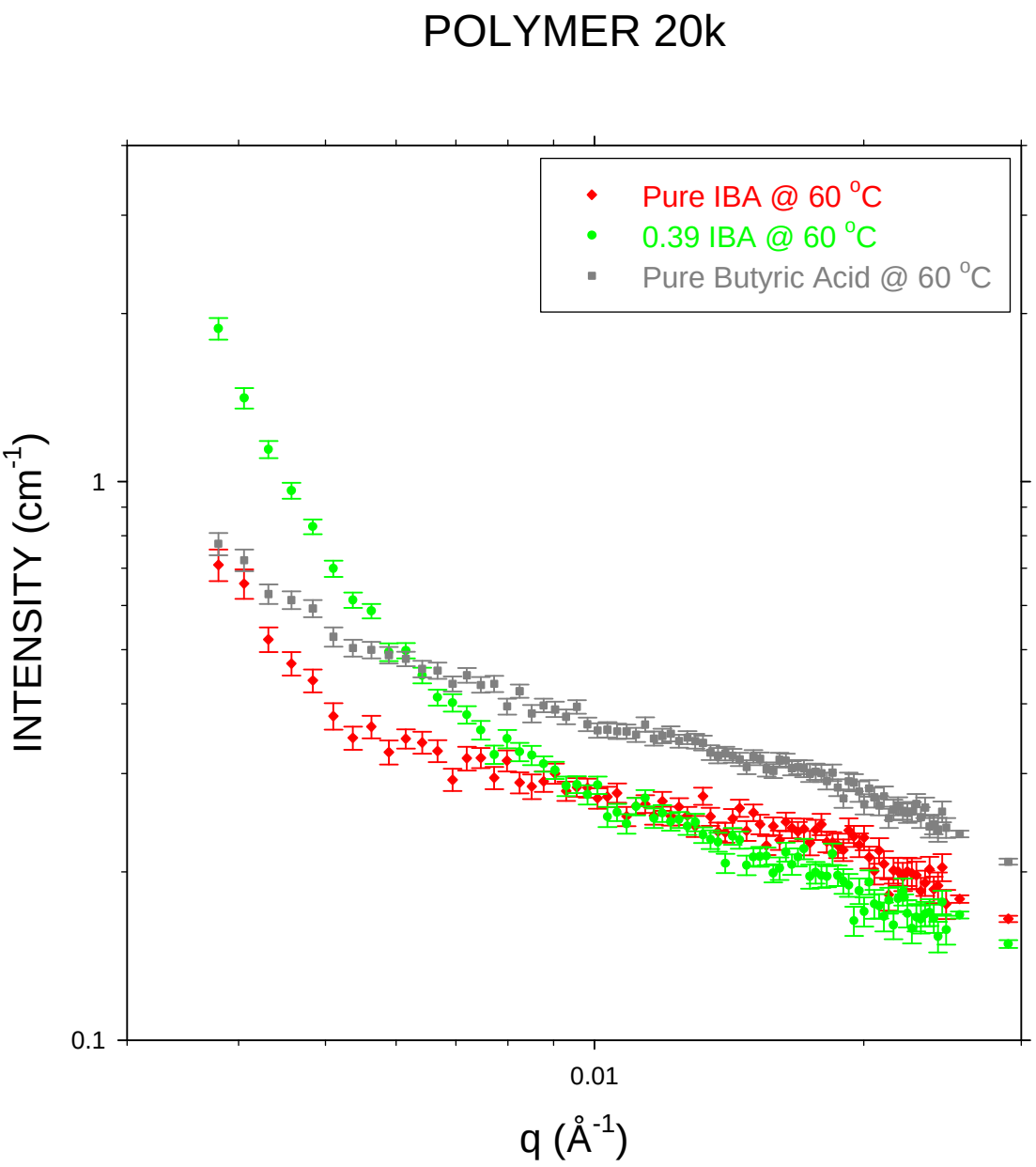

Figure 50. Low-q region of the scattering intensity curves for Polymer 20k showing the aggregation upturn.

Polarimeter

As described in the experimental section, a number of polarimetry runs were carried out to investigate whether the rods formed by PEO in IBA were helices. The solvents were hydrogenated IBA and H_2O. The rotation and sample information for each run is given in the tables below.

Run 1

In Run 1, polymer was added to pure isobutyric acid and to water. The only impurities present were those left from the solvent manufacture. Run 1 samples were not heated to 90 ^oC as was done in Run 3; see Run 3 for more information.

Table 18. Results for polarimetry, Run 1. Absolute rotation, α, and specific rotation, [α], are given. Note that Polymer 20k has a negative rotation, while Polymers 4k and 252k have positive rotations.

Sample	Polymer	Concentration (mg/mL)	Solvent	α	[α] (deg/(dm *g/mL))
I	Polymer 20k	13.6	IBA	-0.0056 ± 0.0001	-0.41
II	Polymer 4k	11.9	IBA	0.0036 ± 0.0001	0.30
III	Polymer 252k	10.5	IBA	0.0077 ± 0.0005	0.73
IV	Polymer 20k	12.7	H_2O	0.0002 ± 0.0001	0.016

All three of the PEO samples in IBA showed a small rotation above the uncertainty of the instrument. Polymer 20k in water, however, showed no statistically significant rotation. Figure 49 shows the absolute value of the specific rotations. This was done to show the apparent linear relationship between the logarithm of the molecular weight and the specific rotation. The aqueous Polymer 20k sample is shown in blue.

This logarithmic behavior occurred only for this lot of IBA. Other lots showed no rotation when PEO was added. We could not reproduce these data, but they motivated us to add chiral impurities deliberately.

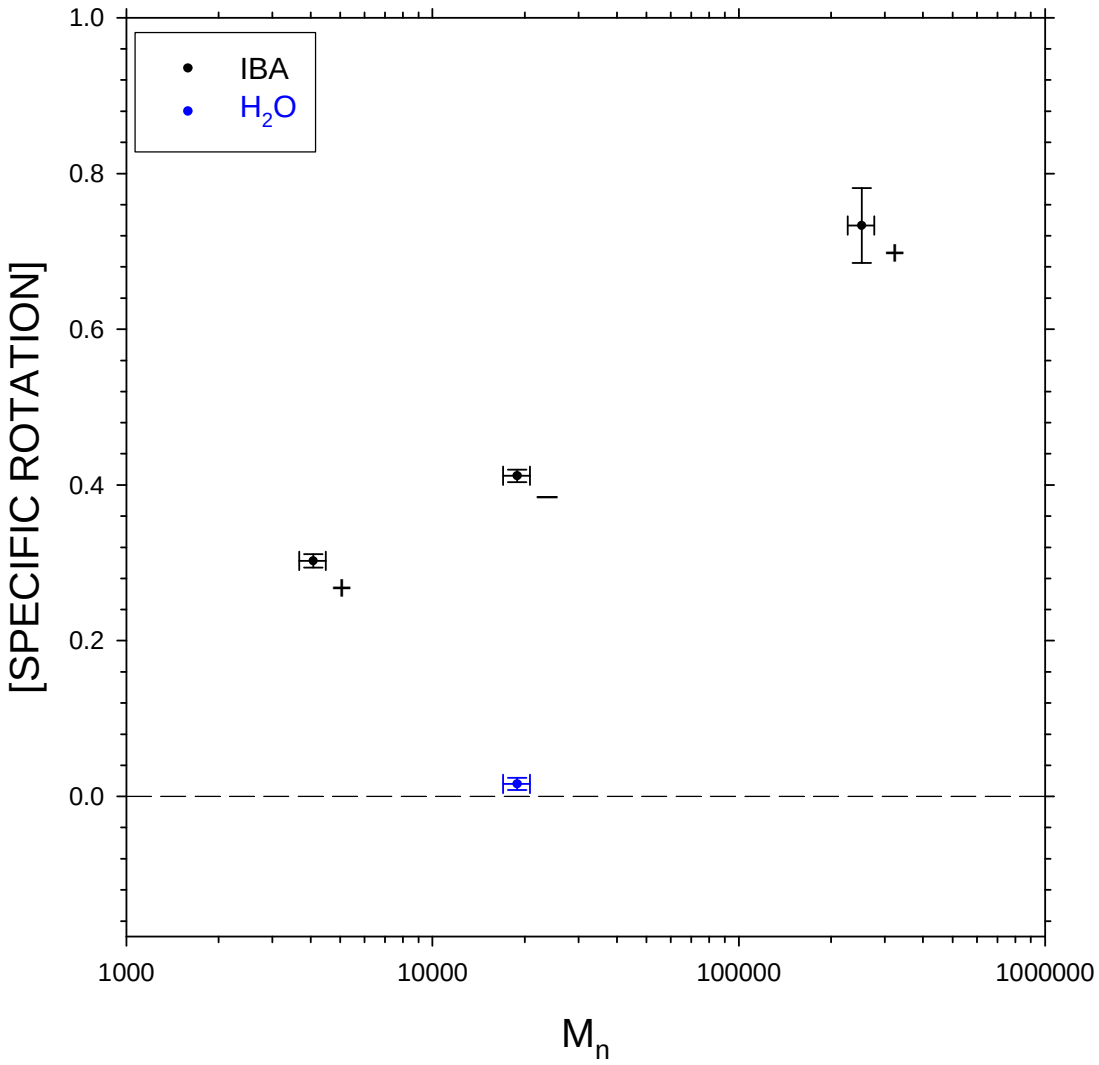

Figure 51. Absolute value of specific rotation versus molecular weight. Note that the abscissa is scaled logarithmically. The signs of the rotations are noted on the figure. The aqueous sample is in blue. Error bars are one standard deviation.

Run 2

Run 2 was carried out with the new IBA sample, Lot # 07710PB. The samples with varying concentrations of polymer in pure IBA (V-IX) showed no statistically significant rotation for any of the concentrations studied; therefore, specific rotations were not calculated since the changing concentrations created an artificial trend. The data for XI, XIV, and XV are plotted in Figure 50. The samples in Run 2 were not heated to 90 ^{o}C; see Run 3 for more information.

Table 19. Rotation and specific rotations for polarimetry, Run 2.

Sample	Polymer	Concentration (mg/mL)	Solvent	α	[α] (deg/(dm *g/mL))
V	Polymer 20k	1.2	IBA	-0.0003	N/A
VI	Polymer 20k	5.1	IBA	-0.0002	N/A
VII	Polymer 20k	15.1	IBA	-0.0004	N/A
VIII	Polymer 20k	20.1	IBA	-0.0003	N/A
IX	Polymer 20k	25.1	IBA	0.0003	N/A
X	Polymer 20k	10.2	IBA + PHL	-0.0038 ± 0.0001	-0.3725
XI	Polymer 252k	12.2	H_2O	0.0006 ± 0.0002	0.049
XII	Polymer 4k	12.3	H_2O	0.0003 ± 0.0003	0.024
XIII	Polymer 20k	12.2	H_2O +TA	0.0000 ± 0.0001	0
XIV	Polymer 20k	12.2	IBA + TA	-0.0042 ± 0.0005	-0.3443
XV	Polymer 252k	10.3	IBA + TA	-0.0076 ± 0.0005	-0.7379

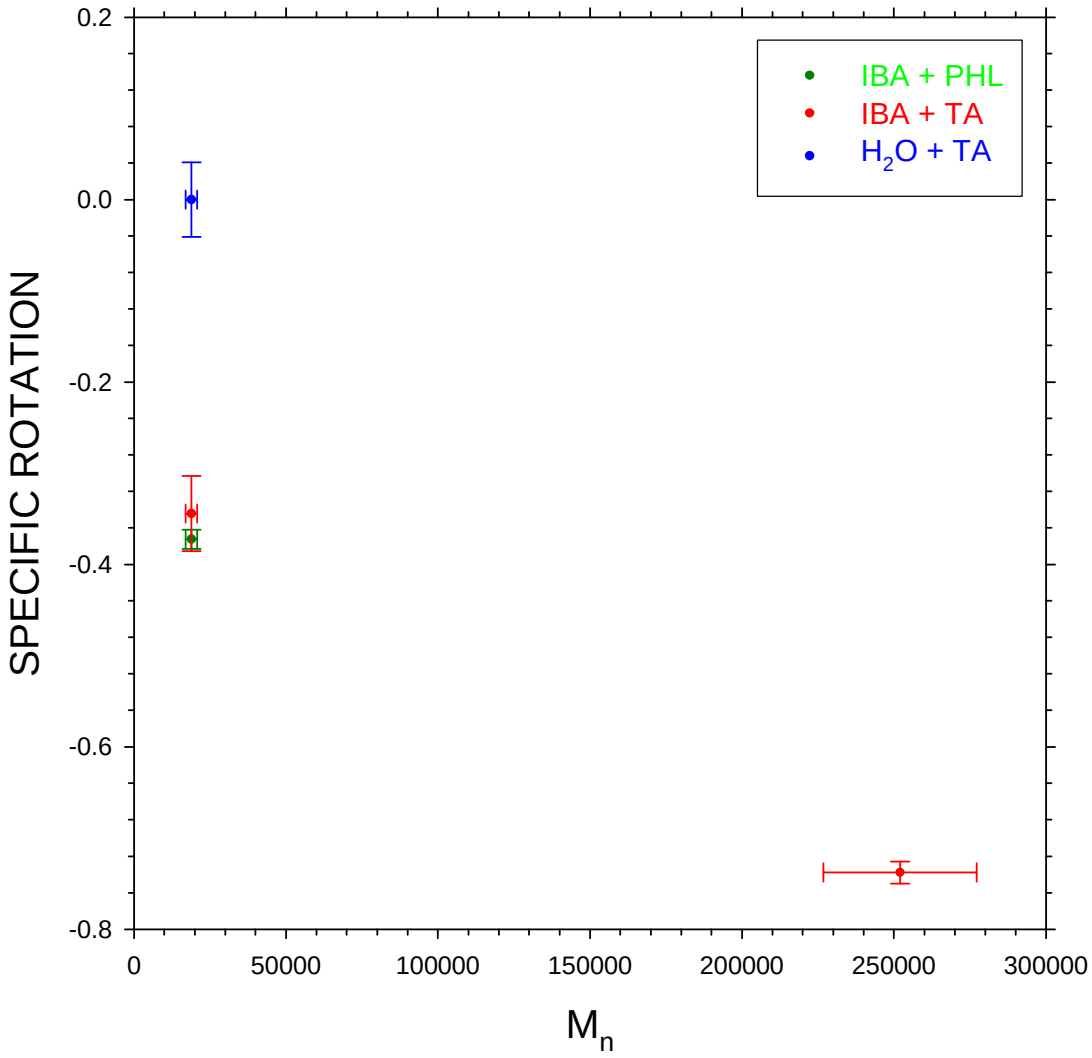

Figure 52. Plot of specific rotation versus molecular weight for Run 2. PHL and TA stand for L-phenylalanine and tartaric acid, respectively. Error bars are one standard deviation.

Figure 50 shows that chiral impurities could be used to influence the rotation. Two different impurities, (-) phenylalanine and (+) tartaric acid, were used. As can be seen from Polymer 20k, the rotations of the two samples were within their uncertainties of each other, but both gave a negative rotation, even though their chiralities were different. Samples of the same polymer, using the same solvent without the impurity were studied at five different concentrations, none of which showed a rotation. In order to rule out the possibility that the chiral impurities were interacting in some way with the polymer and creating an artificial signal, a sample of Polymer 20k in water with tartaric acid added was studied. As can be seen on Figure 50, this sample showed no rotation, which indicates that the signals in IBA are probably due to enantiomeric bias and not artifacts of the chiral impurity

Run 3

Run 3 made use of a chiral impurity, 1,2-propanediol, that had better solubility in IBA and was available in both enantiomers. The samples studied are listed in the table below.

Table 20. Absolute and specific rotations for polarimetry, Run 3. All samples listed have been heated. The column of solvent number refers to Table 11 in the Materials section.

Sample	Polymer	Concentration (mg/mL)	Solvent	α (±0.005)	[α] (deg/(dm *g/mL))
XVI	Polymer 20k	12.3	1	0.00596	0.4846
XVII	Polymer 20k	12.5	2	-0.00227	-0.1819
XVIII	Polymer 252k	12.2	1	0.00373	0.3057
XIX	Polymer 252k	11.1	2	-0.00366	-0.3297
XX	Polymer 10kM	11.6	1	0.00663	0.5716
XXI	Polymer 10kM	11.6	2	-0.00726	-0.6259
XXII	Polymer 4k	12.6	1	0.00230	0.1825
XXIII	Polymer 4k	12.5	2	-0.00502	-0.4016
XXIV	Polymer 2kH	12.5	1	0.00398	0.3184
XXV	Polymer 2kH	12.3	2	-0.00502	-0.4081
XXVI	Polymer 337k	11.9	1	0.00536	0.4504
XXVII	Polymer 337k	12.3	2	-0.00934	-0.7593
XXVIII	Polymer 10kH	11.9	1	0.00320	0.2689
XXIX	Polymer 10kH	11.7	2	-0.00452	-0.3863
XXX	Polymer 10kM	11.3	1	0.00492	0.4354
XXXI	Polymer 10kM	11.6	2	-0.00648	-0.5586
XXXII	Polymer 10kH	12.3	3	0.01030	0.8374
XXXIII	Polymer 10kH	12.6	4	-0.0082	-0.6508
XXXIV	Polymer 10kH	12.3	5	0.00194	0.1577
XXXV	Polymer 10kH	12.4	6	-0.00107	-0.0863

An effect that was mentioned briefly in the experimental section was the effect of temperature upon the rotation of the sample. A sample of Polymer 10kM was accidentally left on a hot plate and reached a very high temperature (~120 ^{o}C) for several hours. When this sample was run there was a significant signal. Samples XVI-XIX, which originally showed little rotation, were then heated to 90 ^{o}C using a vacuum oven. The samples were then run again. The results of this experiment are shown in Figure 53. This behavior, combined with neutron results that show a helix-to-coil transition at elevated temperature, reinforces our belief that enantiomeric amplification is taking place. By heating the sample to above the transition temperature, the helical character remaining from the solid phase is completely removed. As the temperature is decreased, the helix reforms and is influenced by the chiral impurities present in the solvent. Only samples heated above 90 ^{o}C are listed in Table 12 for Run 3.

Figure 51 shows the rotation versus molecular weight (samples XVI-XXIX) using IBA spiked with approximately 1% by mass propanediol. The plot is too noisy to discern a clear trend with molecular weight, but the sign of the rotation clearly follows the sign of chiral impurity added to the IBA. It can also be seen that the plot is fairly symmetrical with respect to 0^{o} of rotation. This plane of symmetry was also seen in Figure 52.

Polymer 252k (sample XVIII-XIX) showed a surprisingly low amount of rotation, which may be due to the monomethyl ether termination, possibly indicating termination effects. Figure 52 shows the two closest molecular weight polymer samples with different terminations. As can be seen, perhaps the methoxy terminated

polymer shows less rotation. The uncertainty in the measurements, however, and the molecular weight differences make a clear distinction of end effects impossible. More samples will need to be studied in order to confirm this result.

An attempt was also made to investigate the effect of the dopant concentration upon the signal. Figure 54 shows the signal from Polymer 10kH at a number of different mass fractions of propanediol. It appears that increasing the amount of propanediol increases the rotation of the polymer. The higher mass fraction sample (0.15% by mass) had an increase in signal that was proportionally greater than the increase of propanediol. This indicates that using higher mass fractions of propanediol could have a greater effect upon the enantiomeric multiplication.

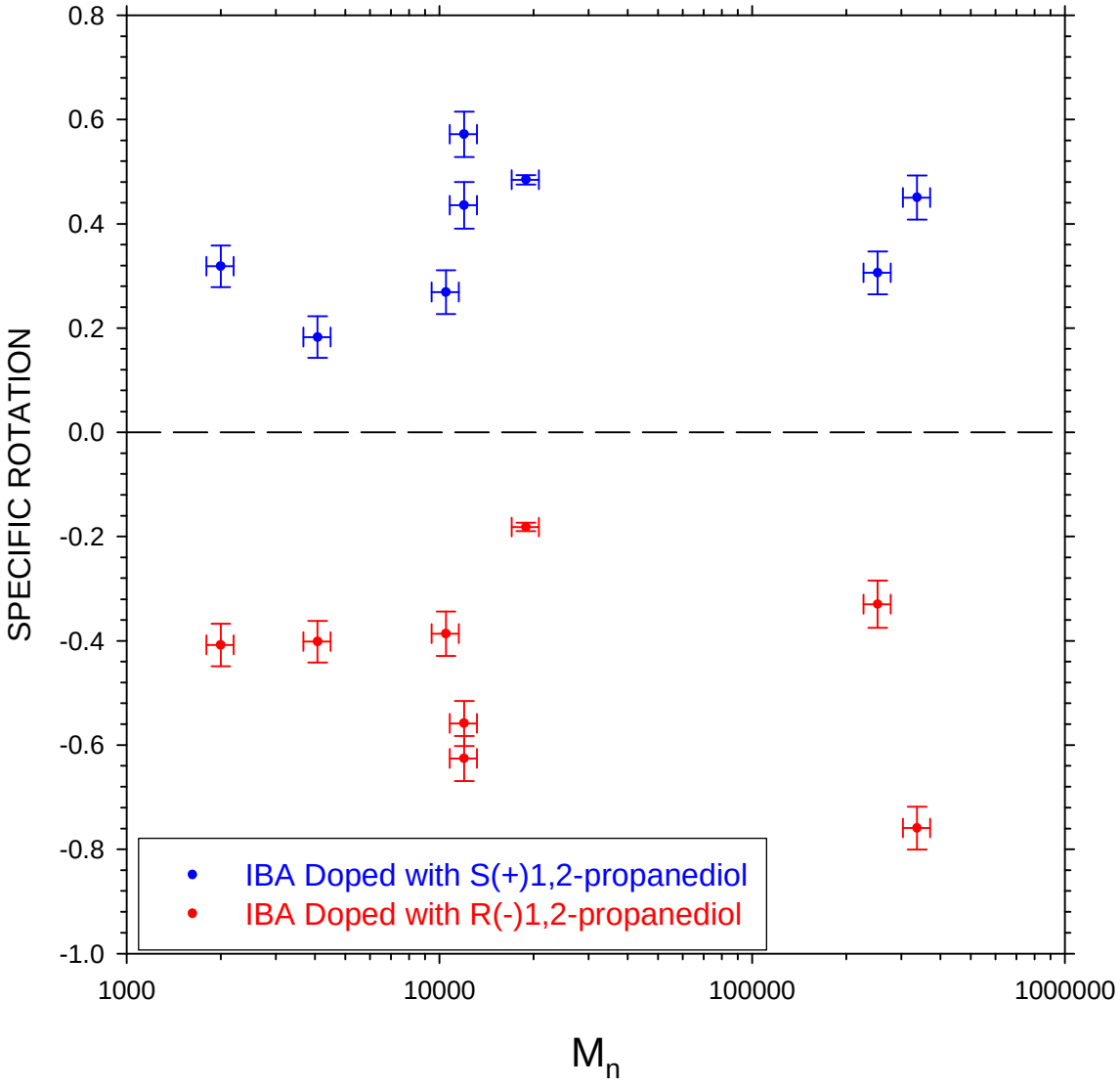

Figure 53. Specific rotation versus molecular weight with propanediol-doped IBA. Samples made with S(+)1,2-propanediol doped IBA are in blue, those made with R(-)1,2-propanediol spiked IBA are red. Note that the abscissa is logarithmically scaled. Error bars are one standard deviation.

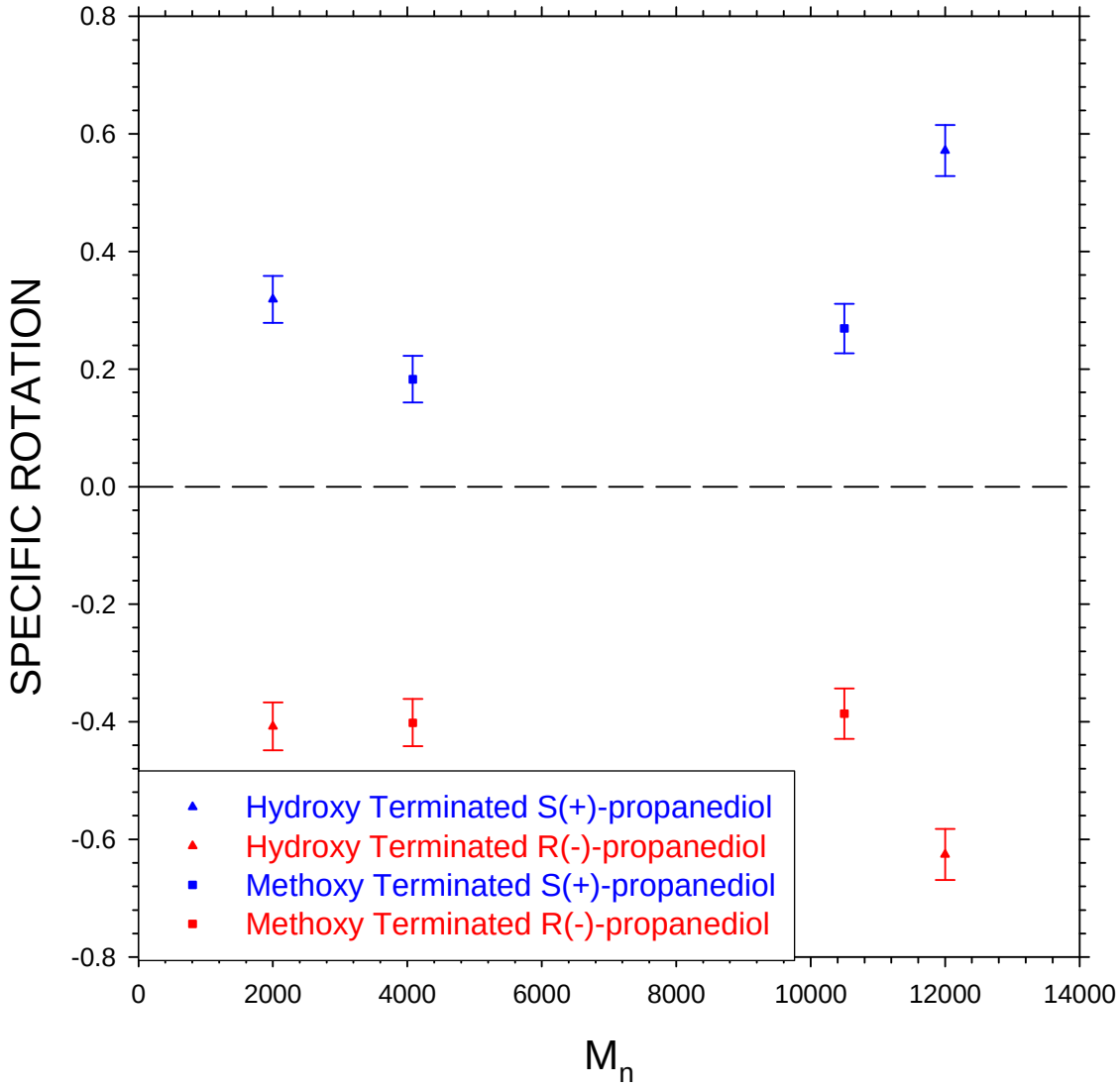

Figure 54. Specific rotation versus molecular weight for methoxy (square) terminated and hydroxy (triangle) terminated PEO. Samples (made with S(+)1,2-propanediol doped IBA are in blue, those made with R(-)1,2-propanediol doped IBA are red. Error bars are one standard deviation.

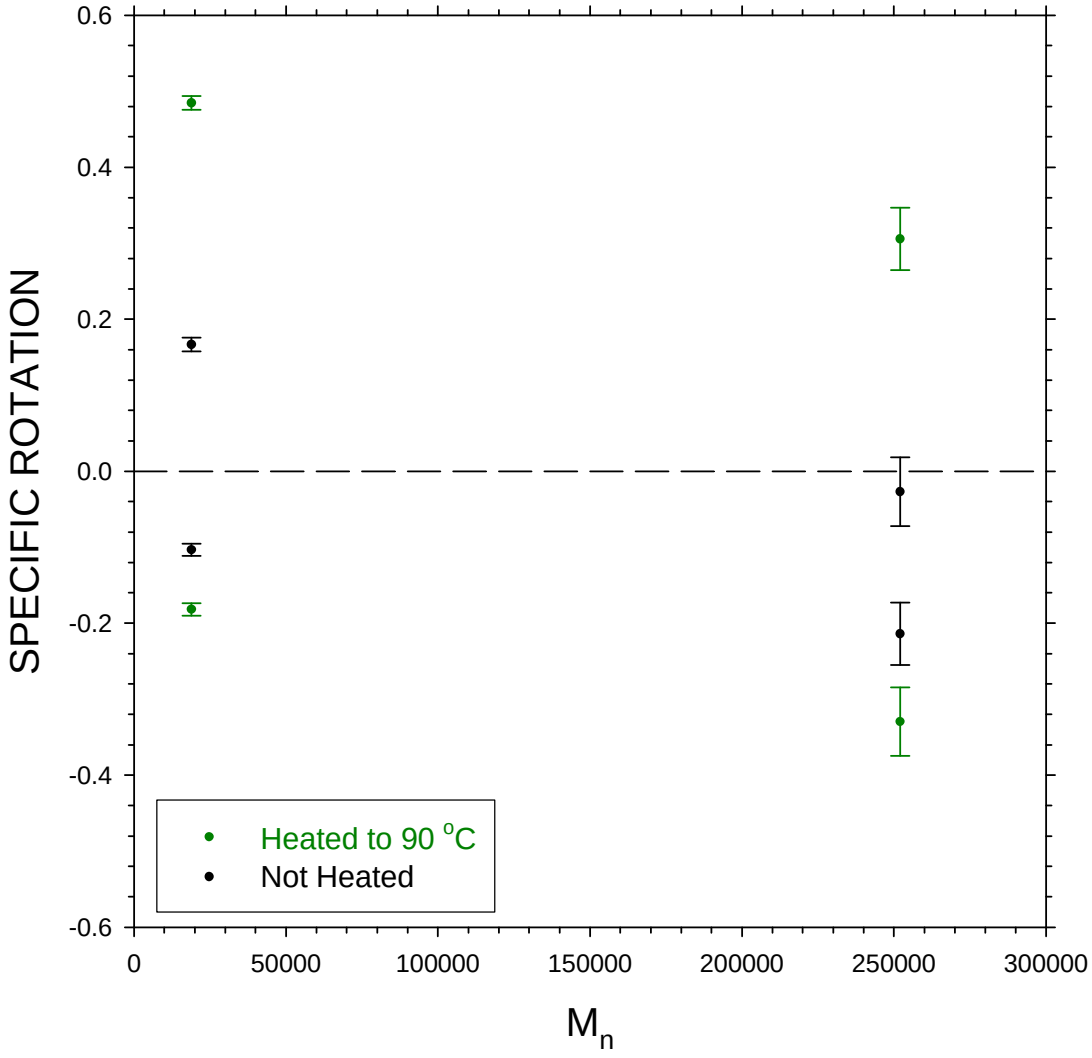

Figure 55. Specific rotation versus molecular weight for samples that were run before (black) and after (green) heating to 90 °C. The unheated samples are not listed in the table for Run 3. Error bars are one standard deviation.

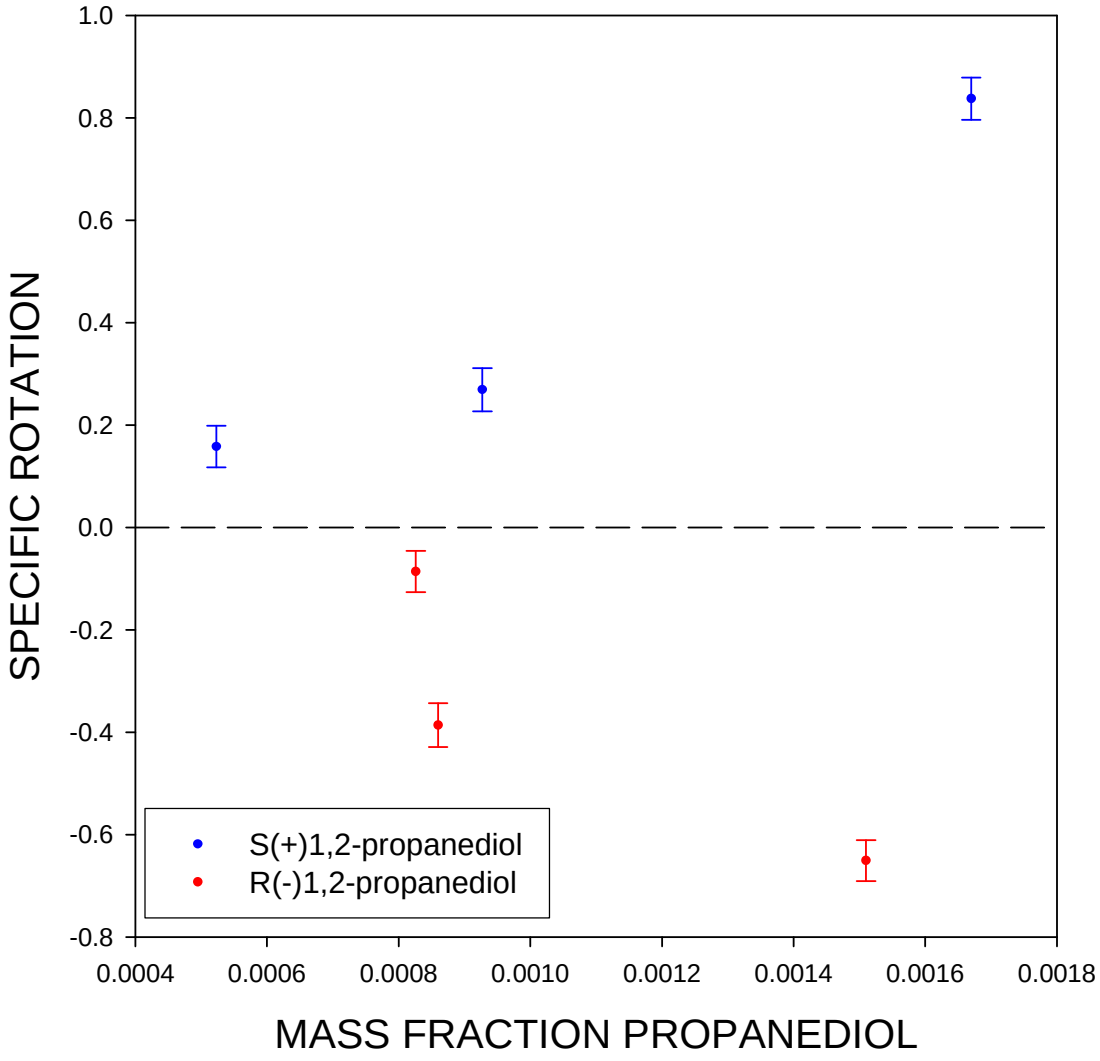

Figure 56. Specific rotation of Polymer 10kH (samples XXXII-XXXV) versus mass fraction of propanediol dopant. Error bars are one standard deviation.

Chapter 5: Conclusions

Neutron Scattering

The formation of a stiff helix by PEO in isobutyric acid was entirely unexpected. PEO is known to form a helix in the solid state, and there is evidence that, on a local scale, PEO has helical content in water,[37,51-55,69-71] but it is certainly not a stiff global helical structure in water. Exploring the causes of this conformation was difficult because of the limited amount of beam time available and the time required for the custom synthesis of the deuterated solvents (greater than six weeks). In spite of these difficulties, we were able to explore the effect of temperature, solvent composition, and molecular weight upon the conformational behavior of PEO in solutions of isobutyric acid. It also appears that the handedness of the helix can be biased by using chiral impurities to cause enantiomeric excess.

Temperature Effects

PEO is often treated as a simple model protein since it contains both hydrophobic and hydrophilic segments on the chain. In addition to these segments, we can now say that PEO, like a protein, also has a secondary structure in solution. The structure shows a reversible transition between a helix and coil between the temperatures of 55 and 60 ^{o}C. This transition results in a drastic decrease in the stiffness ratio and the radius of the worm-like molecule. The helix to coil transition also appears to be reversible, since the neutron scattering samples were all heated to at least 60 ^{o}C before scattering to insure that the polymer was solvated. Further

evidence of this reversibility is given by the polarimetry results, where the solution maintains a signal after heating to well above 60 ^{o}C and cooling back to room temperature. In the temperature range from 30 to 55 ^{o}C, there appears to be little effect of temperature. Polymer 337k may have shown some sign of "softening," but the stiffness ratios were still significantly larger than 1.0.

Solvent Effects

The composition of the solvent plays a strong role in the stiffness of the helix. Starting with pure D_2O and increasing the mass fraction of d-IBA led to a stiffening of the polymer. Using deuterated acids and bases did not have any effect on the conformation of the PEO, indicating that this effect is a consequence of isobutyric acid interactions and is not pH driven. The mechanism of IBA interactions that leads to the helices still not well understood and will be discussed in Future Work.

It has also been shown that the addition of water to isobutyric acid appears to facilitate the aggregation of the PEO molecules. The controversy regarding PEO aggregation has been debated by a number of authors, but it appears that this result, along with the work of Ho *et al.*,[15,32,72] conclusively shows that PEO aggregation is a characteristic of aqueous PEO solutions and is not caused by impurities.

Molecular Weight

The effect of molecular weight upon the solution behavior of PEO has been more difficult to observe. The stiffness ratio of Polymer 337k was significantly larger than the ratio for Polymer 20k, but the significance of this difference is not clear, since the concentration of Polymer 337k may have been above the polymer critical overlap concentration, c^*. There is a lot of uncertainty in the value of c^* because there are two very different relations for R_g of PEO in water,[14,17] and because c^* is smaller for rod-like particles than for coils:[67,73]

$$c^*_{rod} = \frac{M}{N_A L^3} \tag{27}$$

Using the above relation for c^*, where M is the molecular weight of the polymer, N_A is Avogadro's number, and L is the fitted rod length, would give overlap concentrations of 12 and 7 mg/mL for Polymer 20k and Polymer 337k respectively. The fitted length of the rods is also suspect in that the length difference is not sufficient considering the molecular weight difference between Polymer 20k and Polymer 337k. Polymer 20k would consist of approximately 455 monomers, each with a length of about 3 Å, giving an expected end-to-end distance of 1365 Å. Using the radius of the worm-like molecule (5 Å) would mean each turn required about 32 Å. This would be roughly equivalent to 43 turns of the helix or 10.5 monomers per turn. For reference, in the solid state, PEO forms a helix with 3.5 monomers per turn.[7] Using this number of monomers per turn for Polymer 337k would require 725 turns. Unless the packing of the helix is different, i.e., a tighter helix, the rod length for Polymer 337k should be much longer. The idea of a tighter helix is not, however,

implausible since the stiffness ratio of Polymer 337k was much higher than the ratio of Polymer 20k. This would indicate an even more complicated polymer-solvent interaction. The dramatic stiffening may also have been caused by the larger, Polymer 337k, rods reaching c^* before Polymer 20k.

There also appears to be a correlation between molecular weight and the amount of aggregation. The lowest molecular weight polymer studied, Polymer 4k, showed no aggregation in pure d-IBA at 60 ^oC, but strong aggregations in D_2O. The higher molecular weight polymers all showed aggregations, even in pure d-IBA. This may indicate that d-IBA is not a good solvent for high molecular weight PEO. A similar effect was seen by Shresth *et al.*,[3] who saw the higher molecular weight molecules fractionate to the water phase in a binary solution of IBA and water.

Termination Effects

The termination of the polymer did not seem to have any effect upon the stiffening of the molecule. More samples will need to be studied to see if there is a subtle effect that was not obvious in these scattering experiments. Niamke[48] examined the effect of termination on relative fractionation and also saw no effect.

Polarimetry

The conformation of the rods seen by neutron scattering was further investigated by polarimetry. Because a helix has a plane of symmetry, it is expected to generate a signal, as explained in the polarimetry section. It has been shown above that PEO in IBA generates a polarimeter signal, while PEO in water does not. The fact that the rod-like molecules seen in neutron scattering also generate a polarimeter signal provides strong evidence that these rods are actually helical. In addition to proving the helicity of PEO in IBA, we have shown that the direction of the helix can be influenced by using chiral "impurities."

Enantiomeric Effects

Run 1 showed a polarimetry signal that was linear with the logarithm of the molecular weight of the PEO. Changing the lot number of the solvent resulted in a loss of signal, indicating that an impurity in the solvent was causing a bias in the proportion of left- and right-handed helices in Run 1. Run 2 provided further evidence that impurities could affect the signal when the introduction of phenylalanine and tartaric acid into the same sample of PEO in IBA that had previously shown no signal, then had a signal. In Run 3, two enantiomers of 1,2-propanediol were used to specifically influence the ratio of enantiomers. Introducing the + enantiomer resulted in a positive rotation, and the – enantiomer resulted in a negative rotation. This shows an ability to influence the folding of the polymer at a molecular scale.

Temperature Effects

Heating the sample to high temperatures was found to increase the polarimeter signal. This is probably because heating the solution over the helix-to-rod transition, seen in the neutron scattering, removes residual helical structure that may be remaining from the solid phase. It also provides the energy required for the helix reversal in order to shift the ratio of enantiomers, resulting in a polarimeter signal.

Amount of Chiral Impurity

Three concentrations of chiral impurity were studied in this work. With only three samples, it is difficult to get a clear relationship between concentration and signal, but it appears that increasing the concentration results in a nonlinear increase in signal. The number of chiral molecules per polymer molecule does not appear be a direct indicator of signal, since there was no clear influence of molecular weight. Since the mass concentration of polymer was kept fairly constant, the number of polymer molecules decreases as the molecular weight increased. As an example, there are approximately 17 times more individual polymer molecules in a 12 mg/mL sample made with Polymer 20k versus Polymer 337k. For a mass fraction of propanediol of 0.000927, this would result in about 20 propanediol molecules per Polymer 20k molecule and 322 propanediol molecules per Polymer 337k molecule. More molecular weights and dopant concentrations would need to be studied to attempt to derive a relationship between the number of chiral molecules and the subsequent signal, which may be complicated.

Termination Effects

The effect of the termination upon the behavior of the PEO in IBA is still not clear. Polymer 252k, with a monomethyl ether termination, showed an abnormally low signal when compared to the other molecular weights. The termination may have played a role in this. Unfortunately, only two matched molecular weight polymers with different terminations were available. With only two samples, it appears that the hydroxy terminated samples have a higher signal, indicating that the less encumbered end-group may facilitate the helix reversal required to shift the ratio of enantiomers. Without further experiments, though, this remains conjecture.

Summary

Neutron scattering has shown that PEO undergoes a change from a coil to a rod when placed into solution with IBA. The stiffness of the chain has been seen to increase smoothly with increasing IBA content. The reverse rod-to-coil transition was seen to occur between 55 and 60 ^{o}C. Polarimetry experiments have shown that these rods are helices and can, through enantiomeric multiplication, be influenced to undergo a helix reversal, resulting in an off-racemic mixture. The formation of a helix by PEO in solution has not been seen in previous work and represents a simple model protein that can undergo denaturation. These “nanohelices” may also be possible building blocks for nanofabrication.

Chapter 6: Future Work

After analyzing the data from this series of experiments there are several aspects that should be explored further.

Temperature Effects

The helix to coil transition was seen to occur between 55 and 60 ^{o}C. The actual transition temperature is not, however, known with sufficient precision. Further scattering should be carried out in this temperature range to elucidate the transition temperature with more precision. The polarimetry experiments were carried out in hydrogenated systems without temperature control. The rotation signal increased after the samples were heated and then cooled to room temperature, but there was not sufficient time to see the effect of different maximum temperatures on the rotation signal. Jasco, the manufacturer of the polarimeter, has temperature controlled cells that would allow the helix to coil transition to be directly observed in the hydrogenated system. The final temperature effect that may be interesting is the use of differential scanning calorimetry to measure the enthalpy of the transition.

Molecular Weight

Further study of the effect of molecular weight on PEO's behavior in IBA needs to be carried out. Run 4 of the neutron scattering included four molecular weights of PEO in d-IBA, but the temperature of the run (60 ^{o}C) was above the helix to coil transition, and Polymer 252k and Polymer 4k were not studied in earlier runs

in pure d-IBA. Further neutron runs should concentrate upon the behavior of PEO in pure d-IBA, with lower polymer concentrations for the higher molecular weights to insure that the concentration is below c^*. A series of scattering runs with varying polymer concentration may prove informative.

Solvent Effects

Several aspects of solvent effect should also be studied. The mixed solvent samples did not show any of the critical fluctuation effects that we expected.[43-46,74] It may be of interest to revisit this issue with further scattering studies. The mixed solvent samples seemed to have solubility issues and were more difficult to analyze through model fitting in that the models could not be reliably fitted to the data. Using lower molecular weight PEO samples and keeping the samples at an elevated temperature for longer periods of time may help with solubilizing the PEO in the mixed solvents.

Also of interest is why isobutyric acid has this effect on PEO. What is special about isobutyric acid that causes this stiffening? More study of n-butyric acid should be conducted. In addition to n-butyric acid, structural homologues of isobutyric acid should be studied. One possible candidate is isobutanol, which has the same number of carbons and can form hydrogen bonds. The respective structures are shown in the figure below.

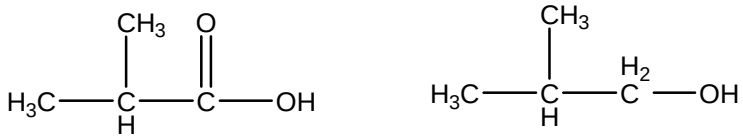

Isobutyric Acid Isobutanol

Figure 57. Chemical structure of isobutyric acid and isobutanol.

The response of these helices to shear is also of interest. At the present time, the only shear cell suitable for neutron scattering requires 15 mL or more of solvent. The custom synthesis of deuterated IBA costs approximately $900.00 for 5 mL. This makes for a prohibitively expensive experiment. In development, however, is a much smaller shear cell that will only require a few mL of solution. Once this cell is on-line, experiments can be carried out shearing the solution and seeing how the rods behave in a shear field. This can play a major role in developing applications for these polymer rods.

The formation of a helix in solution by a simple linear polymer without bulky side groups is an unusual phenomenon that requires more study to fully understand the factors at play. In addition to its possibility as a simple model protein that folds, PEO can conduct electricity when mixed with a salt. This could lead to the fabrication of polymeric nanowires.

Appendix: Model Fits to Neutron Data

Run 2

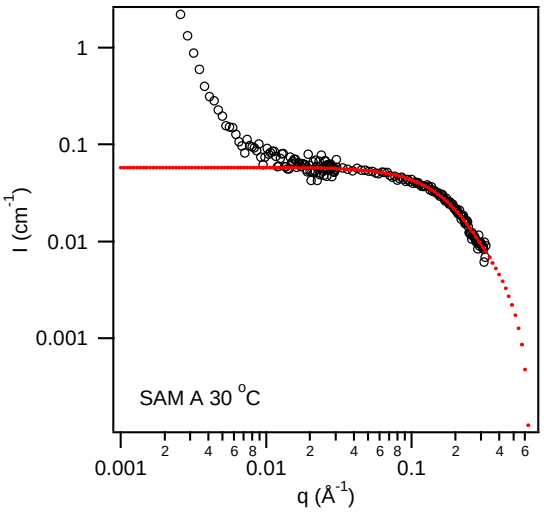

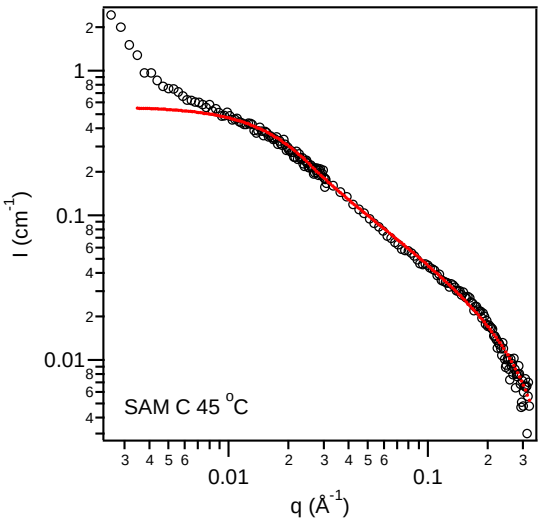

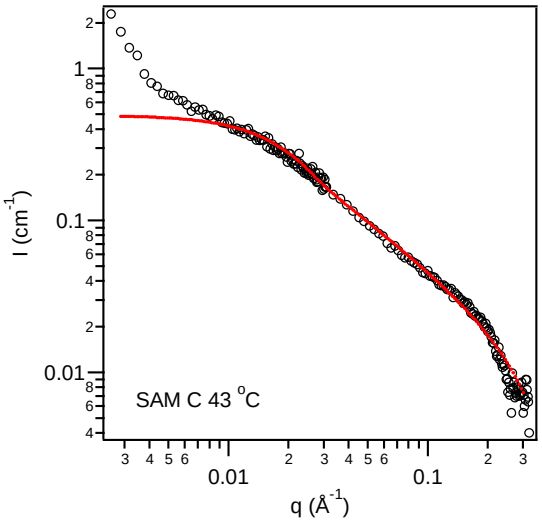

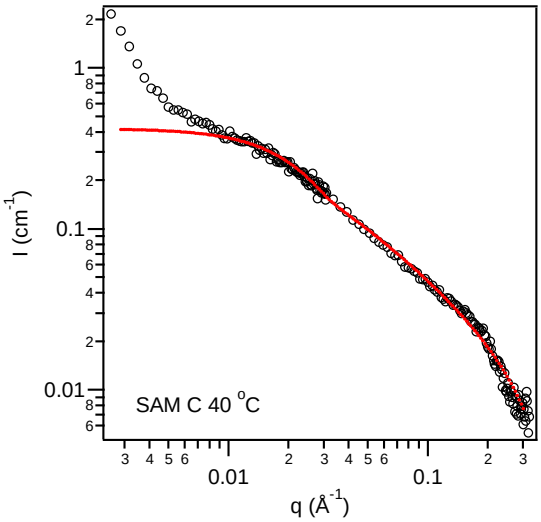

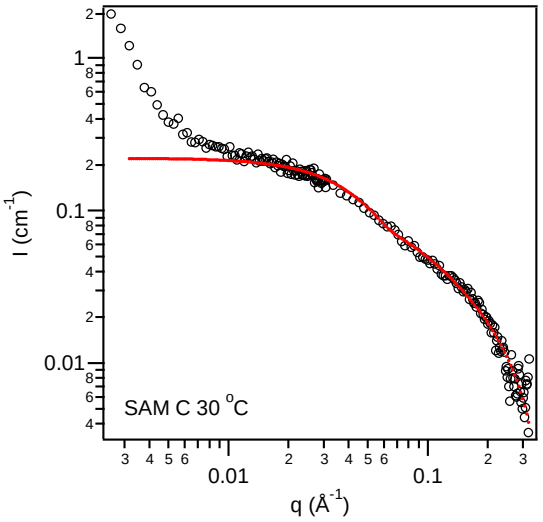
SAM C 30 °C
I (cm-1)
q (Å-1)

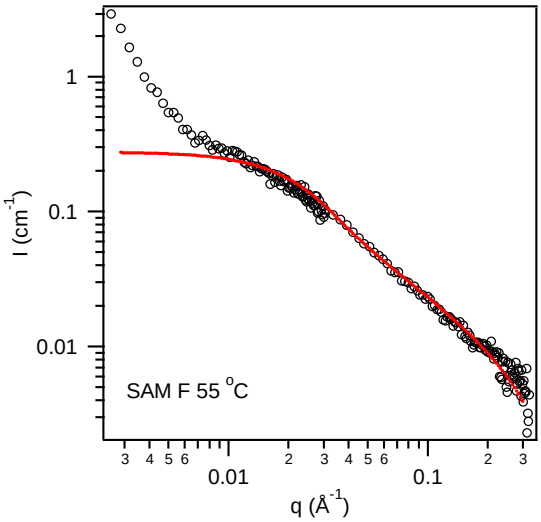
SAM F 55 °C
I (cm-1)
q (Å-1)

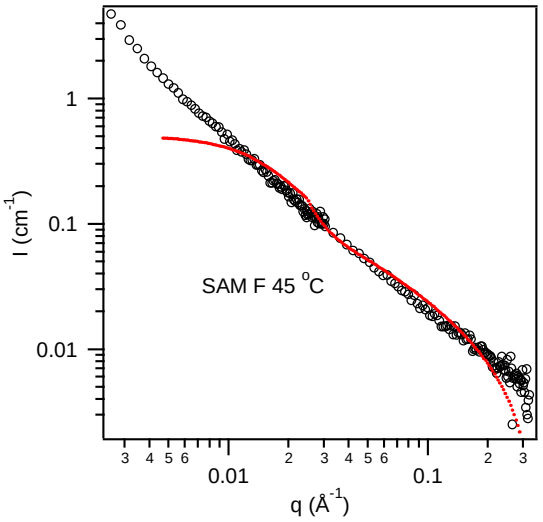
SAM F 45 °C
I (cm-1)
q (Å-1)

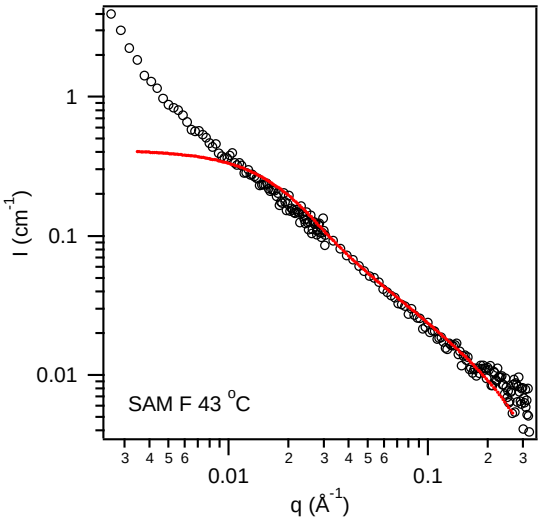
SAM F 43 °C
I (cm-1)
q (Å-1)

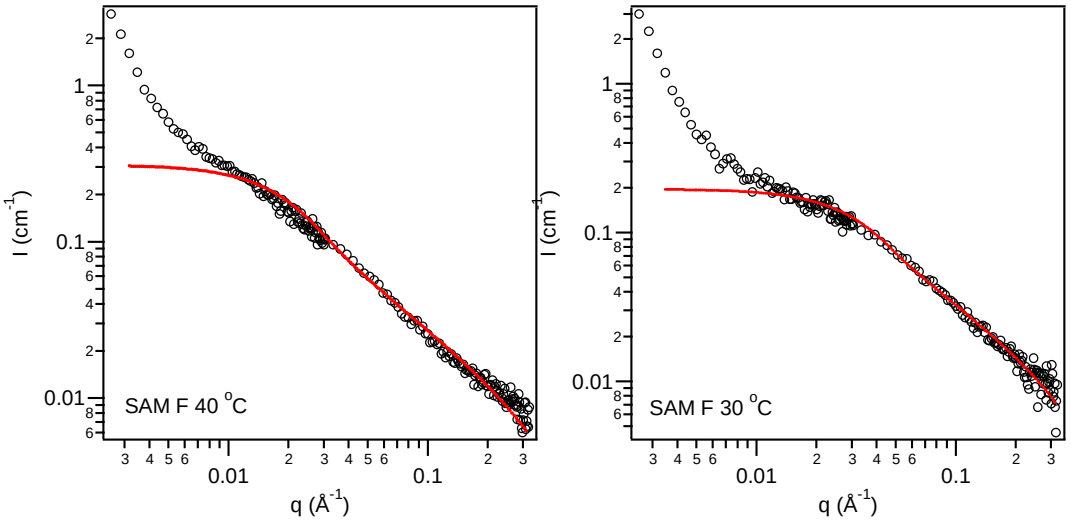
I (cm-1)
SAM F 40 °C
q (Å-1)
I (cm-1)
SAM F 30 °C
q (Å-1)

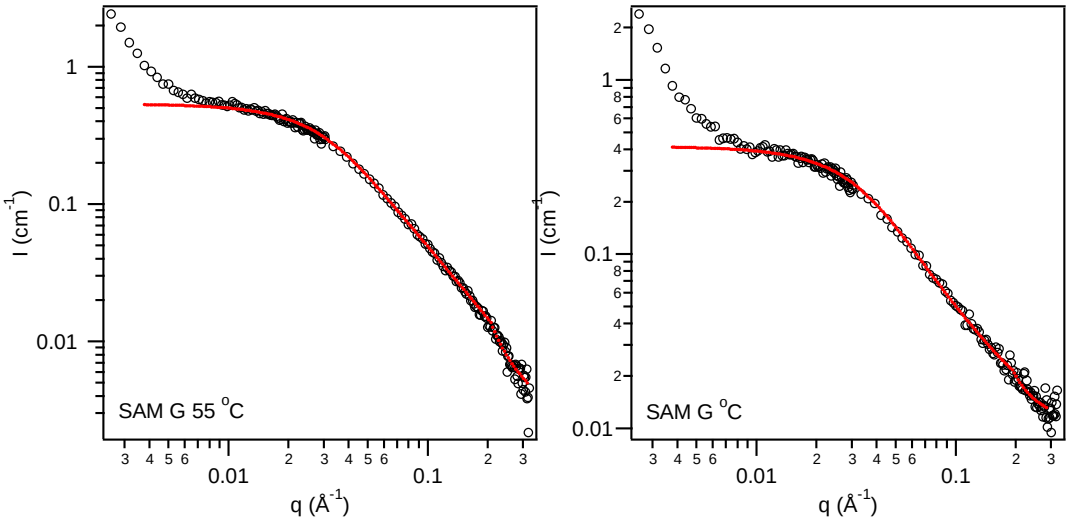
I (cm-1)
SAM G 55 °C
q (Å-1)
I (cm-1)
SAM G °C
q (Å-1)

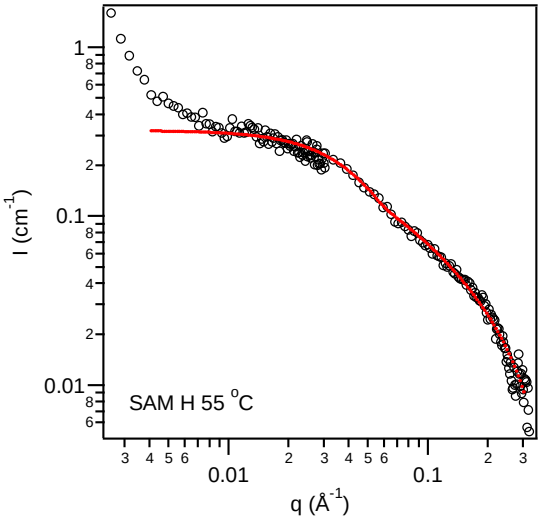
I (cm-1)
q (Å-1)
SAM H 55 °C

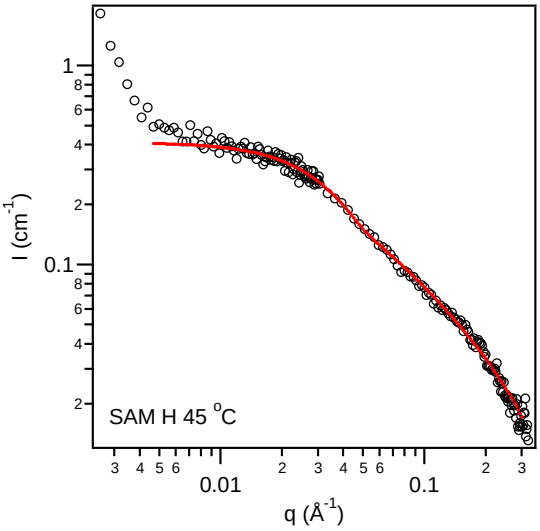
I (cm-1)
q (Å-1)
SAM H 45 °C

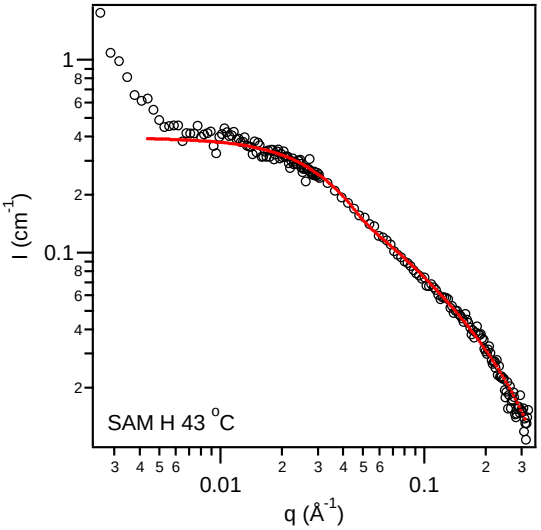
I (cm-1)
q (Å-1)
SAM H 43 °C

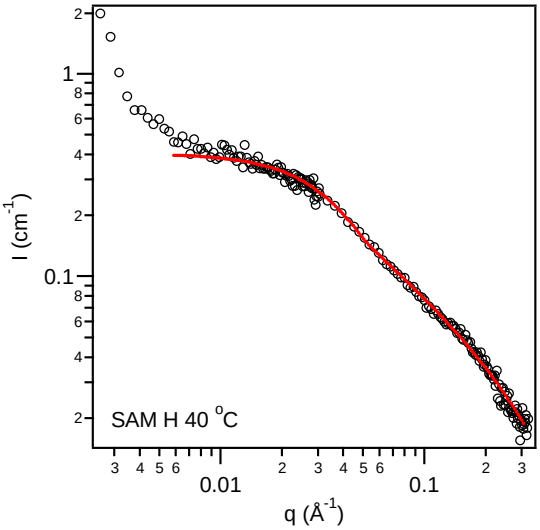
I (cm-1)
q (Å-1)
SAM H 40 °C

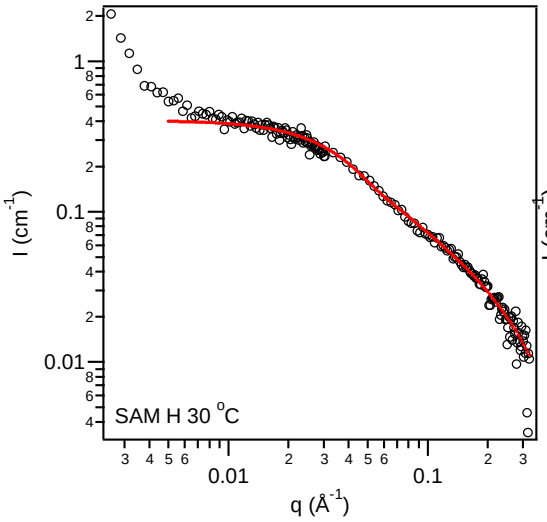
SAM H 30 °C
I (cm-1)
q (Å-1)

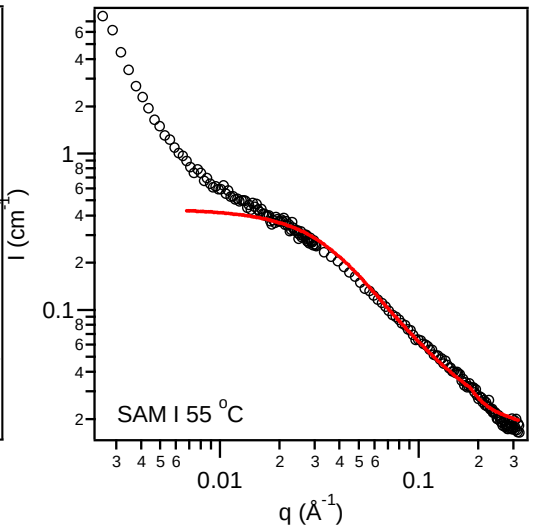
SAM I 55 °C
I (cm-1)
q (Å-1)

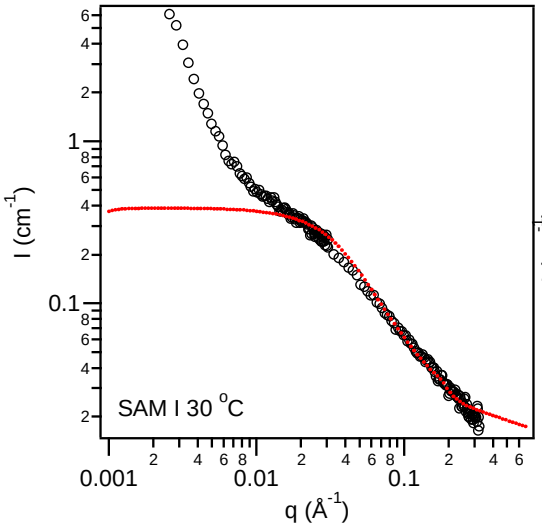
SAM I 30 °C
I (cm-1)
q (Å-1)

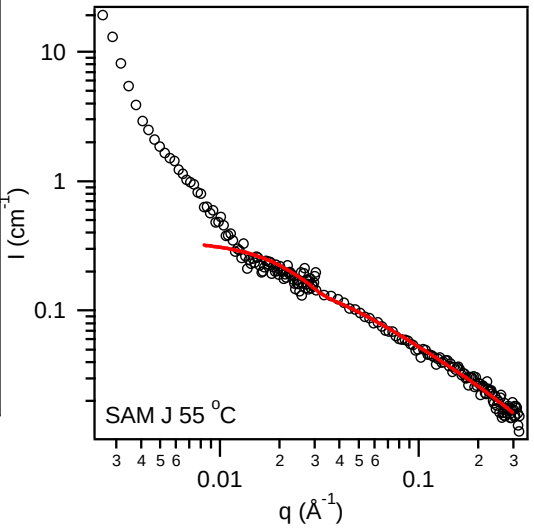
SAM J 55 °C
I (cm-1)
q (Å-1)

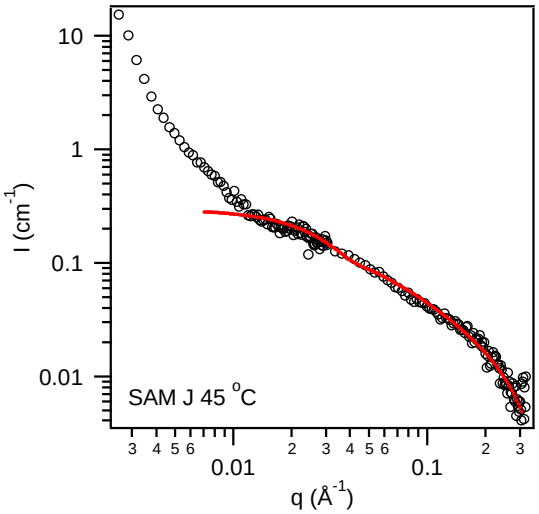
10
1
0.1
0.01
I (cm-1)
SAM J 45 °C
3 4 5 6 0.01 2 3 4 5 6 0.1 2 3
q (Å-1)

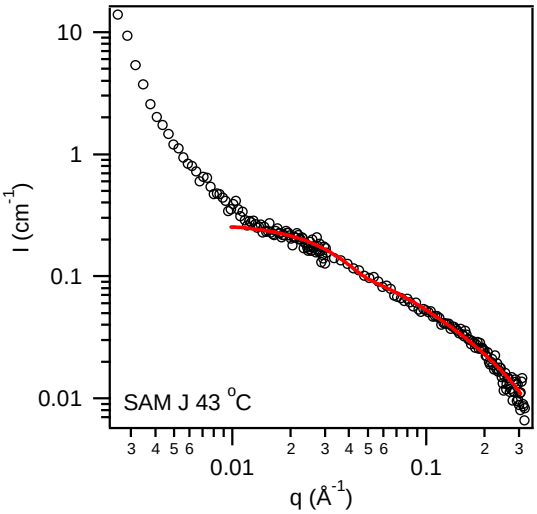
10
1
0.1
0.01
I (cm-1)
SAM J 43 °C
3 4 5 6 0.01 2 3 4 5 6 0.1 2 3
q (Å-1)

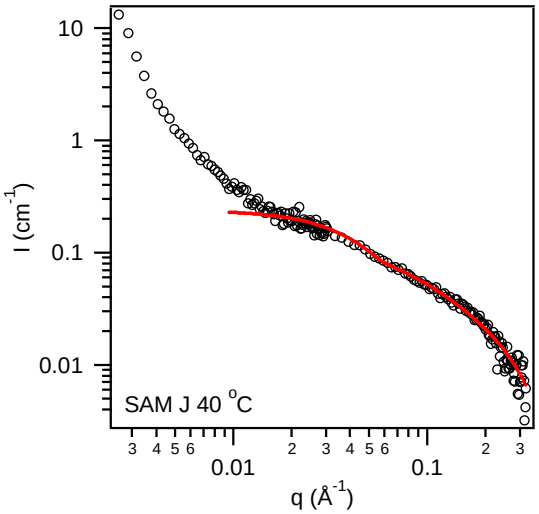
10
1
0.1
0.01
I (cm-1)
SAM J 40 °C
3 4 5 6 0.01 2 3 4 5 6 0.1 2 3
q (Å-1)

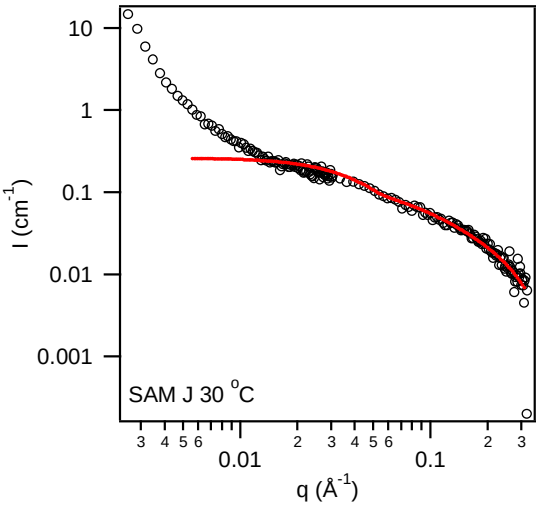
10
1
0.1
0.01
0.001
I (cm-1)
SAM J 30 °C
3 4 5 6 0.01 2 3 4 5 6 0.1 2 3
q (Å-1)

Run 3

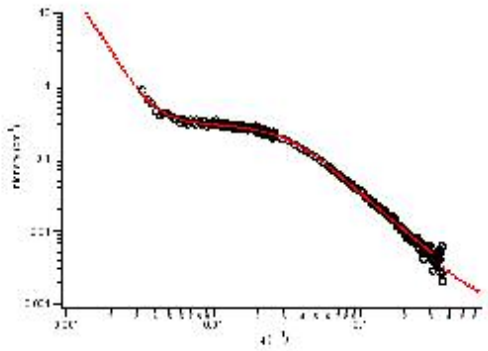

SAM1 @ 25C (Worm-like)

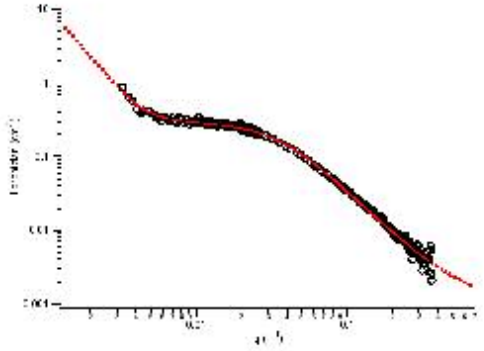

SAM1 @ 25C (Debye)

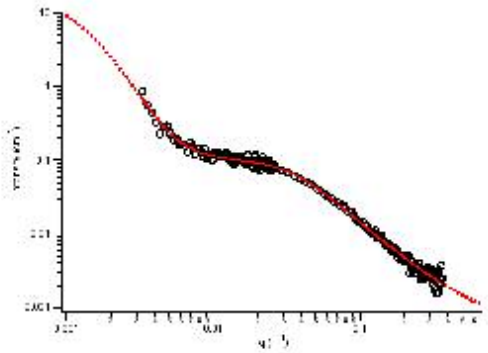

SAM2 @ 25C (Worm-like)

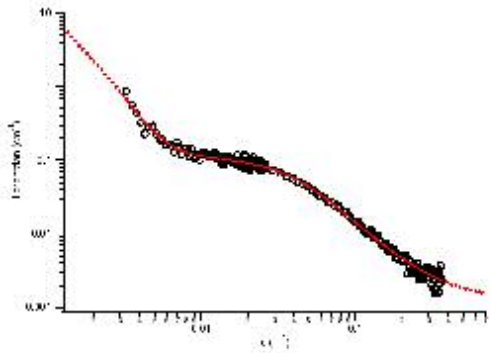

SAM2 @ 25C (Debye)

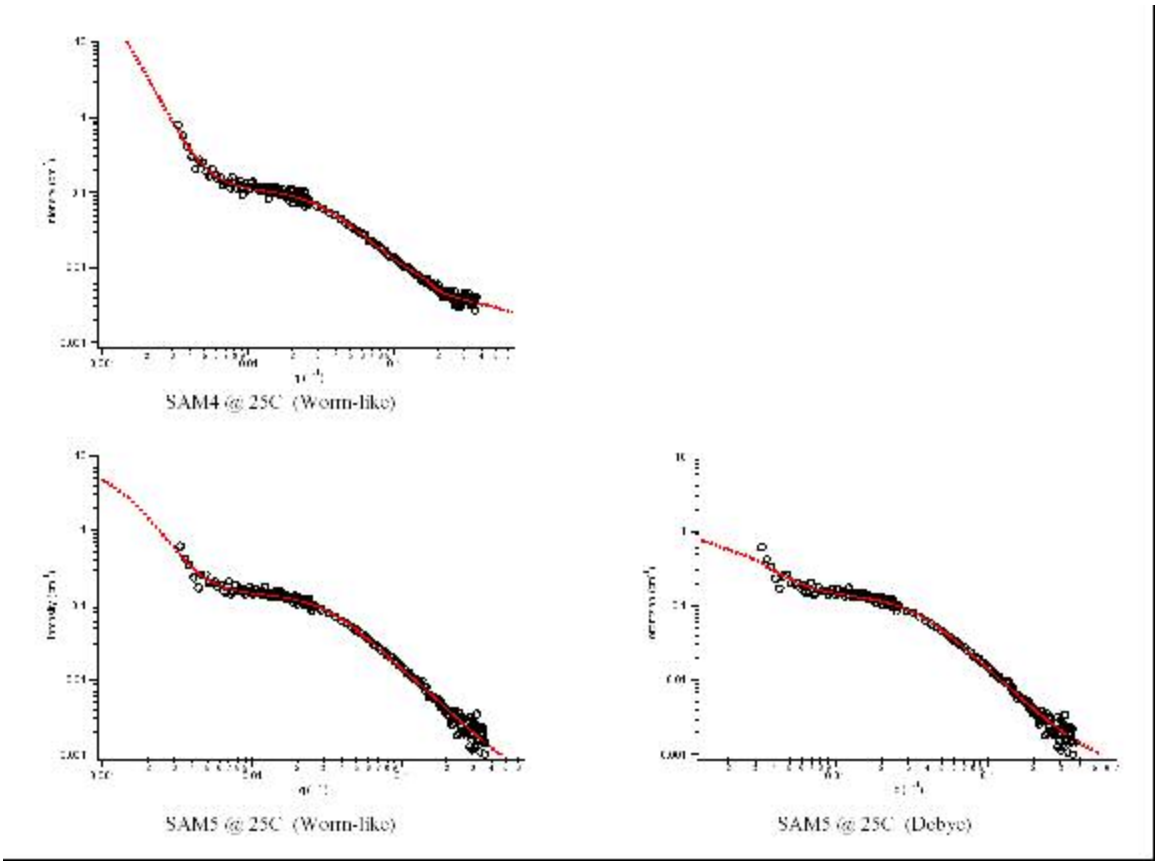

SAM4 @ 25C (Worm-like)

SAM5 @ 25C (Worm-like)

SAM5 @ 25C (Debye)

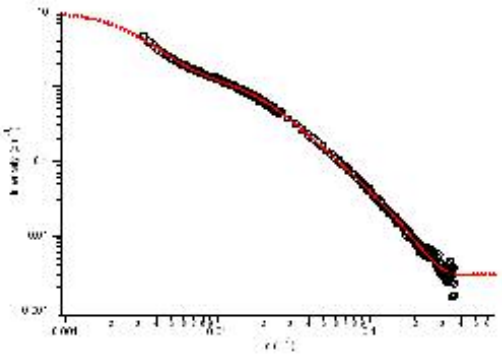

SAM8 @ 55C (Worm-like)

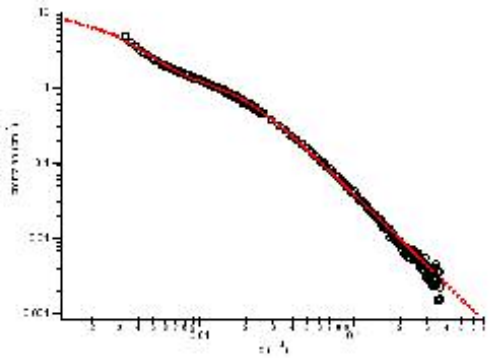

SAM8 @ 55C (Debye)

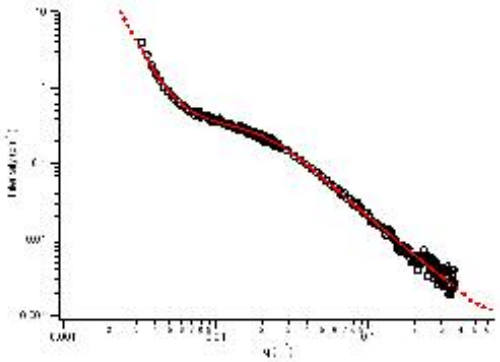

SAM9 @ 55C (Worm-like)

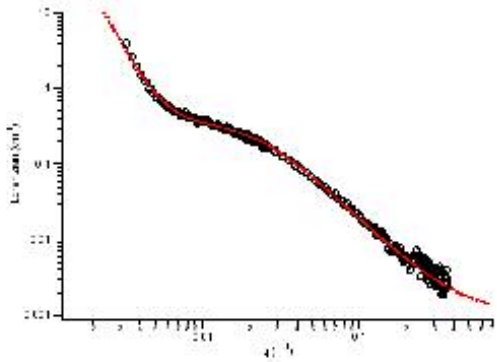

SAM9 @ 55C (Debye)

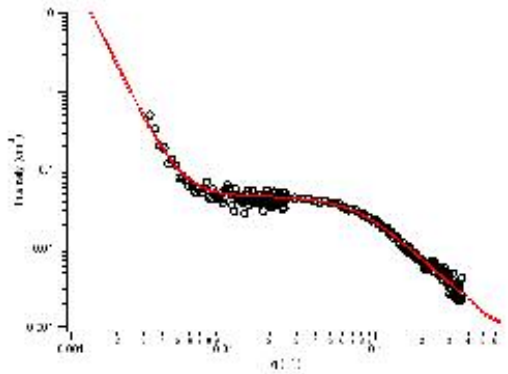

SAM12 @ 55C (Worm-like)

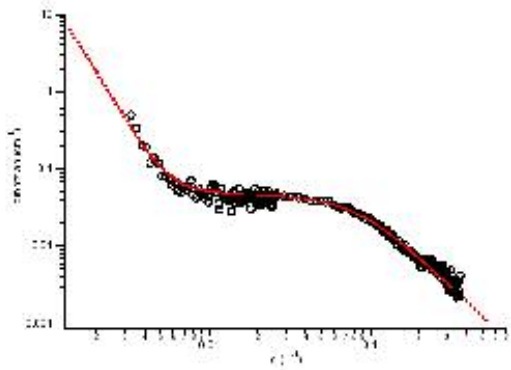

SAM12 @ 55C (Debye)

Run 4

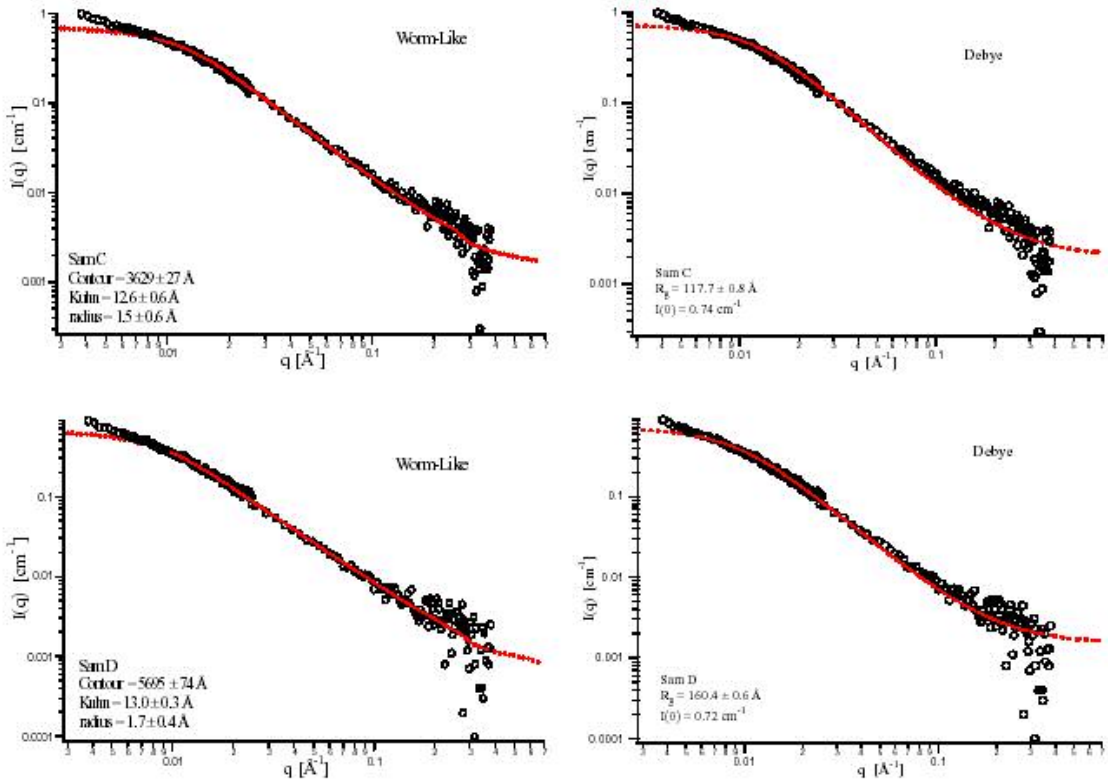
Worm-Like
I(q) [cm^{-1}]
q [Å^{-1}]
SamC
Contour = 3629 ± 27 Å
Kuhn = 12.6 ± 0.6 Å
radius = 1.5 ± 0.6 Å
Debye
I(q) [cm^{-1}]
q [Å^{-1}]
Sam C
R_g = 117.7 ± 0.8 Å
I(0) = 0.74 cm^{-1}
Worm-Like
I(q) [cm^{-1}]
q [Å^{-1}]
SamD
Contour = 5605 ± 74 Å
Kuhn = 13.0 ± 0.3 Å
radius = 1.7 ± 0.4 Å
Debye
I(q) [cm^{-1}]
q [Å^{-1}]
Sam D
R_g = 160.4 ± 0.6 Å
I(0) = 0.72 cm^{-1}

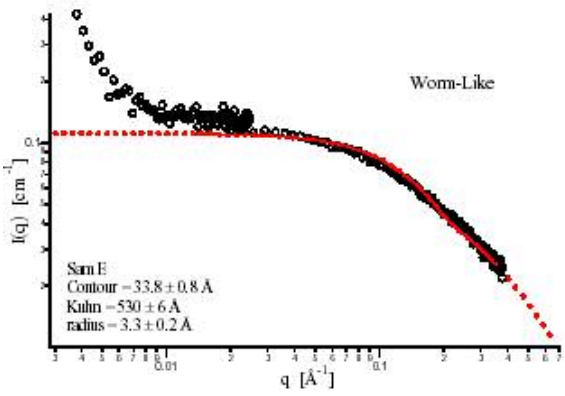
Worm-Like
I(q) [cm^{-1}]
q [Å^{-1}]
Sam E
Contour = 33.8 ± 0.8 Å
Kuhn = 530 ± 6 Å
radius = 3.3 ± 0.2 Å

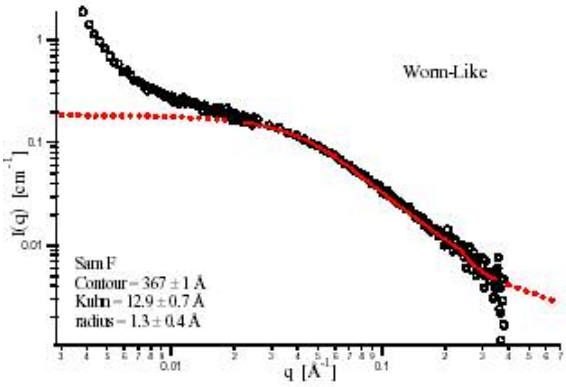
Worm-Like
I(q) [cm^{-1}]
q [Å^{-1}]
Sam F
Contour = 367 ± 1 Å
Kuhn = 12.9 ± 0.7 Å
radius = 1.3 ± 0.4 Å

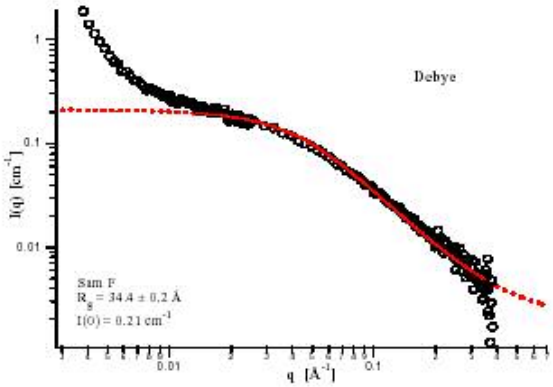
Debye
I(q) [cm^{-1}]
q [Å^{-1}]
Sam F
R_g = 34.4 ± 0.2 Å
I(0) = 0.21 cm^{-1}

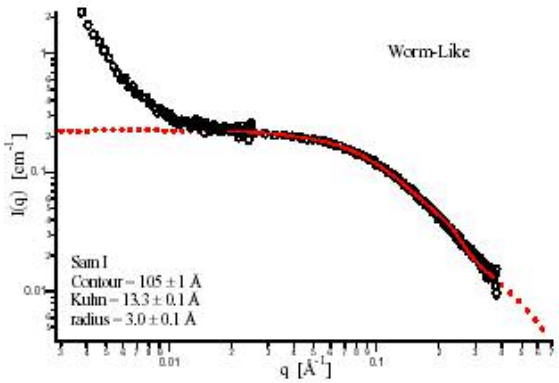
Worm-Like
I(q) [cm^{-1}]
q [Å^{-1}]
Sam I
Contour = 105 ± 1 Å
Kuhn = 13.3 ± 0.1 Å
radius = 3.0 ± 0.1 Å

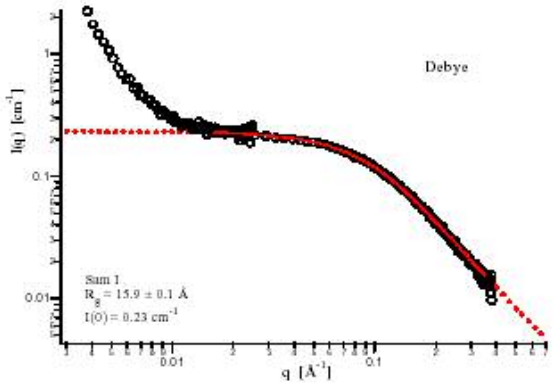
Debye
I(q) [cm^{-1}]
q [Å^{-1}]
Sam I
R_g = 15.9 ± 0.1 Å
I(0) = 0.23 cm^{-1}

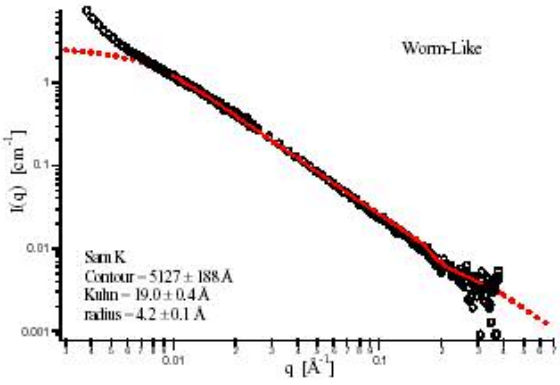
Worm-Like
I(q) [cm^{-1}]
q [Å^{-1}]
Sam K
Contour = 5127 ± 188 Å
Kuhn = 19.0 ± 0.4 Å
radius = 4.2 ± 0.1 Å

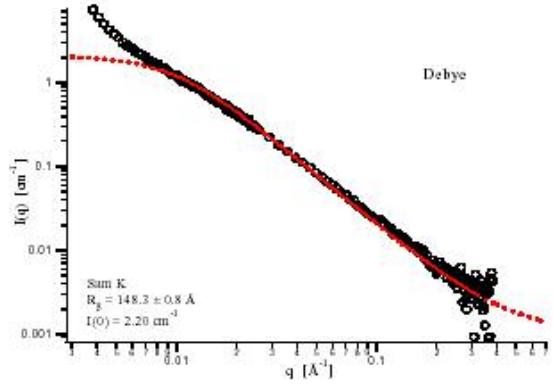
Debye
I(q) [cm^{-1}]
q [Å^{-1}]
Sam K
R_g = 148.3 ± 0.8 Å
I(0) = 2.20 cm^{-1}

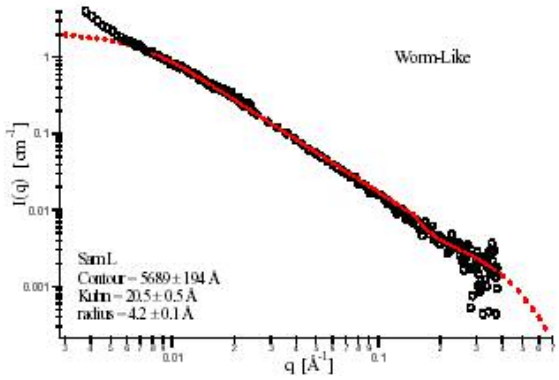
Worm-Like
I(q) [cm^{-1}]
q [Å^{-1}]
SamL
Contour = 5689 ± 194 Å
Kuhn = 20.5 ± 0.5 Å
radius = 4.2 ± 0.1 Å

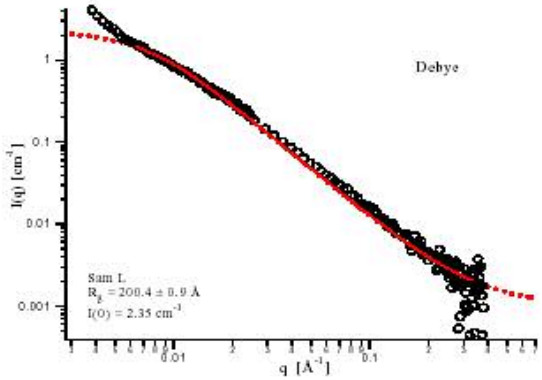
Debye
I(q) [cm^{-1}]
q [Å^{-1}]
Sam L
R_g = 200.4 ± 0.9 Å
I(0) = 2.35 cm^{-1}

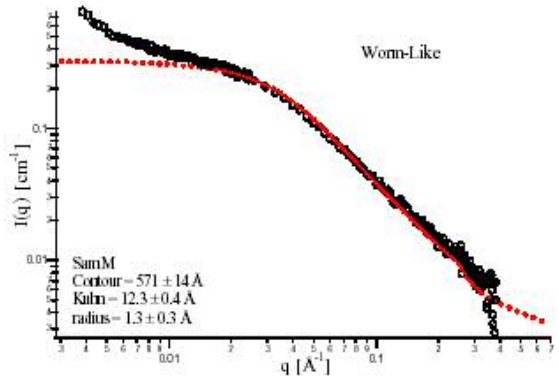
Worm-Like
I(q) [cm^{-1}]
q [Å^{-1}]
SamM
Contour = 571 ± 14 Å
Kuhn = 12.3 ± 0.4 Å
radius = 1.3 ± 0.3 Å

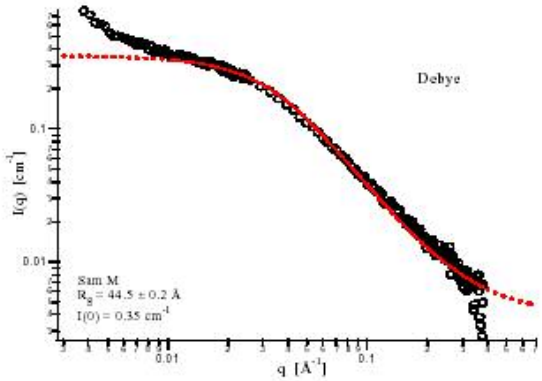
Debye
I(q) [cm^{-1}]
q [Å^{-1}]
Sam M
R_g = 44.5 ± 0.2 Å
I(0) = 0.35 cm^{-1}

Bibliography

(1) Jiang, X.; Lin, H.; Patel, N.; Merkel, T.; Freeman, B. In *North American Membrane Society*: Lexington, Kentucky, 2001.

(2) Flory, P. J. *Principles of Polymer Chemistry*, 2nd ed.; Cornell University Press: Ithaca, 1953.

(3) Shresth, R. S.; McDonald, R. C.; Greer, S. C. *Journal of Chemical Physics* **2002**, *117*, 9037-9049.

(4) Greer, S. C. *Physical Review A* **1976**, *14*, 1770-1780.

(5) Greer, S. C. *Berichte der Bunsen-Gesellschaft- Physical Chemistry Chemical Physics* **1977**, *81*, 1079-1081.

(6) Higgins, J. S.; Benoît, H. *Polymers and Neutron Scattering*; Oxford University Press: New York, 1994.

(7) Kjellander, R.; Florin, E. *Journal of the Chemical Society, Faraday Transactions 1* **1981**, *77*, 2053-2077.

(8) Branca, C.; Faraone, A.; Magazu, S.; Maisano, G.; Migliardo, P.; Triolo, A.; Triolo, R.; Villari, V. *Physica B* **2000**, *276*, 332-333.

(9) Branca, C.; Magazu, S.; Maisano, G.; Migliardo, P.; Tettamanti, E. *Physica B* **1999**, *270*, 350-359.

(10) Branca, C.; Faraone, A.; Maisano, G.; Magazu, S.; Migliardo, P.; Triolo, A.; Triolo, R.; Villari, V. *Journal of Physics-Condensed Matter* **1999**, *11*, 6079-6098.

(11) Vennemann, N.; Lechner, M. D.; Oberthur, R. C. *Polymer* **1987**, *28*, 1738.

(12) Bekiranov, S.; Bruinsma, R.; Pincus, P. *Physical Review E* **1997**, *55*, 577-585.

(13) Sun, T.; King, H. E. *Macromolecules* **1998**, *31*, 6383-6386.

(14) Polverari, M.; van de Ven, T. G. M. *Journal of Physical Chemistry* **1996**, *100*, 13687-13695.

(15) Hammouda, B.; Ho, D.; Kline, S. *Macromolecules* **2002**, *35*, 8578-8585.

(16) Devanand, K.; Selser, J. C. *Nature (London)* **1990**, *343*, 739.

(17) Devanand, K.; Selser, J. C. *Macromolecules* **1991**, *24*, 5943-5947.

(18) Blandamer, M. J.; Fox, M. F.; Powell, E.; Stafford, J. W. *Makromolekulare Chemie* **1969**, *124*, 222-&.

(19) Dormidontova, E. E. *Macromolecules* **2002**, *35*, 987-1001.

(20) Hirschfelder, J.; Stevenson, D.; Eyring, H. *Journal of Chemical Physics* **1937**, *5*, 896.

(21) Karlström, G. *Journal of Physical Chemistry* **1985**, *89*, 4962-4964.

(22) Saeki, S.; Kuwahara, N.; Nakata, M.; Kaneko, M. *Polymer* **1976**, *17*, 685-689.

(23) Panayiotou, C.; Sanchez, I. C. *Macromolecules* **1991**, *24*, 6231-6237.

(24) Panayiotou, C.; Sanchez, I. C. *Journal of Physical Chemistry* **1991**, *95*, 10090-10097.

(25) Veytsman, B. *Journal of Physical Chemistry* **1990**, *94*, 8499-8500.

(26) Veytsman, B. *Journal of Physical Chemistry B* **1998**, *102*, 7515-7517.

(27) Matsuyama, A.; Tanaka, F. *Physical Review Letters* **1990**, *65*, 341-344.

(28) Gupta, R. B.; Panayiotou, C.; Sanchez, I. C.; Johnston, K. P. *AIChE Journal* **1992**, *38*, 1243-1253.
(29) Malcolm, G. N.; Rowlinson, J. S. *Transactions of Faraday Society* **1957**, *53*, 921-931.
(30) Bae, Y. C.; Lambert, S. M.; Soane, D. S.; Prausnitz, J. M. *Macromolecules* **1991**, *24*, 4403.
(31) Woodley, D. M.; Dam, C.; Lam, H.; LeCave, M.; Devanand, K.; Selser, J. C. *Macromolecules* **1992**, *25*, 5283-5286.
(32) Ho, D. L.; Hammouda, B.; Kline, S. R. *Journal of Polymer Science Part B-Polymer Physics* **2003**, *41*, 135-138.
(33) Fischer, V.; Borchard, W. *Journal of Physical Chemistry B* **2000**, *104*, 4463-4470.
(34) Fischer, V.; Borchard, W.; Karas, M. *Journal of Physical Chemistry* **1996**, *100*, 15992-15999.
(35) Branca, C.; Magazu, S.; Maisano, G.; Migliardo, P.; Migliardo, F.; Romeo, G. *Physica Scripta* **2002**, *66*, 175-179.
(36) Branca, C.; Magazu, S.; Maisano, G.; Migliardo, F.; Migliardo, P.; Romeo, G. *Journal of Physical Chemistry B* **2002**, *106*, 10272-10276.
(37) Begum, R.; Matsuura, H. *Journal of Chemical Society, Faraday Transactions* **1997**, *93*, 3839-3848.
(38) Bailey, F. E.; Koleske, J. V. *Poly(ethylene oxide)*; Academic Press: New York, 1976.
(39) Smith, G. D.; Bedrov, D. *Journal of Physical Chemistry B* **2003**, *107*, 3095-3097.
(40) Scott, R. L. *Journal of Chemical Physics* **1949**, *17*, 268.
(41) Shultz, A. R.; Flory, P. J. *Journal of Polymer Science* **1955**, *15*, 231-242.
(42) Magda, J. J.; Fredrickson, G. H.; Larson, R. G.; Helfand, E. *Macromolecules* **1988**, *21*, 726-732.
(43) Brochard, F.; de Gennes, P. G. *Ferroelectrics* **1980**, *30*, 33-47.
(44) Stapper, M.; Vilgis, T. A. *Europhysics Letters* **1998**, *42*, 7-12.
(45) To, K.; Choi, H. *Physical Review Letters* **1998**, *80*, 536-539.
(46) To, K.; Kim, C. A.; Choi, H. J. *Physica A* **1998**, *254*, 292-299.
(47) Morita, S.; Tsunomori, F.; Ushiki, H. *European Polymer Journal* **2002**, *38*, 1863-1870.
(48) Niamke, J. Masters Thesis in Chemical Engineering; University of Maryland, 2004.
(49) Shresth, R. S. Doctoral Dissertation in Chemistry; University of Maryland, 2002.
(50) Rupp, B., Circular Dichroism Spectroscopy: http://www-structure.llnl.gov/cd/cdtutorial.htm, 2004.
(51) Masatoki, S.; Takamura, M.; Matsuura, H.; Kamogawa, K.; Kitagawa, T. *Chemistry Letters* **1995**, 991-992.
(52) Matsuura, H.; Fukuhara, K. *Journal of Molecular Structure* **1985**, *126*, 251-260.
(53) Matsuura, H.; Sagawa, T. *Journal of Molecular Liquids* **1995**, *65-6*, 313-316.
(54) Maxfield, J.; Shepherd, I. W. *Polymer* **1975**, *16*, 505-509.

(55) Begum, R.; Masatoki, S.; Matsuura, H. *Journal of Molecular Structure* **1996**, *384*, 115-120.
(56) Begum, R.; Sagawa, T.; Masatoki, S.; Matsuura, H. *Journal of Molecular Structure* **1998**, *442*, 243-250.
(57) Green, M.; Reidy, M. *Journal of the American Chemical Society* **1989**, *111*, 6452-6454.
(58) Singleton, D. A.; Vo, L. K. *Organic Letters* **2003**, *5*, 4337-4339.
(59) Soai, K.; Sato, I.; Shibata, T. *Chemical Record* **2001**, *1*, 321-332.
(60) Soai, K.; Sato, I.; Shibata, T.; Komiya, S.; Hayashi, M.; Matsueda, Y.; Imamura, H.; Hayase, T.; Morioka, H.; Tabira, H.; Yamamoto, J.; Kowata, Y. *Tetrahedron-Asymmetry* **2003**, *14*, 185-188.
(61) Sato, I.; Urabe, H.; Ishiguro, S.; Shibata, T.; Soai, K. *Angewandte Chemie International Edition* **2003**, *42*, 315-317.
(62) Sato, I.; Ohno, A.; Aoyama, Y.; Kasahara, T.; Soai, K. *Organic and Biomolecular Chemistry* **2003**, *1*, 244-246.
(63) Sato, I.; Kadowaki, K.; Urabe, H.; Jung, J. H.; Ono, Y.; Shinkai, S.; Soai, K. *Tetrahedron Letters* **2003**, *44*, 721-724.
(64) Singleton, D. A.; Vo, L. K. *Journal of the American Chemical Society* **2002**, *124*, 10010-10011.
(65) Kline, S., SANS Data Reduction and Analysis with IGOR Pro: http://www.ncnr.nist.gov/programs/sans/manuals/data_anal.html, 2002.
(66) Pedersen, J. S.; Schurtenberger, P. *Macromolecules* **1996**, *29*, 7602-7612.
(67) Teraoka, I. *Polymer Solutions*; John Wiley & Sons: New York, 2002.
(68) Guinier, A.; Fournet, G. *Small-Angle Scattering of X-Rays*; John Wiley, 1955.
(69) Borodin, O.; Douglas, R.; Smith, G. A.; Trouw, F.; Petrucci, S. *Journal of Physical Chemistry B* **2003**, *107*, 6813-6823.
(70) Branca, C.; Faraone, A.; Magazu, S.; Maisano, G.; Migliardo, P.; Triolo, A.; Triolo, R.; Villari, V. *Journal of Applied Crystallography* **2000**, *33*, 709-713.
(71) Tasaki, K.; Abe, A. *Polymer Journal* **1985**, *17*, 641-655.
(72) Ho, D.; Hammouda, B. *Unpublished work in progress* **2004**.
(73) Borsali, R.; Nguyen, H.; Pecora, R. *Macromolecules* **1998**, *31*, 1548-1555.
(74) Dondos, A.; Benoît, H. *Makromolekulare Chemie* **1970**, *133*, 119.